ABSTRACT

Title of Document:	PROCESSING OF CELLULOSE FOR THE ADVANCEMENT OF BIOFUELS
	Brian J. Watson, *Doctor of Philosophy, 2011*
Directed By:	Professor Isabel Lloyd (Co-Chair) Department of Materials Science and Engineering
	Professor Steven Hutcheson (Co-Chair) Department of Cell Biology and Molecular Genetics

The enzymatic degradation of cellulose polymers is currently a rate-limiting step in the bioconversion of biomass to biofuels. Cellulose polymers self assemble to form crystalline structures stabilized by a complex network of intermolecular interactions such as hydrogen bonding. The network of interactions in crystalline cellulose (cellulose nanostructure) poses an energy barrier that limits enzymatic degradation as apparent from the activity of Cel5H. To improve the degradability of cellulose the intermolecular interactions must be disrupted. The interactions of the cellulose nanostructure prevent solubilization by water and most other common solvents, but some organic solvents aid degradation of cellulose suggesting they influence cellulose nanostructure. The objective of this work is to understand the influence of solvents on cellulose nanostructure with the goal of improving the degradability of cellulose nanostructure using solvents.

To understand solvent interaction with cellulose, phosphoric acid was used to first solubilize cellulose (PAS cellulose) followed by adding an organic liquid or water to wash the phosphate from the system. The Flory Huggins theory was used to predict wash liquids that could favorably interact with cellulose. A favorable wash liquid was

predicted to prevent the reformation of crystalline domains to yield a disrupted cellulose nanostructure, which should be more degradable. Low molecular weight alcohols and glycols were calculated to be favorable wash liquids.

Washing PAS cellulose with the predicted favorable liquids yielded semi-transparent gel-like materials compared to the opaque white precipitate formed when water or unfavorable solvents were used in the wash. Fractal analysis of small angle neutron scattering (SANS) of these apparent gels indicated cellulose polymers likely have the properties of clustered rods. This partial disruption increased degradability relative to the water washed PAS cellulose. The apparent rod-like cellulose nanostructures suggested the presence of intra and interpolymer hydrogen bonding. Characterization of the hydrogen bonding network by Fourier transform infrared resonance (FTIR) indicated the gel-like material formed by ethanol washes was the result of heterogeneous interpolymer hydrogen bond cross-links.

The interactions leading to gel-like materials were evaluated using Hansen solubility parameters, which predicted mixtures of ethanol and water may be most effective for disrupting cellulose nanostructure. Fractal analysis by SANS indicated 40 % ethanol/water was most effective. Similar results were obtained when 40 % ethanol was used to disrupt the cellulose nanostructure in municipal office waste (MOW). Ethanol washes increased the degradability of MOW by at least 30 % relative to conventional water washing. This is significant because increased degradability of MOW could further the development of cellulosic biofuels by reducing the amount of enzyme required to digest the material.

PROCESSING OF CELLULOSE FOR THE ADVANCEMENT OF BIOFUELS

By

Brian James Watson

Dissertation submitted to the Faculty of the Graduate School of the
University of Maryland, College Park, in partial fulfillment
of the requirements for the degree of
Doctorate of Philosophy
2011

Advisory Committee:
Professor Isabel Lloyd, Co-Chair
Professor Steven Hutcheson, Co-Chair
Professor Robert Briber
Professor Joonil Seog
Professor Dorothy Beckett

Dedication

I dedicate this dissertation to my father, Dr. James F. Watson. His optimism, encouragement, and support, have contributed to my life long journey of learning and the pursuit of my dreams.

Acknowledgements

I would like to acknowledge the people and organizations that helped me earn my Ph.D. I would like to thank Mr. Steve Beeland and the Department of External Relations for providing me with my first graduate assistantship, which enabled me to attend the University of Maryland. I would also like to thank the National Science Foundation (DEB0621297), the University of Maryland Energy Research Center and the Maryland Industrial Partnerships Program (MIPS - 4516) for funding my research. I would also like to thank the Department of Cell Biology and Molecular Genetics for providing me with teaching assistantships that enabled me to support myself.

I would also like to express my sincere gratitude to the staff of the NIST Center for Neutron Research for their assistance working with SANS and several other characterization techniques. The guidance and assistance from Dr. Boualem Hammouda, Dr. Ken Rubinson, Dr. David Mildner, and Ms. Kim Tomassi was especially critical to the success of this work.

I also want to thank the staff of Zymetis Inc. for their support and assistance. I would especially like to thank Dr. Haitao Zhang for all of his advice and friendship.

Table of Contents

List of Tables

List of Figures

List of Terms

Cellobiohydrolase – An enzyme that degrades cellulose processively from a specific polymer end

Cellulose solvent – A chemical that can dissolve the structure of crystalline cellulose

Disruption of cellulose – Impeding the formation of crystalline domains during the washing of PAS cellulose

Disrupted cellulose – Cellulose that has both cellulose II and amorphous fractions

Endoglucanase – An enzyme that degrades cellulose at random sites of the polymer

Hydroxymethyl group – The C6 – O6 exo-cyclic group of the glucopyranose ring

Intrapolymer interactions – Bonds that form within the same polymer

Interpolymer interactions– Bonds that form between different polymers

Phosphoric acid solubilization (PAS) – When the polymers of the cellulose structure are dissolved in phosphoric acid

Wash liquid – The liquid added to PAS cellulose to wash the phosphate from the system

1. Introduction

The urgent demand for alternatives to fossil fuels has promoted research in developing biofuels from biomass (1). The structural backbone of biomass is the cellulose microfibril, which is composed of linear glucose polymers (2, 3). Cellulose is produced through a biosynthetic process in which the polymers self assemble to yield para-crystalline structures with both crystalline and amorphous regions (Figure 1.1) (4-6). The crystal structure of cellulose is stabilized by its backbone β-1,4 linkage, hydrogen bonding, van der Waals forces and hydrophobic interactions (in the presence of water) (2, 7, 8). This network of interactions poses an energy barrier to degradation which is a rate limiting step in the biofuels process (1, 2). Understanding how the interactions of cellulose can be manipulated to increase degradability is the subject of this dissertation.

One of the most promising means of degrading cellulose is by using enzymes to catalyze the conversion of polymeric to monomeric glucose (1, 2). The most efficient enzymes degrade cellulose processively, which means they release multiple glucose units from the structure per binding event (9). The mechanism of the *Saccharophagus degradans* cellulolytic system was investigated and several new processive enzymes were identified. The degradation of cellulose by these processive enzymes was inversely dependent on cellulose crystallinity, which demonstrated the necessity for disrupting the ordered interactions of cellulose.

Numerous protocols have been developed to fractionate the components of biomass to increase cellulose accessibility for enzyme degradation (10, 11). The fractionation of cellulose is typically accomplished by solubilizing biomass in acid followed by the addition of an extraction solvent (10, 12). Extraction solvents include

acetone and ethanol, but vary depending on biomass composition (13, 14). The use of solvents has been empirically determined to increase the degradability of cellulose, but how the interactions in the structure are affected is not well understood (15).

The network of intermolecular interactions causes cellulose polymers with seven or more glucose units to be insoluble in water and most other liquids (16). To overcome the energy barrier to solvation of cellulose phosphoric acid, a cellulose solvent, was used to first solubilize the cellulose polymers (17). The acidic conditions of the phosphoric acid solubilized (PAS) cellulose denature enzymes, which necessitated the use of a liquid to wash the phosphate from the system (17). The wash liquid caused the cellulose polymers to precipitate and thus reform a structure (17). The goal of the washing process was to have the wash liquid favorably interact with cellulose to disrupt precipitation.

The interactions between the wash liquid and cellulose are important because they affect the properties and morphology of the precipitate (18, 19). The Flory Huggins theory was used to predict the interactions between the cellulose polymers and wash liquid (20, 21). The Flory Huggins interaction parameter χ, which predicts favorable or unfavorable interactions in a polymer/solvent system (20, 21), identified low molecular weight alcohols and glycols as having potential favorable interactions with cellulose. To test the predicted interactions PAS cellulose was washed with predicted favorable and unfavorable liquids. The optical density of washed PAS cellulose in suspension was used to characterize the state of polymer aggregation (21). In this work, optical density indicated the precipitates had unique gel-like and opaque white properties depending on the wash liquid.

Different polymer morphologies suggested unique nano scale properties, which effect enzyme accessibility and thus degradation (22, 23). Small angle neutron scattering (SANS) was used to characterize the washed PAS cellulose on the scale of 10 – 800 nm (24-26). The scattering data exhibited fractal behavior and was fitted using a power law model. The fitted power law exponent, α, represented the clustering of cellulose nanostructures of each washed PAS cellulose (24, 25, 27). The α of the gel-like precipitates was lower relative to the α of the opaque white precipitate formed by water washing, which indicated a possible reduction in clustering of cellulose nanostructures.

The precipitation of clustered nanostructures suggested the presence of hydrogen bonding. Fourier transform infrared resonance (FTIR) was used to characterize the molecular interactions of the washed PAS cellulose structures. In cellulose structures hydrogen bonding can occur both between cellulose polymers (inter) and within the same polymer (intra) as well as between cellulose sheets (intersheet) (28-31). The patterns in hydrogen bonding represented the tendency to form intrapolymer bonds in the opaque white precipitates versus interpolymer bonds in the gel-like material. Understanding how washing PAS cellulose with organic liquids and water affected hydrogen bonding enabled the optimization of disruption.

The properties of the wash liquids that yielded cellulose gel-like precipitates were quantified using Hansen solubility parameters (δ) which enabled formulation of mixtures to most effectively disrupt real materials. Hansen solubility parameters were used to plot the $\delta_{\text{Hydrogen Bonding}}$ versus δ_{Polarity} to identify a region of approximate gel-like formation (32). Based upon the Hansen solubility parameters, solvent mixtures were used to expand the region of gel-like formation. Ethanol/water mixtures were determined to

yield the most disruption and were applied to disrupt the cellulose structures of municipal office waste (MOW). In this work the investigation of wash liquid/cellulose interactions was applied to increase the enzymatic degradability of an actual recycled material.

Figure 1.1 - The structure of lignocellulosic biomass

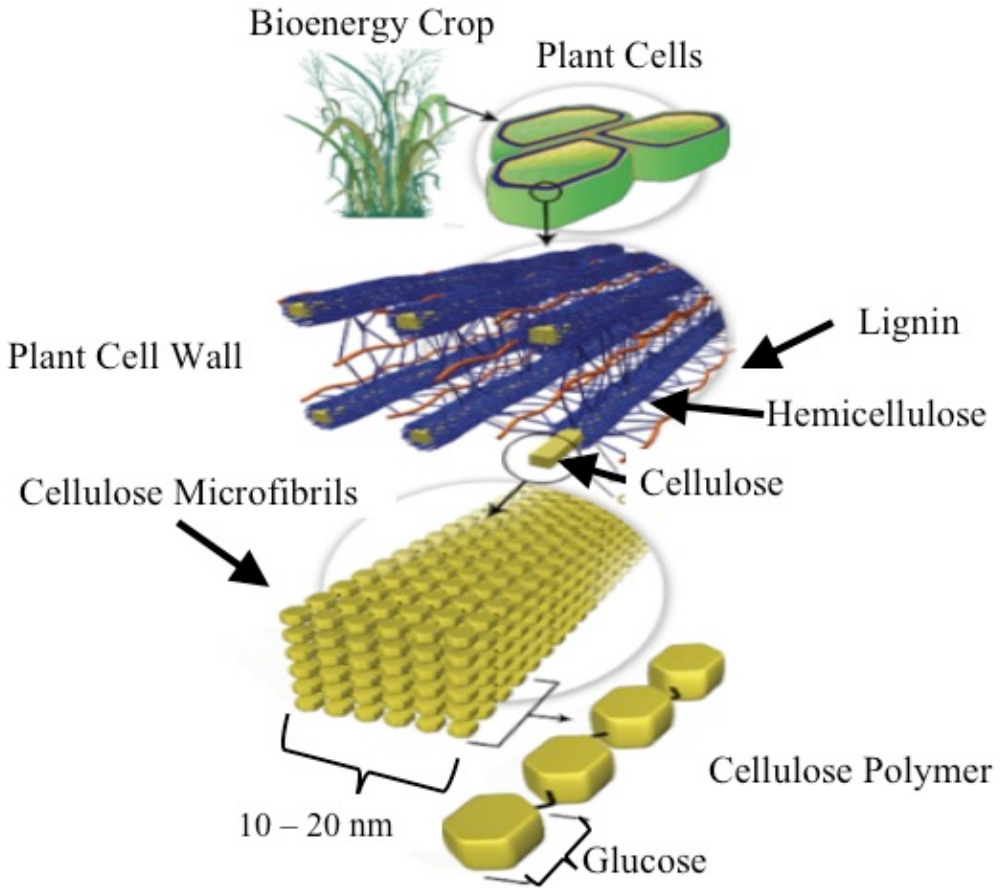

U.S. Department of Energy Genome Programs: http://genomics.energy.gov.

2. Background on Cellulose

2.1. Components of the plant cell wall

The cell wall gives plants the strength and rigidity to withstand the elements of nature such as wind, and attack from animal and insect species (3). The cell wall is composed of a diverse collections of polysaccharides (≈70 %) and phenolic alcohols (≈30 %) which yield the strength to withstand tensile and compressive forces (3, 5). The backbone structural unit is the cellulose microfibril which is formed by assembly of unbranched β-1,4 glucose polymers which form hexagonal shaped, rod-like para-crystalline structures (2, 3). The para-crystalline cellulose structures are encased by a diverse matrix of hemicellulose/pectin and lignin that protect the cellulose microfibrils from degradation (1, 2).

The linkages and side chain functional groups of each polysaccharide determines the degree of branching and distinguishes cellulose, hemicellulose and pectin components (3, 5). Hemicellulose is most commonly composed of β-1,4 linked xylan (5 carbon sugar) and mannan (6 carbon sugar) (3, 5). Due to the heterogeneity of the hemicellulose polymers they generally do not form crystalline structures like cellulose (33). The possibility of multiple linkages also hinders the formation of ordered structures. Pectin is similar to hemicellulose, but contains a more diverse collection of linkages and side-polymer units, such as arabinan, galactan, and glucuronic acid (5).

Lignin forms a matrix which binds the hemicellulose/pectin and cellulose structures (2, 3). Lignin is composed of phenolic alcohols which form a complex cross-linked network that is not polymeric since there is no repeating unit (1). The aromatic compounds of lignin act to inhibit the enzymatic degradation of cellulose (2). The

encased cellulose microfibrils aggregate into larger bundles that retain the ordered structure of the individual microfibrils (1, 2).

2.2. Cellulose

Cellulose is a major component of lignocellulosic biomass (≈30 – 40 %) (1, 2). Cellulose exists as high molecular weight β-1,4 linked glucose polymers (degree of polymerization ≈200 – 10,000) (Figure 2.1A) (34, 35). Each cellulose polymer has one reducing and one non-reducing end (2). These ends are useful for detecting sugars and are used by enzymes to recognize their binding site (35). At the reducing end the C1 carbon is linked to an oxygen atom as an aldehyde group (35). The non-reducing end is simply where the polymer no longer forms a β-1,4 linkage and is not able to act as a reducing agent (35).

The individual glucose monomers have a chair conformation, which orients the hydroxyl groups into equatorial positions and aliphatic hydrogen atoms into axial positions (2, 8). This conformation induces interpolymer hydrogen bonding, which contributes to the formation of planar sheets (2). The planar sheets of cellulose stack through hydrophobic and van der Waals interactions (8, 36). These interactions cause cellulose polymers to self-assemble in water during synthesis of the plant cell wall to form highly ordered, para-crystalline microfibrils (Figure 2.1B) (2, 5).

A typical cellulose microfibril is composed of 36 cellulose polymers in a para-crystalline (degree of crystallinity ≈70 %), linear, hexagonal arrangement with a ≈20 nanometer diameter (Figure 2.1B) (2, 37). Crystalline cellulose forms a stable structure due to multiple hydrogen bonds linking cellulose polymers in plane and van der Waals and hydrophobic interactions between planes (2, 30, 38). The stability of crystalline

cellulose is evident in its onset temperature of decomposition of approximately 310 °C and lack of an obvious melting temperature (39).

The ordering of cellulose polymers within the microfibril is effected by the conformation of the 6th carbon of each glucose unit (40). Each glucose unit of cellulose is a 5 carbon glucopyranose ring that has a 6th, exo-cyclic carbon, not in the ring structure (41). The exo-cyclic 6th carbon is linked to a hydroxyl group and together are referred to as the "hydroxymethyl group" (Figure 2.2) (42). The hydroxymethyl group is important because its conformation effects intrapolymer, interpolymer and intersheet interactions (42). The conformation is defined by two torsion angles that are each represented by a single letter. The first letter refers to the angle between the O5 – C5 – C6 – O6, and the second refers to the angle between the C4 – C5 – C6 – O6 (40). When the angle is either 60 ° or -60 ° the letter is *g (gauche)* and when the angle is 180 ° the letter is *t (trans)* (40). Three conformations of the hydroxymethyl group exist in cellulose: *tg, gt, and gg (40)*. The most important concept of the hydroxymehtyl group conformation is that 180 ° *tg* means the hydroxyl group is in the horizontal plane of cellulose polymers, while the hydroxyl group in the *gg* and *gt* conformations extends out of the plane.

Figure 2.1 – The cellulose polymer and microfibril

(A)

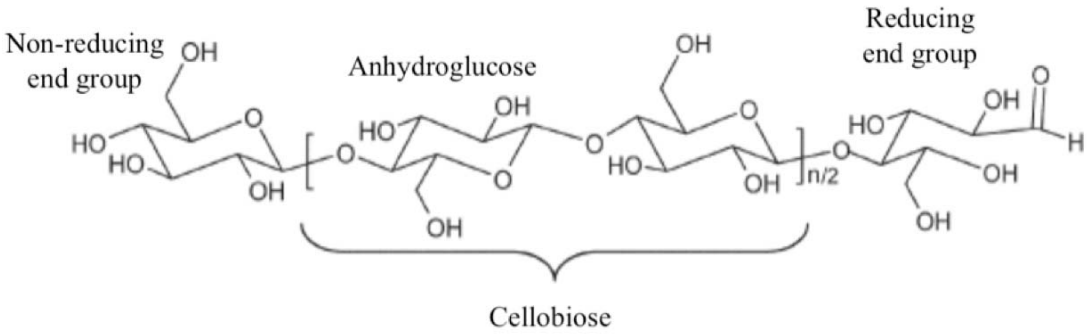

(B)

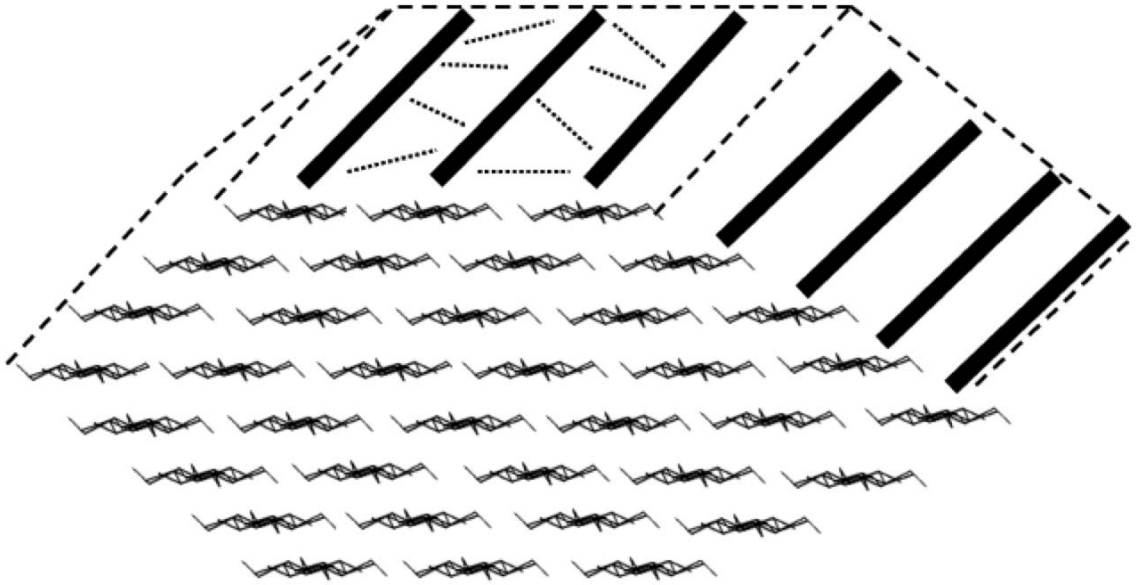

(A) The cellulose polymer with a reducing and non-reducing end. Reproduced with permission (43). (B) The cellulose microfibril is composed of 36 cellulose polymers in a hexagonal geometry (2). The view is of the end of a cellulose microfibril. The large dashed lines represent the edges of the microfibril. The small dashed lines in between polymers represent hydrogen bonds. The solid black lines represent the cellulose polymers.

Figure 2.2 – The hydroxymethyl group of cellulose

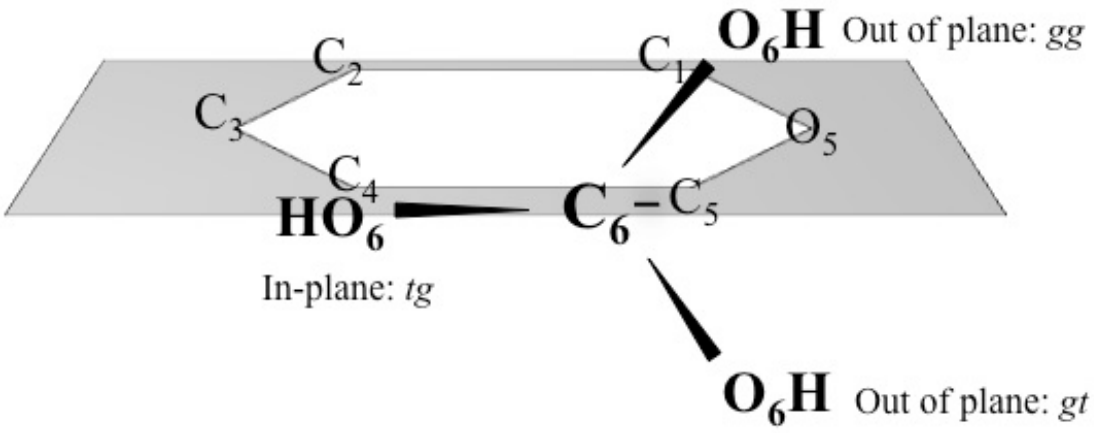

The three possible conformations of the hydroxymethyl group. The glucopyranose ring structure is represented by the hexagon. In the drawing the *tg* conformation is in the plane of the glucopyranose ring.

2.3. Synthesis and crystallization of cellulose

Cellulose is created through a biosynthetic process by cellulose biosynthetic enzymes (4, 5). Cellulose biosynthetic enzymes are found in families of algae, slime mold, bacteria, cyanobacteria and tunicates (4, 5, 39). The cellulose biosynthetic enzymes form a membrane structure called a terminal complex (TC), which has six fold symmetry and a diameter of ≈30 nm (4, 5, 39). The TC has six units that each have six individual cellulose biosynthetic enzymes (Figure 2.3A) (4, 5, 39).

The first step in the formation of cellulose structures is the polymerization of glucose to yield β-1,4 linked cellulose polymers (4, 5). Cellulose biosynthetic enzymes in the TC have been observed performing the three steps of polymerization: initiation, elongation and termination using uridine diphosphate-α-glucose (UDP-α-glucose) as the substrate (4, 5, 39). Cellulose biosynthetic enzymes act processively with two UDP-α-glucose units in the active site at a time (4, 5, 39).

After extrusion from the TC, the cellulose polymers interact through hydrogen bonding, van der Waals and hydrophobic interactions to form cellulose structures (44, 45). Cellulose polymers with 7 or more glucose units are insoluble in water and most organic solvents (16). The crystallization of native cellulose is a two-step process described by Cousins and Brown (44, 45). Each unit of the TC extrudes six cellulose polymers, which form mini-crystals (5). The cellulose mini-crystals form sheets through hydrogen bonding which stack due to van der Waals interactions to form a mini-crystal composed of six cellulose polymers which aggregate to form cellulose microfibrils (Figure 2.3B) (44, 45).

Figure 2.3 – The terminal complex (TC) of cellulose biosynthetic enzymes

(A)

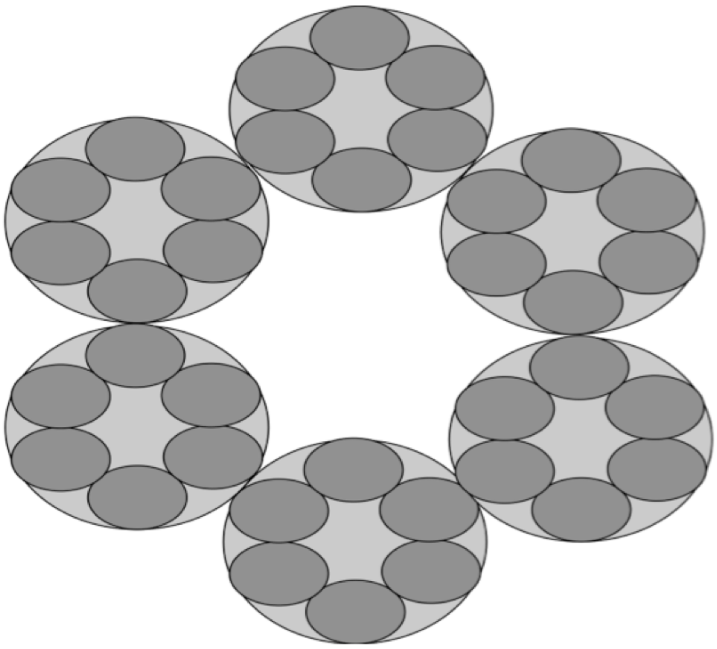

(B)

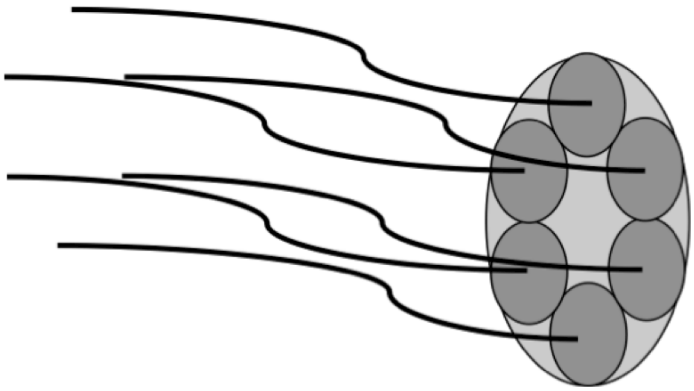

(A) The TC consists of six units with six cellulose biosynthetic enzymes each (4, 5). (B) Each cellulose biosynthetic enzyme extrudes a single cellulose polymer, which assemble to form mini-crystals with the six nearest polymers and then aggregate into 36 polymer microfibrils (4, 5).

2.4. The crystal structure of cellulose

2.4.1. Lattice structure of native cellulose (cellulose I)

Native cellulose has two unique phases depending on the alignment of the cellulose polymers (8). In native cellulose, each cellulose polymer is extruded from the TC in parallel, which means the hydroxymethyl groups align in the same direction (2, 46) (Figure 2.4A). The alignment of the parallel cellulose polymers yields two dominant crystal phases, alpha (I_α) and beta (I_β) (Figure 2.4B) (30, 31). The alpha phase exists mostly in bacterial and algal sources of cellulose while the beta phase predominately exists in higher plants (30, 31). Using synchrotron x-ray and neutron fiber diffraction the crystal structures of both I_α and I_β have been established (30, 31).

The unit cell of the I_α phase is triclinic and has one cellulose polymer (Figure 2.5A). Each polymer is offset by 25 % the length of the polymer repeat direction (31). The unit cell belongs to the P1 space group (P refers to a primative unit cell with a 1 fold axis of rotation) (47). The lattice parameters of the unit cell are: a = 6.7 Å, b = 6.0 Å, c = 10.4 Å, α = 118.1 °, β = 114.8 °, γ = 80.4 ° (31). The (110) is the plane of hydrogen bonding and the (100) and (010) are both planes of hydrophobic and van der Waals interactions (31). The a and b directions represent intersheet distances while the c directions represents the polymer repeat direction.

The I_β phase has two cellulose polymers per unit cell with a polymer located at the center and corners of the lattice (Figure 2.5B) (30). The polymer at the center of the unit cell is offset by 25 % in the polymer repeat direction relative to the corner polymers (30). This causes the glucose monomers to appear staggered when viewed on the (011) face of the structure (8, 30). This ordering of cellulose polymers yields a monoclinic unit cell

with a $P2_1$ space group (P refers to a primitive monoclinic unit cell, 2 refers to a two-fold axis of rotation and the sub-1 refers to the mirror plane) (30, 47). The plane of hydrogen bonding is the (010), while hydrophobic and van der Waals interactions occur in the (100), (110), and (1$\bar{1}$0) planes. The lattice parameters are a = 7.8 Å, b = 8.2 Å, c = 10.4 Å, $\alpha = \beta = 90°$, $\gamma = 96.5°$ (Figure 2.4B) (30). (a) is the direction of the cellulose sheets and (b) is the direction of hydrogen bonding within the cellulose sheets and (c) is the polymer repeat direction (30).

Figure 2.4 – The alignment of cellulose polymers

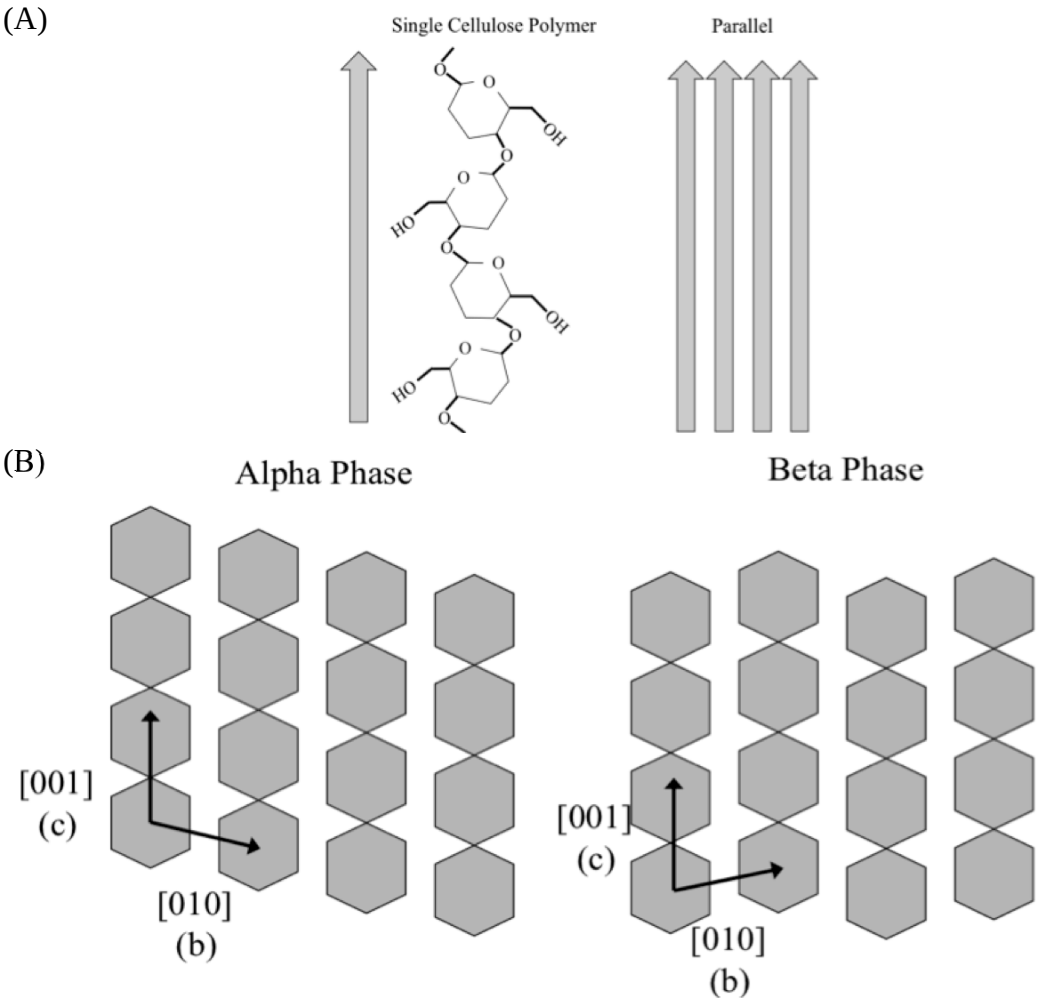

(A) The repeat unit of cellulose is cellobiose, due to the conformation of the hydroxymethyl groups (other hydroxyl groups not shown) (2). (B) The offset of cellulose polymers affects the unit cell of the lattice structure (8). The view is of the (011).

Figure 2.5 – The lattice structure of native cellulose

The view in (A) and (B) is orthogonal to the polymer repeat direction (c)

(A)

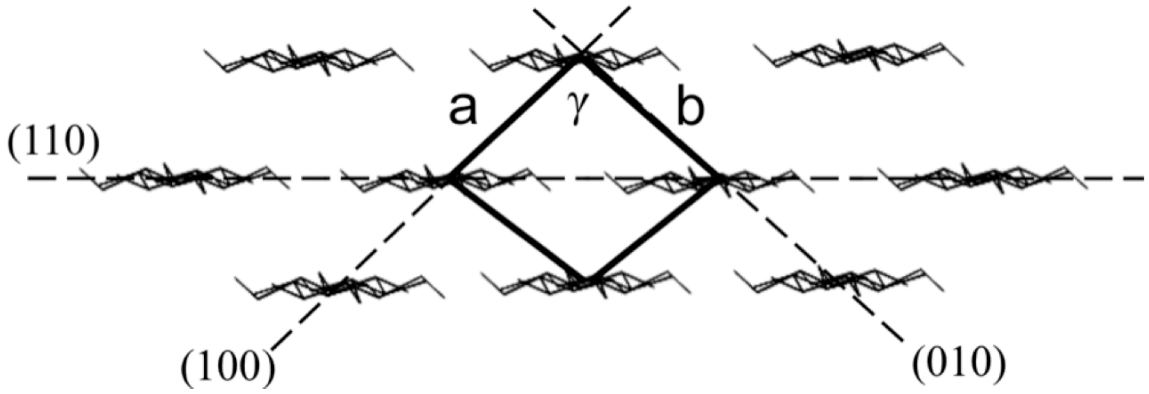

(B)

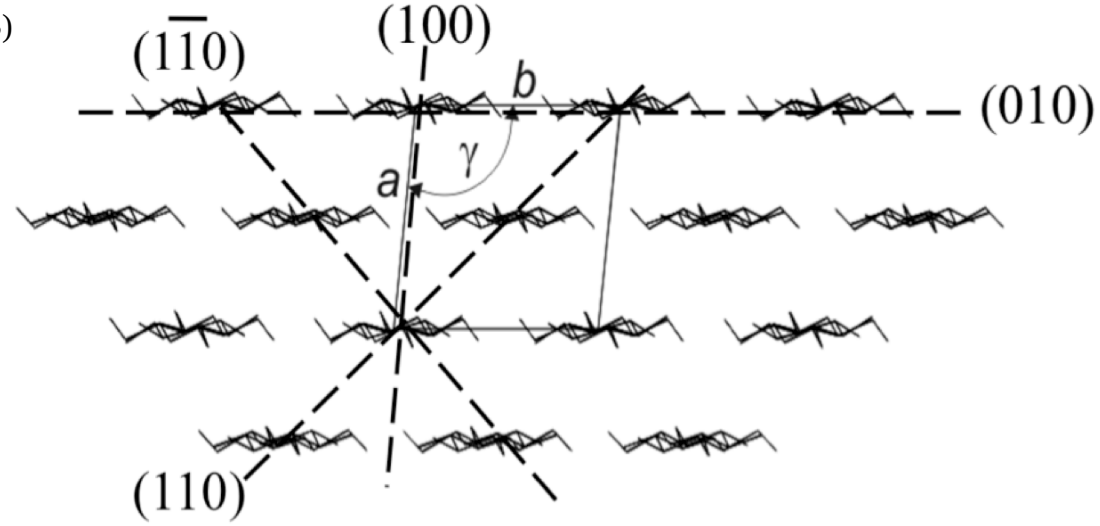

(A) The lattice structure of the I_α phase (31). (B) The lattice structure of the I_β phase

2.4.2. Lattice structure of cellulose II

Native cellulose can be processed to yield cellulose II (48, 49). In cellulose II the polymers are anti-parallel which yields opposite locations of the hydroxymethyl groups (29). In native cellulose the dipole moments of each chain are forced into a parallel conformation. During the transition the chains become swollen which allows some of the microfibrils to be mobile. Opposite dipoles attract microfibrils of opposite charge to become intertwined, which is called interdigitation (29, 50). Interdigitation is driven by attractive polar interactions, which causes the anti-parallel structure to form (50, 51). In the anti-parallel structure the hydroxymethyl groups are in the *gt* conformation, which enables hydrogen bonding in the (110) plane (29, 38). structure of cellulose II is more stable than native cellulose because of the added plane of hydrogen bonding (52). The unit cell of cellulose II is monoclinic with two polymers per cell: a = 8.0 Å, b = 9.0 Å, c = 10.4 Å with $\alpha = \beta = 90°$, $\gamma = 117.1°$ (Figure 2.6A) (29). The most notable difference between the native cellulose and cellulose II lattice structures is the angle, γ, which is 96.5 ° for native cellulose (I_β) compared to 117.1 ° in cellulose II (29).

2.4.3 Lattice structure of cellulose III

Native cellulose or cellulose II can be transformed to cellulose III (52, 53). The cellulose polymers of cellulose III are parallel with one polymer per unit cell (Figure 2.6B) (54). The hydroxymethyl groups are in the *gt* conformation which enables intersheet interactions similar to those of cellulose II, however the parallel alignment of the polymers causes a unique structure to form (54). The transition of native cellulose to cellulose III is reversible upon heating (55). The unit cell of cellulose III is monoclinic ($P2_1$) with lattice parameters a = 4.5 Å, b = 7.9 Å, c = 10.4 Å and $\gamma = 105.1°$ (54).

Figure 2.6 – The lattice structure of cellulose II and III

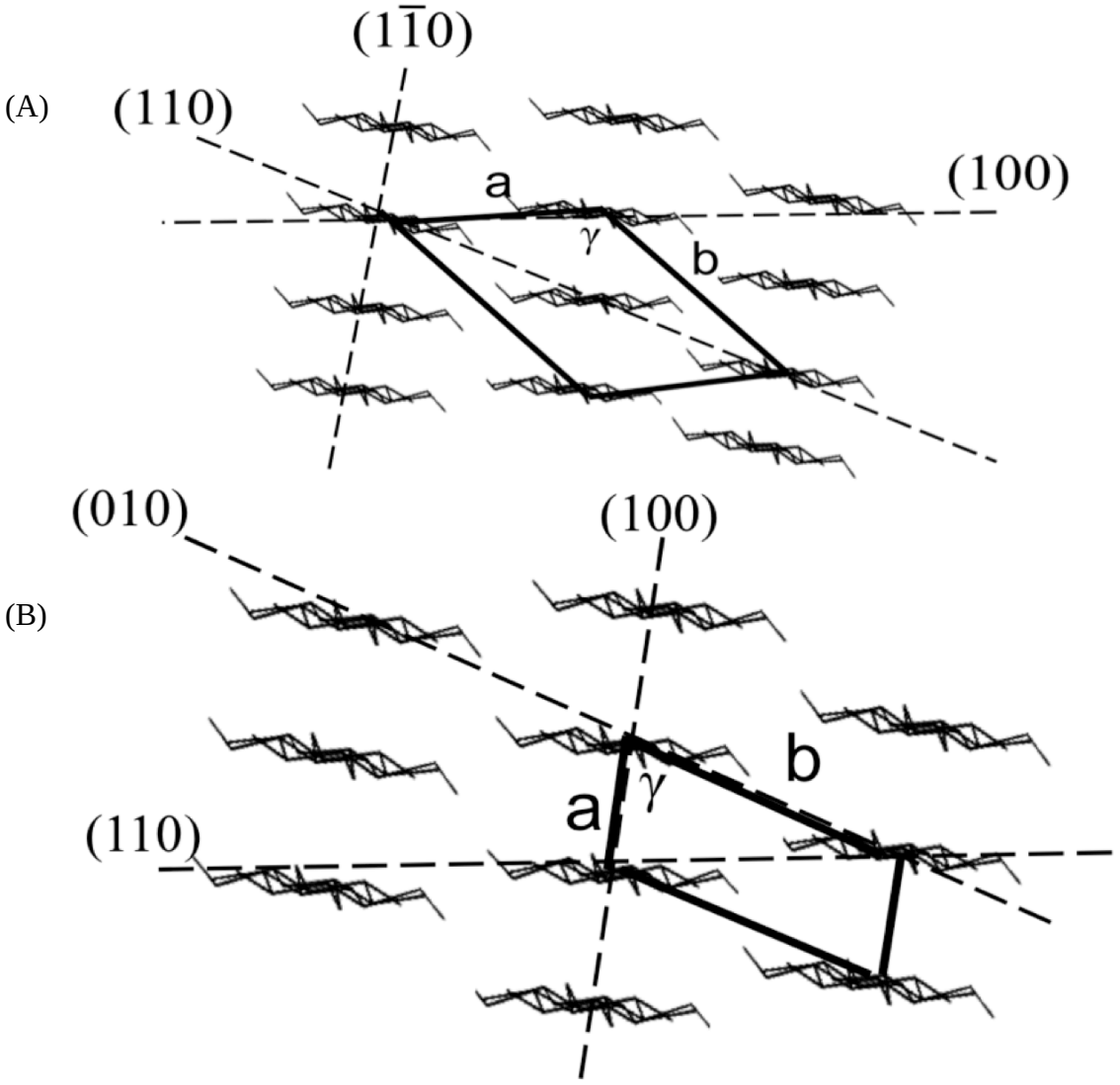

(A) The lattice structure of cellulose II. (B) The lattice structure of cellulose III.

2.4.4 Cellulose IV

Cellulose IV is formed from native cellulose after processing to an intermediate cellulose II or cellulose III structure (52, 56). The unit cell of cellulose IV is tetragonal with the P1 space group (56). There are two polymers per unit cell in cellulose IV with lattice parameters of a = 8.0 Å, b = 8.1 Å and c = 10.4 Å (56). The angles α, β, and γ are equal to 90 ° in a tetragonal structure (47).

2.4.5. Amorphous cellulose

By definition the structure of amorphous cellulose is highly disordered and does not have defined lattice structure (42). Amorphous regions are present in native cellulose between the ordered crystalline domains (2). During extrusion of cellulose polymers from the TC, it is possible for some of polymers to misalign which causes disorder (4, 5). The misalignment yields regions of weakened interactions due to increased distance and non-linear bond angles.

2.5. Hydrogen bonding in cellulose structures

The crystal lattice of cellulose is stabilized, in part, by a complex network of hydrogen bonding (2). The hydrogen bonding network of cellulose forms both inter and intra polymer bonds in each polymorph (38, 40). These bonds have a range of ≈2.6 – 3.1 Å and generally form near linear angles (57). For this bond length and angle, the bond energy, given in units of enthalpy is ≈5 kcal/mol (58, 59). When there are as many as three hydrogen bonds per glucose unit, the theoretical energy is approximately ≈15 kcal/mol. This energy is near the energy of the covalent β-1,4 linkages which has been reported as ≈23 – 30 kcal/mol (60, 61). Since the energy holding each monomer in the

lattice is near, although still less than, that of the backbone β-1,4 linkage there is not a distinguishable melting and decomposition temperature (7).

The three primary hydrogen bonds in native cellulose are the interpolymer: O6H – O3, and intrapolymer: O3H – O5 and O2H – O6 (Figure 2.7A) (2, 40, 62). Interpolymer bonding maintains sheets of cellulose, while intrapolymer bonding reinforces the stiffness of each cellulose polymer (2). Intersheet hydrogen bonding occurs only rarely in native cellulose due to the high ordering of in plane hydroxymethyl groups (*tg* conformation) (63).

In cellulose II the most frequent hydrogen bonding occurs between intrapolymer: O3H – O6 and O3H – O5 and interpolymer O6H – O2 (Figure 2.7B) (29, 57). Polarized FTIR spectroscopy indicates there are 11 possible bonds that can form in cellulose II (57). The less frequently occurring hydrogen bonds have bond distances of ≈3.0 Å which yields weak bonds with energy on the order of ≈2 – 4 kcal/mol (58).

Figure 2.7 – The hydrogen bonds in native cellulose and cellulose II

(A)

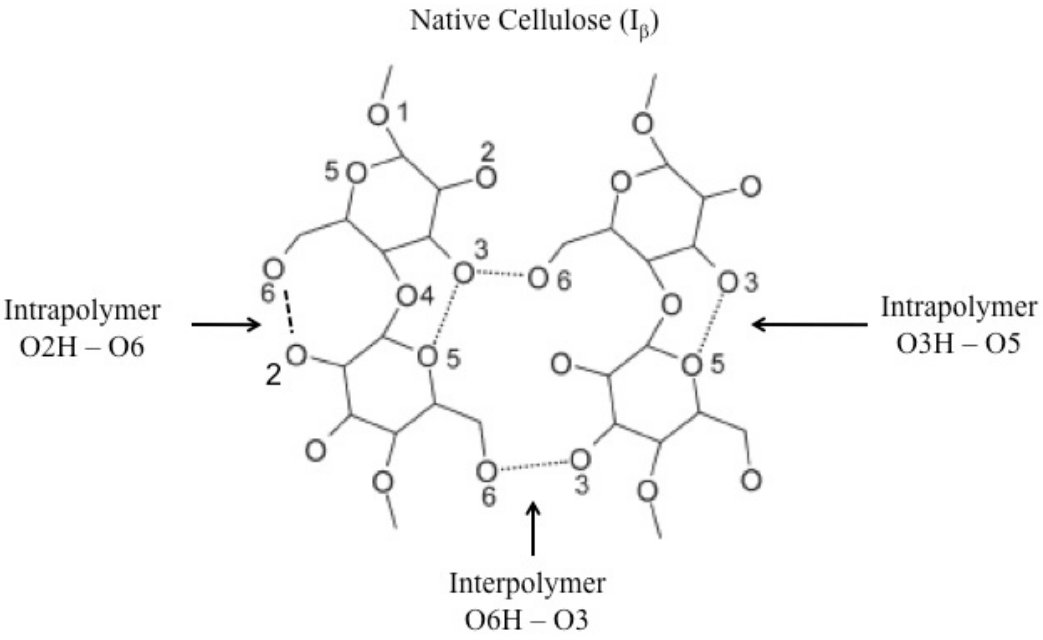

(B)

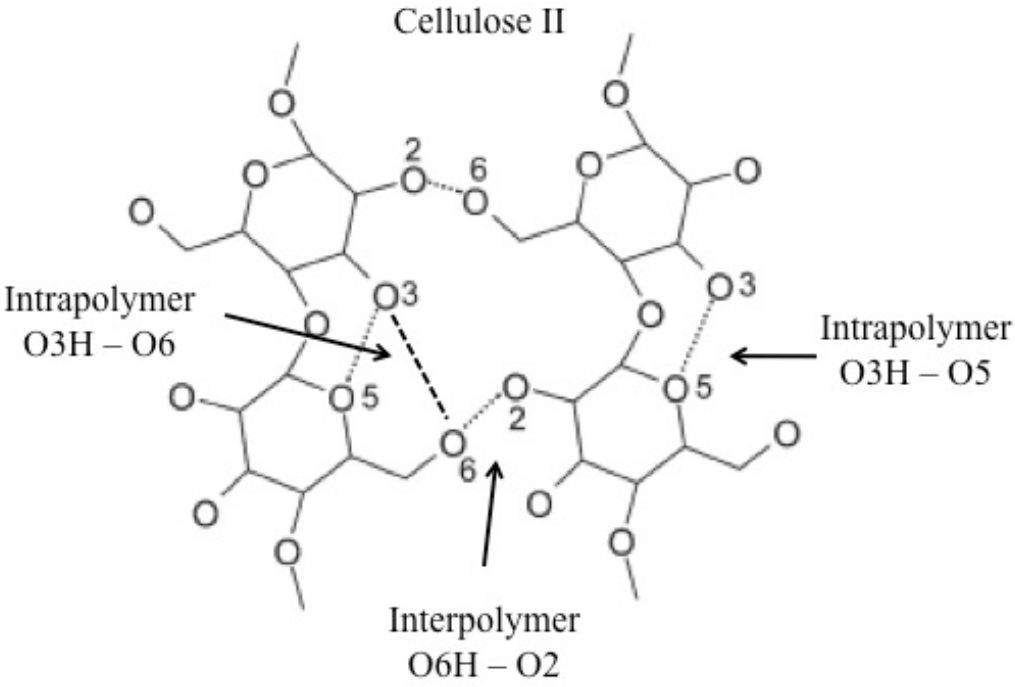

(A) The most common hydrogen bonding network is native cellulose (I_β). (B) The most common hydrogen bonding network in cellulose II. Reproduced with permission (43).

2.6. Enzymatic degradation of cellulose structures

Degrading cellulose structures to release glucose is necessary to produce the precursors for biofuels production (1). One of the most promising means for releasing glucose from cellulose is by using enzymes to degrade the cellulose structure (1, 2). In the enzymatic degradation process, enzymes called cellulases catalyze the conversion of polymeric glucose (cellulose) to glucose (2). The enzymatic degradation of crystalline cellulose is a rate limiting step in the conversion of cellulose to glucose sugar (2). Cellulase accessibility to its substrate and the network of intermolecular interactions in the cellulose structure limits degradability (22, 23, 64).

A retaining mechanism is commonly used by cellulases such as *Thricoderma Reesei* Cel7A (One of the most common commercially available cellulases) and is likely used by the *Saccharophagus degradans* cellulolytic family to degrade cellulose (37, 65, 66). The first step is cleavage of the β-1,4 linkage (65, 66). This is accomplished by a carboxyl group in the catalytic cleft of the enzyme which acts as an acid catalyst by protonating the oxygen of the β-1,4 linkage (65, 67). A second carboxylic group in the catalytic cleft of the enzyme acts as a nucleophile to form a covalent enzyme/cellulose intermediate (60, 65). The glucose molecule is released when water is deprotonated by the carboxyl group which protonated the β-1,4 linkage (60). The conformation of the hydroxyl group at the C1 anomeric carbon is retained (same as before degradation) (65).

This retaining mechanism is used by two classes of enzymes to degrade the crystalline structure of cellulose (60). The crystalline structure limits access to cellulases called endoglucanases, so they act primarily on amorphous regions of the cellulose nanostructure (Figure 2.7) (68, 69). The other class of cellulase is called the

cellobiohydrolase, which requires a specific end of the polymer, such as one of the ends created by the activity of an endoglucanase, to begin degradation (Figure 2.8) (68, 69). These cellobiohydrolases then degrade unidirectionally from that end (70). This means only one enzyme can act on an available end of a cellulose polymer and this 1:1 enzyme-substrate correspondence increases the amount of enzyme needed to process the material (2). The primary difference between the two enzymes is that cellobiohydrolases generally perform multiple processive rounds of cleavage before dissociation from the substrate (70, 71).

Since each cellobiohydrolase requires a specific end, either reducing or non-reducing, only the glucose units at the end of each cellulose microfibril are accessible for degradation (70). The binding energy of each glucose unit varies depending on its position within the microfibril (2, 72). For example the combined intersheet and interpolymer interaction energies for the middle polymers is reported from simulations as ≈-9.84 kcal/mol, whereas the total binding energy of the three polymers on the (100) surface is ≈-8.14 kcal/mol (72). The difference in energy binding on the (100) surface suggests only 3 glucose units at the end of the cellulose microfibril are available to begin digestion. A cellulose microfibril with 36 polymers each having a degree of polymerization of 200 has 7,200 glucose units, but only 3 that are easily accessible. The most accessible are the glucose units on the surfaces with only 3 cellulose polymers each. This means only 0.04 % of the glucose units are accessible which shows how the interactions of the cellulose structure limits degradation. In order to overcome this low accessibility high enzyme loadings are required which are expensive (2, 73).

Figure 2.8 – The conventional cellobiohydrolase/endoglucanase mechanism for enzymatic degradation of cellulose

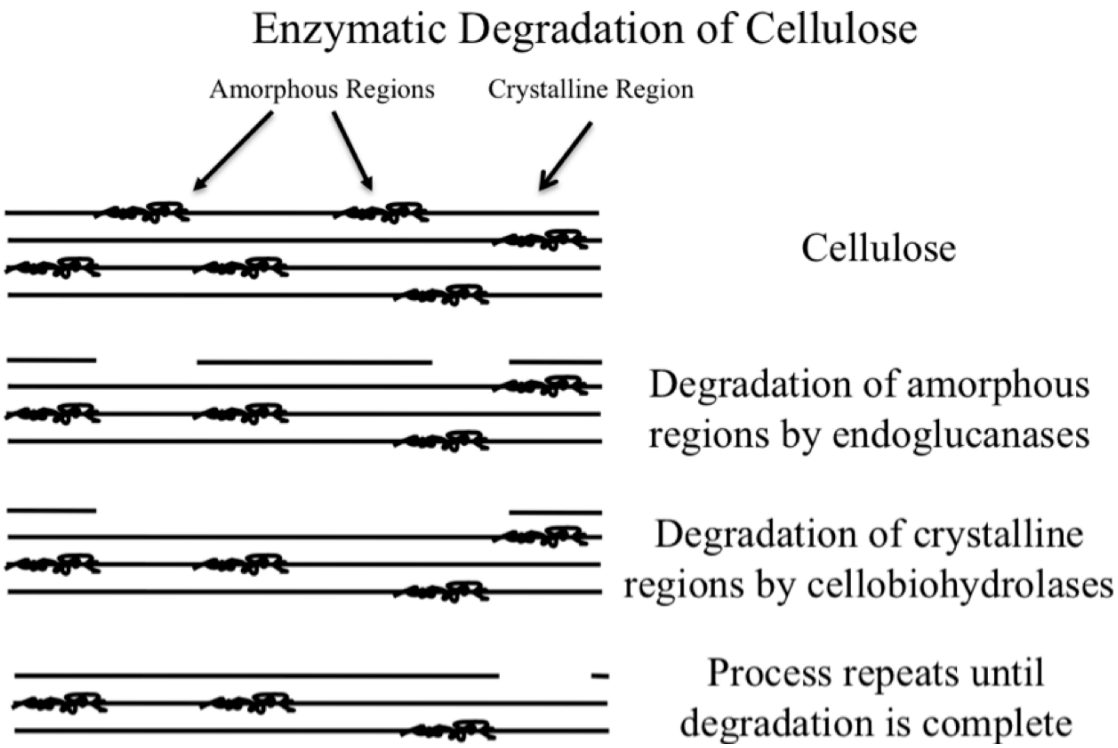

2.7. The conversion of native cellulose to other cellulose polymorphs

2.7.1. The conversion of native cellulose to cellulose II

The transformation of native cellulose to cellulose II can occur via two pathways: alkali swelling, known as the Mercer process, or through acid regeneration (Figure 2.9) (48, 74). In the Mercer process, strong base (x > 20 % by mass NaOH or $Ca(OH)_2$) is added to an aqueous suspension of cellulose (48, 75). The hydroxyl ion penetrates the interstitial space, which causes the polymers to shift to anti-parallel through the process of interdigitation (29, 48). This expands the lattice structure through electrostatic repulsion (29, 48, 75). After a period of 24 hours the cellulose is washed with water to remove the hydroxyl ions and cations (11, 75). Since cellulose II has a lower energy than native cellulose, the transition is irreversible (52). Dissolution of the cellulose polymers does not occur in the Mercer process, which is the notable difference from acid regeneration.

Acid regeneration mixes cellulose with an acid (typically H_2SO_4 or H_3PO_4), which solvates crystalline cellulose, while generally leaving the backbone β-1,4 linkage intact (74, 76). The increase in protonation competes with the hydrogen bonding network of cellulose, while the anion penetrates the lattice structure similar to the Mercer process (17). The anion (e.g. $H_2PO_4^-$) is required to provide the electronegative driving force to break the hydrogen bonding network (17). Upon the addition of a wash liquid (typically water) the polymers precipitate to form cellulose II with amorphous regions (17). **The term "disrupted cellulose" is used in this dissertation to describe cellulose nanostructures with disorder similar to amorphous cellulose with regions of cellulose II.**

Figure 2.9 – The conversion process from native cellulose to each cellulose polymorph

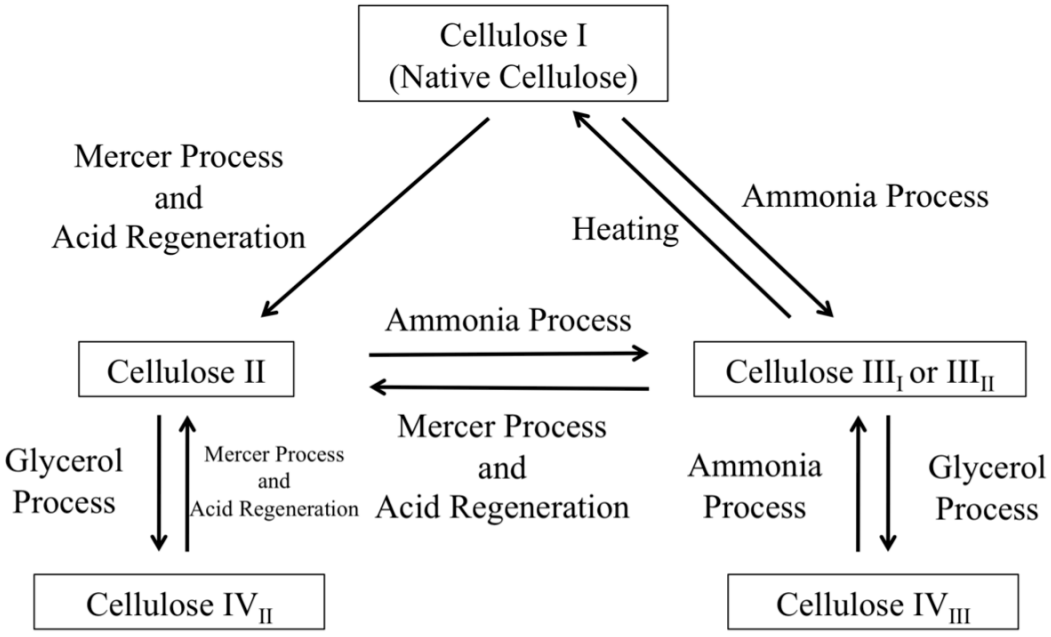

2.7.2 The conversion of native cellulose and cellulose II to cellulose III

Ammonia processing is used to convert raw biomass and cellulose II to cellulose III (53, 77). Cellulose III processed from native cellulose is called cellulose III_I and cellulose III_{II} when processed from cellulose II (53, 78). However, the structure has been determined to be almost identical for cellulose III_I and cellulose III_{II} (53). In ammonia processing 1-2 g of ammonia per gram of biomass is heated to 110 – 130 °C and pressurized to approximately 4.5 MPa (53, 79). The ammonia ion disrupts electrostatic interactions similar to that of the Mercer process, but causes cellulose polymers to be parallel in the structure (54, 55). The transformation of cellulose I to cellulose III is reversible upon heating above 200 °C (55). Cellulose III can also be transformed to cellulose II by Mercerization or acid regeneration (52).

2.7.3. The conversion of cellulose II and III to cellulose IV

Cellulose I is transformed to cellulose IV, via a cellulose II or III intermediate (56, 80). Cellulose II or III is transformed to cellulose IV by heating at 260 °C in glycerol (56, 80). There is debate as to how cellulose II and III are transformed to cellulose IV and how the structure differs from the other polymorphs (80).

2.8. Insolubility of cellulose in water and most solvents

Solvation of a structure occurs when the free energy of mixing is negative based on entropic and enthalpic contributions (20, 21). The entropy of a high molecular weight polymer such as cellulose decreases as molecular weight increases which increases the free energy (20, 21). The increase in free energy causes cellulose polymers with seven or more glucose units to be insoluble in water (16, 81). Cellulose is also insoluble in several common organic solvents such as ethanol and acetone even though they have a tendency

to form hydrogen bonding and polar interactions (16, 82, 83). Cellulose is amphiphilic which means it has polar and non-polar regions that contribute to the enthalpic interactions (82). The polar hydroxyl groups contribute to hydrogen bonding while the non-polar faces of each glucopyranose ring contribute to hydrophobic and van der Waals interactions (82). In general an amphiphilic polymer is best solvated by an amphiphilic solvent which also has both polar and non-polar functional groups (82).

2.9. Intermolecular interactions between cellulose and solvents

The term "solvents" in this dissertation is used to describe chemicals that dissolve cellulose. The term "wash liquids" refers to chemicals that interact with cellulose during washing of the cellulose solvent.

2.9.1. Mineral acids

Mineral acids are routinely used to fractionate cellulose and even hydrolyze cellulose to glucose (11, 76, 84). Sulfuric acid has been used extensively due to low cost and high strength (pK_a = -3.0) (14, 41). Phosphoric acid is a relatively weaker acid (pK_a values: $H_2PO_4^{1-}$ = 2.15, HPO_4^{2-} = 7.20, PO_4^{3-} = 12.37) (41), which is used to prevent hydrolysis of the β-1,4 linkage (17). The phosphate ion forms cellulose esters through electrostatic interactions at the hydroxymethyl group which disrupts interpolymer hydrogen bonding and causes the cellulose polymers to dissociate (17). This disruption is caused by the electronegativity of the phosphate ion, and not simply the pH of the mixture (17, 76). An increase in protonation affects the properties of the phosphate ion, but does not disrupt cellulose by itself due to the lack of an electronegative driving force. The formation of cellulose esters is reversible upon addition of a wash liquid that is used to precipitate cellulose which yields disrupted cellulose (17, 48).

Sulfuric acid is used extensively to break down corn stalks to glucose (14, 85). Mixing sulfuric acid with biomass at temperatures exceeding 200 °C causes the β-1,4 linkages to degrade (76). High temperature acid pretreatment yields toxic cellulose derivatives, such as furfuryls, which inhibits downstream processing (86). The process of degrading biomass directly to glucose is energy intensive and thus expensive, which are reasons why alternatives are currently being sought (87).

2.9.2 Alkali

Strong bases such as sodium hydroxide have been used extensively in textile production to swell cellulose fabrics to increase dyeability (88). The hydroxyl ion of the strong base penetrates the interstitial space of cellulose (75). The electrostatic interactions cause repulsion between the hydroxyl ion and the hydroxyl groups of cellulose, which causes the polymers to shift to an anti-parallel conformation (29, 48, 75). The anti-parallel conformation is formed through interdigitation, in which opposite polar forces cause microfibrils to become intertwined (51). Several alkali species including calcium, potassium, and ammonium hydroxide have been incorporated into pretreatments (11). Sodium hydroxide is advantageous since it disrupts cellulose at low temperatures and low cost (11, 48). However, the process is slow, often taking hours or days and is corrosive (11).

2.9.3. Ammonia

Ammonia processing transforms native cellulose to a structure (cellulose III) that is more degradable by enzymes (79, 89). Under high temperatures and pressures, ammonia penetrates the lattice of cellulose causing electrostatic interactions similar to those caused by sodium hydroxide (53). Although pretreating cellulose with ammonia

produces cellulose that is significantly more degradable by enzymes, the high temperature and pressure increases cost (79).

2.9.4. Ionic liquids

Ionic liquids have been developed to optimize cellulose dissolution and are defined as liquid salts at temperatures under 100 °C (90, 91). Synthetic ionic liquids form a complex with cellulose through electrostatic interaction with the hydroxymethyl group, while also having hydrophobic groups to interact with the glucose ring structure (90, 91). Ionic liquids, such as 1-ethyl methylimidazolium chloride, are made through synthetic processes which can be used to tailor the groups participating in hydrogen bonding and hydrophobic interactions (90). Ionic liquids are advantageous due to their chemical stability, low vapor pressure, and reusability, but often cost 10 times greater than organic solvents (90, 92). Ionic liquids have a high charge distribution, which causes them to also denature cellulase enzymes (92, 93). This means the ionic liquid has to be washed from the material similar to the process for mineral acids. Due to cost and incompatibility with enzymes, ionic liquids are prohibitively expensive for use on the large scale.

2.10. Fractionation of cell wall components

While cellulose is a huge reservoir of sugars, their release by enzymes is impeded, in-part, by the complex structure of biomass that has evolved to be highly resistant to degradation (2, 23). In order to make cellulose more degradable by enzymes, pretreatments are required to fractionate cellulose, hemicellulose/pectin and lignin into separate streams (10, 11, 94). Fractionation significantly improves the degradability of the complex polysaccharides in biomass, in part, by increasing enzyme accessibility (23).

Pretreatments can employ a variety of processing conditions including dilute acid to solubilize the components of biomass or caustic conditions such as in ammonia fiber explosion (AFEX) (11). Pretreatment of corn stover using AFEX increased the production of sugars and the ethanol yield, but it was only 60 % of the maximum theoretical yield (79). Other pretreatments for corn stover have been reported to yield 96 % glucan degradability when high enzyme loadings are employed (15 FPU/gram glucan in the substrate) (12, 14). Cellulose structure hinders enzymatic degradation, which was evident in the degradation of Avicel using *T. reesei* Cel7A (37). The degradability of Avicel (≈70 % crystalline) using *T. reesei* enzyme was ≈10 % compared to ≈80 % degradability on acid pretreated Avicel (> 10 % crystalline) (23).

Cellulases, in general, act on individual polymers of cellulose (2). The ordering of cellulose microfibrils and bundles at the nano scale, in turn, effects enzyme accessibility to cellulose polymers (95). Solvents such as acetone and ethanol can be incorporated into pretreatment processes to disrupt cellulose structure and to improve cellulose degradability (10, 12, 14). In the pretreatment of corn stover, for example, AFEX reduces the degree of cellulose crystallinity by 14 %, as measured by x-ray diffraction, but the use of dilute acids increases the degree of cellulose crystallinity by 2 % (85, 96). The degree of crystallinity does not yield information on cellulose nanostructure or its hydrogen bonding network (18, 96, 97).

2.11. Influence of cellulose solvent on pretreated material

Cellulose solvents yield conditions that are not suitable for enzymatic degradation due to high polarity and strong electrostatic interactions (92, 93). To yield conditions suitable for enzymatic degradation the cellulose solvent is separated from the material by

washing with a liquid (17). As the cellulose solvent is diluted a precipitation process occurs in which the solubilized cellulose reforms a structure (17). The wash liquid is most commonly water, but can include a variety of organic solvents (15, 17). The properties of the wash liquid affect the precipitation of cellulose yielding polymers with unique morphologies (19, 98).

Water is the most common liquid used to wash cellulose due to low cost and the necessity for a near neutral pH environment for enzymatic degradation (11). Water has a strong tendency to form hydrogen bonds with cellulose which contributes to the formation of ordered cellulose nanostructures (82). The high level of ordering restores significant crystallinity in the form of cellulose II, and thus limits enzymatic degradation (23). Due to these drawbacks, non-aqueous liquids are used in cellulose processing (10).

Organosolvent pretreatment uses acid or ionic liquid to solubilize cellulose followed by washing with a non-aqueous liquid (15, 94, 99-101). Industrial processes have experimented with a variety of wash liquids including acetone, ethanol, methanol and glycols to empirically determine which wash liquids yield the most degradable cellulose (12, 14, 15). Most work has focused on the liquids that yield the highest recovery of each biomass component, thus yielding maximum enzyme accessibility (12, 14, 15). The solubility of hemicellulose and lignin in different liquids typically governs which solvent is employed in the process and there is no uniform protocol (10). Ethanol organosolvent pretreatment is used most frequently because of increase glucose yields per mass of feedstock relative to other protocols (15, 99). Industrial processes primarily focus on biomass fractionation and have largely ignored understanding the effects to the crystalline structure of cellulose during washing by non-aqueous liquids (15).

3. Processive Endoglucanases mediate the degradation of cellulose by *Saccharophagus degradans*

3.1 Introduction

The microbial degradation of cellulose is of interest due to applications in the sugar-dependent production of alternative biofuels (1). There are well-characterized cellulolytic systems of bacteria and fungi that employ multiple endo-acting glucanases and exo-acting cellobiohydrolases in the degradation of cellulose (2). For example, the noncomplexed cellulase system of the wood soft rot fungus, *Hypocrea jecorina (*anamorph *Trichoderma reesei),* the source for most commercially available cellulase preparations, produces up to eight secreted β-1,4-endoglucanases (Cel5A, Cel5B, Cel7B, Cel12A, Cel45A, Cel61A, Cel61B, Cel61C), two cellobiohydrolases (Cel6A, Cel7A), and several β-glucosidases (e.g., Bgl3A) (102). Cellobiohydrolases are critical to the function of these systems as, for example, Cel7A comprises in excess of 60% of the cellulases secreted by this organism (64).

Another well-characterized noncomplexed cellulase system is found in *Thermobifida fusca*, a filamentous soil bacterium that is a major degrader of organic material found in compost piles (70). This bacterium also secretes several endoglucanases and end-specific cellobiohydrolases to degrade cellulose (70). An alternative mechanism to degrade cellulose is found in microorganisms producing complexed cellulolytic systems, such as those found in cellulolytic clostridia. In these microorganisms, several β-1,4-endoglucanases and cellobiohydrolases assemble on surface-associated scaffoldin polypeptides to form a cellulose-degrading multiprotein complexes known as cellulosomes (69, 103). The unifying theme in either complexed or

noncomplex systems is the importance of cellobiohydrolases in converting cellulose and cellodextrins to soluble cellobiose.

Recently a complete cellulolytic system was reported in the marine bacterium *Saccharophagus degradans* 2-40 (104-106). This bacterium is capable of growth on both crystalline and noncrystalline cellulose as sole carbon sources and produces multiple glucanases that can be detected in zymograms of cell lysates (104). The work of Weiner and Taylor annotated the genome sequence of this bacterium, which predicted the function of the cellulolytic system of this bacterium (104, 105). An annotation is a predicted function of an enzyme based on comparing amino acid sequences with enzymes with known functions as described by Henrissat (28). The annotation done by Weiner and Taylor analyzed the amino acid sequences of each enzyme in the *S. degradans* cellulolytic system which suggested the presence of ten GH5-containing β-1,4-endoglucanases (Cel5A, Cel5B, Cel5C, Cel5D, Cel5E, Cel5F, Cel5G, Cel5H, Cel5I, Cel5J), two GH9 β-1,4-endoglucanases (Cel9A, Cel9B), one cellobiohydrolase (Cel6A), five β-glucosidases (Bgl1A, Bgl1B, Bgl3C, Ced3A, Ced3B) and a cellobiose phosphorylase (Cep94A) (104, 105). The apparent absence of a homolog to a scaffoldin in the genome sequence and to dockerin-like domains in the proposed glucanases suggests this bacterium produces a noncomplexed cellulolytic system. Two unusual features of this cellulolytic system are the large number of GH5 endoglucanases and the presence of only one annotated cellobiohydrolase, Cel6A (104, 105). The apparent deficiency of cellobiohydrolases in this system raised the question as to the mechanism by which this bacterium degrades cellulose.

To understand the mechanism for degradation of cellulose, the biochemical activity for the predicted cellobiohydrolase Cel6A and each of the GH5 glucanases predicted for the *S. degradans* cellulolytic system was evaluated. Cel6A exhibited properties of a classic endoglucanase but three of the originally annotated endoglucanases, Cel5G, Cel5H and Cel5J were shown to be processive, forming cellobiose as the end product. Processive endoglucanases substitute for cellobiohydrolases in this system to play a major role in the degradation of cellulose.

This chapter has been published in part: Watson, B.J. *et al. J. Bacteriol.* **191** 5697-5705 (2009). Reproduced with permission from the American Society of Microbiology.

3.2 Materials and Methods

Bacterial growth media and conditions

Saccharophagus degradans 2-40^T (ATCC 43961) was grown at 30 °C in minimal medium containing (per liter) 2.3 % Instant Ocean (Aquarium Systems, Mentor, Ohio), 0.05 % Yeast Extract, 0.5 % (w/v) ammonium chloride, and 16.7 mM Tris-HCl, pH 8.6 supplemented by 0.2 % carbon source using standard protocols. *Escherichia coli*, DH5α (Invitrogen, Frederick, MD) and Rosetta2™ (DE3) (Novagen, Madison, WI) strains were grown at 37 °C in Luria-Bertani (LB) broth or agar supplemented with the appropriate antibiotics. Antibiotics were added to media at the indicated concentrations (in μg/ml): chloramphenicol, 30; and kanamycin, 50.

Molecular cloning and expression were performed by Dr. Haitao Zhang

Purification of glucanases

20 ml of overnight *E. coli* Rosetta™2 (DE3)(pHZ-Cel) culture were inoculated into 500 ml LB broth and grown at 37 ºC for 2 hours. Expression of cloned genes was induced by

the addition of IPTG to a final concentration of 0.1 mM when the OD600 approached 0.6. The culture was then incubated overnight at 15 ºC with mild shaking. Cells from induced cultures were harvested and resuspended in 50 mM sodium phosphate, 300 mM sodium chloride, 10 mM imidizole, pH 8.0 and 0.5 mM phenyl methyl sulfonyl fluoride. Lysozyme was added to a concentration of 1 mg/ml and the cell suspension incubated on ice for 30 minutes. Lysis of cells was completed using five 30 second cycles in a Bead Beater™ (Biospec Products). The lysate was clarified by centrifugation at 10,000 RPM for 20 minutes. The expressed proteins in cleared lysates were purified using Ni-NTA (Nitriltriacetic acid) chromatography according to the manufacturer's recommendations (Qiagen, 2003). The protein concentration was determined by the Pierce microBCA protein assay reagent kit (23235) using bovine serium albumin (BSA) as the standard.

Enzyme Assays

Most assays were performed at pH 6.5 and 50 °C in a reaction mixture containing 1 % Instant Ocean™, 20 mM PIPES buffer, and 0.01 – 1.0 nmol purified enzyme for soluble substrates and 0.1 – 2.0 nmol purified enzyme for insoluble substrates. For alternative pH conditions, 20 mM MES (2-(*N*-morpholino)ethanesulfonic acid) for pH 3-6, 20 mM PIPES (1,4-Piperazinediethanesulfonic acid) for pH 6-7 or 20 mM Tris (2-Amino-2-(hydroxymethyl)propane-1,3-diol) for pH 7-8.5 were employed. The ionic strength of the reaction mixture was adjusted by the addition of 0-10 % (w/v) Instant Ocean™. All assays were performed in triplicate and reported as the mean with standard deviation.

The carboxymethyl cellulose (CMC) assay was performed with 1 % substrate in a total volume of 0.4 ml for a 15 min reaction time. Phosphoric acid swollen cellulose

(PASC) was prepared as described (17). The PASC (1 mg) assay was performed in a total volume of 0.15 ml for 30 minutes. The DNS (dinitrosalicylic acid) assay was used to detect product formation in these reactions (107). Degradation of Avicel (1 mg) or Whatman #1 filter paper (3 mg) was assayed in a total volume of 0.15 ml for 2 hours. The reaction was stopped by incubation for 3 minutes at 95 °C and the substrate separated by centrifugation at 10,000 rpm. The products of filter paper or Avicel degradations were then digested with 0.45 nanomoles of the β-glucosidase *S. degradans* Bgl1A in a total volume of 0.2 ml at 50 °C for 1 hour. After 1 hour at 50 °C, the β-glucosidase was inactivated by incubation for 3 minutes at 95 °C. Glucose oxidase (Sigma GAGO-20) was added to a volume of 0.6 ml and incubated at 37 °C for 30 minutes. 0.4 ml of 12 N sulfuric acid was added and the glucose concentration was measured at OD540 with a glucose standard curve (108). Release of cellobiose was calculated at 50 % the rate of glucose accumulation.

Assessment of Synergy

Evaluation of synergy was one method used to determine endoglucanase versus cellobiohydrolase activity of *S. degradans* cellulases. Synergy was evaluated using the filter paper assay as described above. *T. fusca* Cel6A (endo), *T. fusca* Cel9B (endo) and *T. fusca* Cel6B (exo, cellobiohydrolase) were used as reference enzymes of known activity (gifts of Professor David Wilson, Cornell University). Each assay utilized 1.0 nmol of *S. degradans* enzyme and 0.1 nmol of the indicated *T. fusca* enzyme. The yield of glucose of each enzyme on filter paper was independently measured as described above. The combined yield of glucose from two enzymes together in the filter paper assay was also measured. The degree of synergy was calculated by dividing the

combined glucose yield by the sum of the glucose yield of each enzyme independently. If the degree of synergy was less than 1 the enzymes were considered anti-synergistic and synergistic if greater than 1.

Viscosity measurements

Viscosity was monitored using a cross-arm viscometer (ASTM D455 and D2170). *T. fusca* Cel6B (0.01 nmol), *S. degradans* Cel5H (0.01 nmol) or *T. fusca* Cel9B (0.001 nmol) was added to 2.0 ml of 1 % CMC solubilized in assay buffer. The viscosity of the reaction mixture was measured periodically between 0.5 – 20 minutes.

Thin Layer Chromatography

One μl samples were spotted onto Fisher (5729-6) silica gel 60 plates and air dried. Chromatograms were developed using nitromethane, 1-propanol, and water (2:5:1.5) (v:v:v) (109). Two ascents of the solvent were used to ensure high resolution. The plate was dipped in 5 % (v/v) sulfuric acid in methanol and heated to 140 ºC for 5 minutes to visualize resolved products.

Processivity

The processivity was evaluated by measuring the ratio of soluble to insoluble reducing sugar released during the filter paper assay as described by Zhang with minor modifications (71). Reducing sugar in the soluble fraction was measured using glucose oxidase method described above and reported in μmols of cellobiose. The insoluble reducing sugar was determined using a modified 2,2'-bicinchoninate (BCA) assay as described by Doner and Irwin (110). At the end of the assay period, the filter paper was washed with 6 M guanidine hydrochloride to remove bound protein. The filter paper disc was then washed 4 times with assay buffer and water (71). The retained insoluble

reducing sugar was measured using the Pierce microBCA reagent kit using glucose standards. The processivity was determined using 0.1 – 1 nmol of the indicated *S. degradans* glucanase and 0.1 nmol of *T. fusca* Cel6A (endo) and *T. fusca* Cel9B (processive endo).

3.3 Results

Cellulose degradation by S. degradans

The genome of *S. degradans* is annotated to produce a multi-component cellulolytic system (104, 105), but the mechanism of cellulose degradation was not clear. To estimate the products formed as a result of the activity of the secreted components of the *S. degradans* cellulolytic system, *S. degradans* was grown on Avicel to induce expression of glucanases. The degradation products released from cellulose by the activity of the secreted glucanases were determined. Irrespective of the cellulosic substrate or reaction time, cellobiose was the primary product released by the glucanase activity of *S. degradans* culture filtrates with a lower amount of cellotriose also observed (Figure 3.1). Larger cellodextrin products were not apparent. This suggests that the cellulolytic system of *S. degradans* has an efficient mechanism to release cellobiose during the degradation of cellulose.

Figure 3.1 – Degradation of cellulose by *S. degradans*

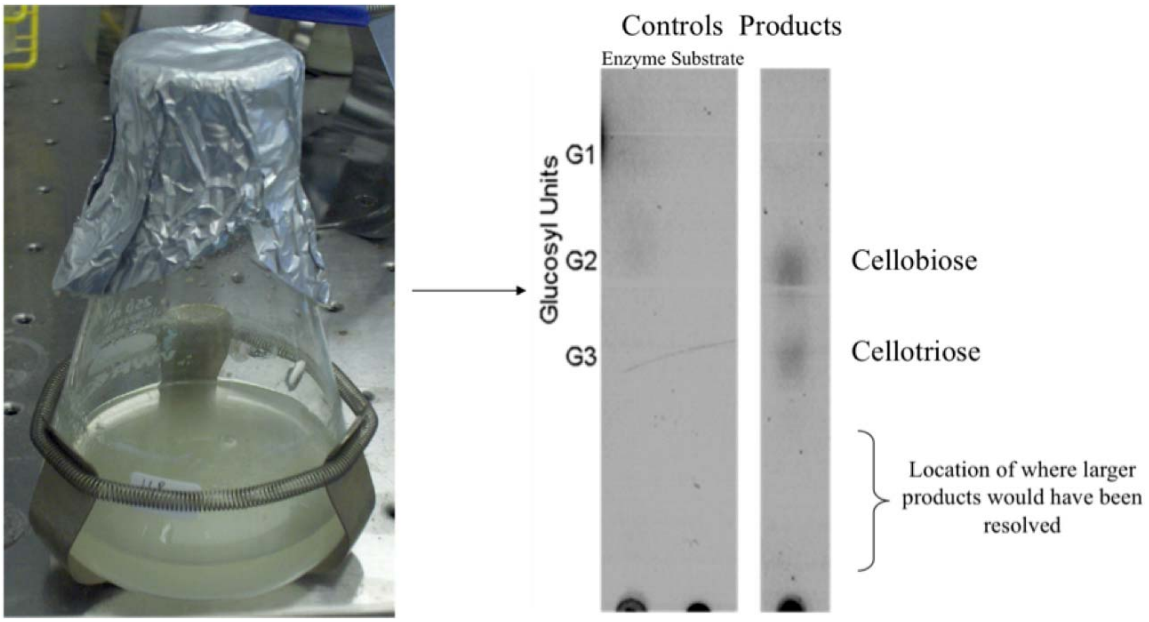

S. degradans was grown on Avicel to induce expression of glucanases (left). After 24 hours 1 µl of the culture media was plated on TLC plates for product analysis. Samples of the enzyme preparation and of the Avicel growth media at time zero were used to control the TLC product analysis, to ensure the sugars observed were the products of *S. degradans* activity.

Activity of Cel6A

Cellobiose can be formed by the processive exoglucanase activity of a cellobiohydrolase. The only annotated cellobiohydrolase in the *S. degradans* genome is Cel6A (104). The *cel6A* gene had been cloned into pET28b in a form that lacked His-tags. Cell lysates containing Cel6A released reducing sugar from CMC consistent with its annotation as a glucanase. The processivity ratio (ratio of soluble to insoluble products) of Cel6A activity and synergisms were values expected for an endoglucanase (Table 3.1). Furthermore, the activity reduced the viscosity of CMC. This activity is typical of a classic endoglucanase, indicating that other enzymes must be contributing to the formation of cellobiose.

Expression of glucanases

Work by Dr. Haitao Zhang indicated that *cel5H* was the highest induced cellulase in the *S. degradans* cellulolytic system and thus likely to be essential for cellulose degradation.

Table 3.1 – Properties of *S. degradans* Cel6A

Degree of Synergy[a]	
S. degradans Cel6A + *T. fusca* Cel6A (Endo)	0.64 (anti-synergistic)
S. degradans Cel6A + *T. fusca* Cel6B (Exo)	1.58 (synergistic)
Impact on Viscosity[b]	-53%
Processivity[c]	1.02 ± 0.11

[a] The degree of synergy: In general, two enzymes with the same type of activity will be anti-synergistic, while two enzymes with different activity with be synergetic. Crude lysate preparations of *S. degradans* Cel6A expressed in *E. coli* Rosetta ™ 2 (DE3) were used. The independent yield of glucose was: *S. degradans* Cel6A: 0.87 ± 0.15 μg, *T. fusca* Cel6A: 7.57 ± 0.44 μg, *T. fusca* Cel6B: 0.34 ± 0.02 μg. The combined yield of glucose for *S. degradans* and *T. fusca* cellulases: *S. degradans* Cel6A + *T. fusca* Cel6A: 5.43 ± 0.27 μg, *S. degradans* Cel6A + *T. fusca* Cel6B: 1.91 ± 0.26 μg. The degree of synergy was calculated by dividing the combined yield by the sum of the independent yield of each cellulase.

[b] The reduction of viscosity of a CMC solution. In parallel experiments, the exoglucanase *T. fusca* Cel6B caused a 30% increase in viscosity, whereas the endoglucanase *T. fusca* Cel9B caused an 84% decrease in viscosity.

[c] The processive ratio is defined as the μmol cellobiose released divided by μmol insoluble sugar (glucose standard) (71).

Activity of Cel5H

For determination of the biochemical activity of Cel5H, the gene had been cloned to create His-tagged derivatives, which enabled purification (Zhang *et al.*). After transformation into *E. coli* Rosetta™2 (DE3), expression was induced by IPTG (Isopropyl β-D-1-thiogalactopyranoside). The expressed Cel5H migrated at the expected mass during SDS-PAGE and hydrolyzed β-glucan and HE (hydroxyethyl) cellulose in zymograms consistent with its annotation. This enzyme appeared to be very active as lystates of *E. coli* Rosetta™2 (DE3) transformants expressing Cel5H had to be diluted to picomolar concentrations before a well-defined zone of activity typical of an individual polypeptide could be resolved. After purification from Rosetta™2 (DE3) transformants to near homogeneity by using nickel-NTA (nitriltriacetic acid) affinity chromatography, the glucanase activity of the purified Cel5H exhibited a pH optimum of 6.5 and retained greater than 84 % of its activity in the range between pH 6.0 – 7.0. Activity increased linearly up to 50 °C but lost activity at higher temperatures. Addition of 1 % Instant Ocean™ enhanced the activity of the enzyme 2.5 fold. The specific activity of purified Cel5H was highest on swollen cellulose and CMC but activity was retained on filter paper and Avicel relative to controls (Table 3.2).

To evaluate whether Cel5H is an endoglucanase like other GH5 enzymes (111), its effect on the viscosity of CMC solutions was monitored. *S. degradans* Cel5H rapidly decreased the viscosity of CMC similar to the endoglucanase *T. fusca* Cel9B (a gift of D. Wilson). In contrast, the exo-acting *T. fusca* Cel6B (a gift of D. Wilson) increased the viscosity of CMC as expected (Figure 3.2).

Table 3.2 – Specific activity of *S. degradans* Cel5H on cellulosic substrates

Enzyme	Specific activity on the indicated substrate (μmol reducing sugar / minute / μmol enzyme [a,b])			
	CMC[d]	Swollen Cellulose[c]	Filter Paper[c]	Avicel[c]
Cel5H	643 ± 148	792 ± 119	2.21 ± 0.1	1.45 ± 0.1

[a] Reducing sugar released from CMC and swollen cellulose was measured using a DNS assay relative to a cellobiose standard curve whereas cellobiose released from filter paper and avicel was measured using the glucose oxidase method after treatment with an excess of β-glucosidase. Mean of triplicate trials and one standard deviation are reported.

[b] μmol protein measured using BSA as the reference

[c] The approximate degree of crystallinity for each substrate (% crystallinity) (35): carboxymethyl cellulose CMC (0%), PASC (<10 %), filter paper (50%), and Avicel (70%)

Figure 3.2 – Effect of endo- and exo-glucanases on CMC viscosity

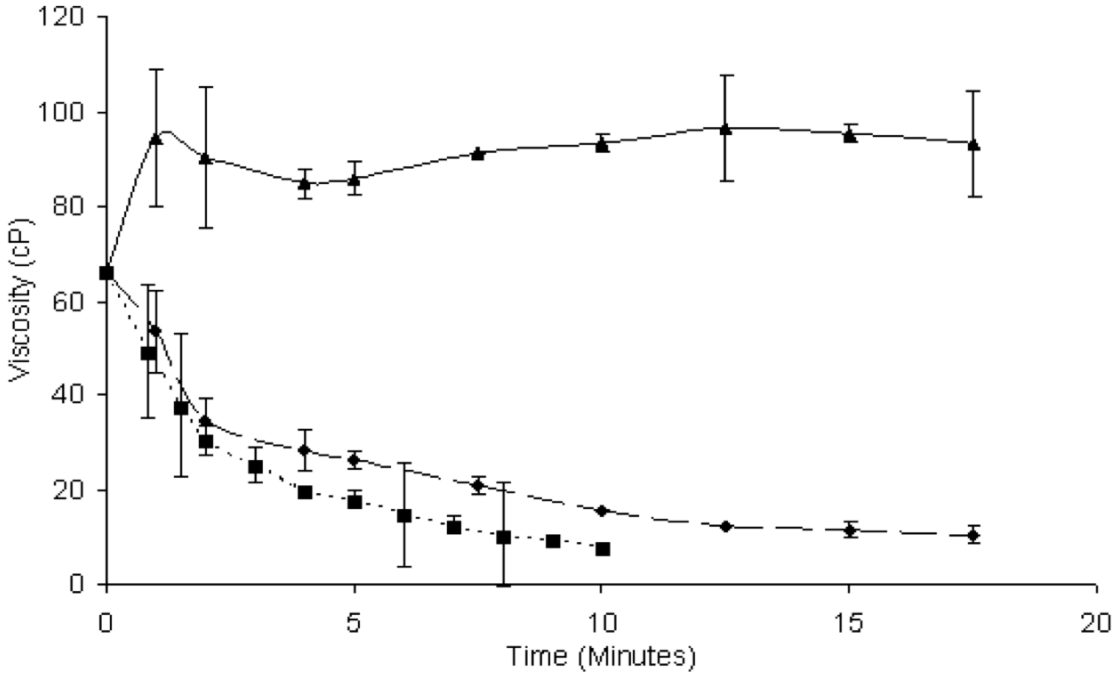

S. degradans Cel5H (-♦-), *T. fusca* Cel9B (Endo) (-■-) and *T. fusca* Cel6B (Exo) (-▲-) were added to a 1 % CMC solution. The error bars represent one standard deviation from triplicate trials.

Synergistic interactions between glucanases also provide an indication of the activity of the enzymes. *S. degradans* Cel5H acted synergistically with the exoglucanase *T. fusca* Cel6B, producing at least 30 % more product when acting together than each individually (Table 3.3). In contrast, anti-synergism was observed with the endoglucanase *T. fusca* Cel9B with combined activities 15-25 % lower than theoretical as seen previously in the interaction of classical endoglucanases (112).

Table 3.3 – Synergy of *S. degradans* and *T. fusca* glucanases

			Yield of Glucose (μg)			
Enzyme	Activity	nmol	Independent Yield[a]	Theoretical Yield[b]	Observed Yield	DoS[d]
S. degradans Cel5H		1	12.6 ± 0.9			
T. fusca Cel9B	endo	0.1	5.9 ± 0.5	18.5	14.3 ± 0.4	0.77
T. fusca Cel6B	exo	0.1	2.7 ± 0.0	15.3	20.1 ± 0.9	**1.31**
S. degradans Cel5G		1	10.5 ± 1.3			
T. fusca Cel9B	endo	0.1	5.9 ± 0.5	16.4	14.1[e]	0.86
T. fusca Cel6B	exo	0.1	2.6 ± 0.0	13.2	20.4 ± 0.9	**1.55**

[a] The yields were measured after two hours as described for the filter paper assay. Mean of three trials and the standard deviation reported are rounded to tenths

[b] The sum of the μg glucose produced by the indicated *S. degradans* and the *T. fusca* glucanases during independent degradations.

[c] The yield obtained under the same conditions as the independent reactions in a degradation containing Cel5H or Cel5G together with *T. fusca* Cel9B or Cel6B

[d] DoS: The degree of synergy: product formed when both enzymes are present in the reaction mixture divided by the sum of the yields from equivalent amounts of the same enzymes under identical conditions.

[e] Representative of single trial due to lack of *T. fusca* endoglucanase

Cel5H is processive

Cellobiose was the primary product released from swollen cellulose, filter paper, and Avicel by the activity of purified Cel5H in heat stopped reactions, irrespective of the time of degradation (Figure 3.3). Products larger than cellotriose were not apparent during 45 second degradations or thereafter. The amount of Cel5H used did not affect the product distribution.

The production of cellobiose by Cel5H activity could be an indication of processivity. To evaluate the processivity of Cel5H, the ratio of soluble and insoluble products was measured and compared to that of *T. fusca* Cel9A (processive endoglucanase; a gift of D. Wilson) and *T. fusca* Cel6A (classical endoglucanase) (70). Like the processive *T. fusca* Cel9A and in contrast to the classical endoglucanase *T. fusca* Cel6A (113), 82 % of the products formed by the activity of the *S. degradans* Cel5H were soluble (Table 3.4). For both *T. fusca* Cel9A and *S. degradans* Cel5H the rates of soluble product formation exceeded that of insoluble products throughout a 2-hour time course (Figure 3.4).

Figure 3.3 – Products formed by *S. degradans* Cel5H activity

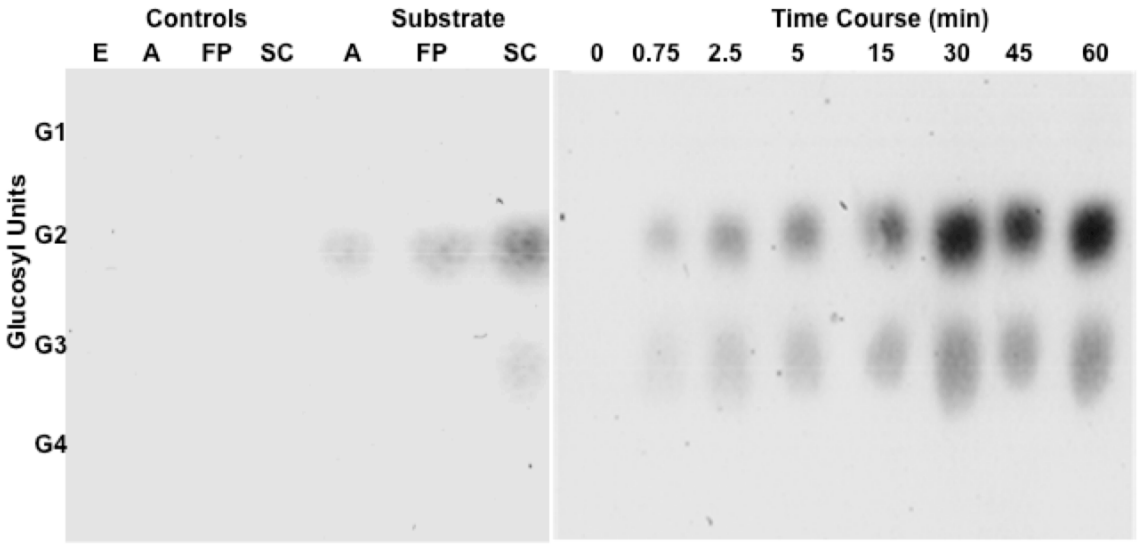

Controls: E, Enzyme alone; A, Avicel alone; FP, Filter paper alone; SC, phosphoric acid swollen cellulose alone. Substrate: Products formed by the activity of purified Cel5H on the indicated substrate**:** A, Avicel; FP, filter paper; and SC, phosphoric acid swollen cellulose. The markers, G1-G4, represent the migration of glucose, cellobiose, cellotriose and cellotetraose. Time course: Time course of products (min) released by the activity of *S. degradans* Cel5H on swollen cellulose.

Table 3.4 – Processivity of *S. degradans* Cel5H

Enzyme[a]	Specific Activity[b]	Processive Ratio[c]	Soluble Reducing Sugar[d]	Insoluble Reducing Sugar[d]
T. fusca Cel9A (Proc. Endo)	0.70 ± 0.01	4.72 ± 0.43	82.5 %	17.5 %
T. fusca Cel6A (Endo)	1.33 ± 0.14	2.55 ± 0.28	71.9 %	28.1 %
S. degradans Cel5H	1.66 ± 0.07	4.26 ± 0.71	81.4 %	18.6 %

[a] 0.1 nmol of each endoglucanase was used in each 2 h degradation of filter paper.

[b] The specific activity is reported as μmol reducing sugar / minute / μmol enzyme.

[c] The processive ratio is defined as the μmol soluble reducing sugar (cellobiose standard) divided by μmol insoluble sugar (glucose standard) as described in the Materials and Methods.

[d] The mass fractions of soluble and insoluble products given as percentages.

Figure 3.4 – Processivity of Cel5H activity

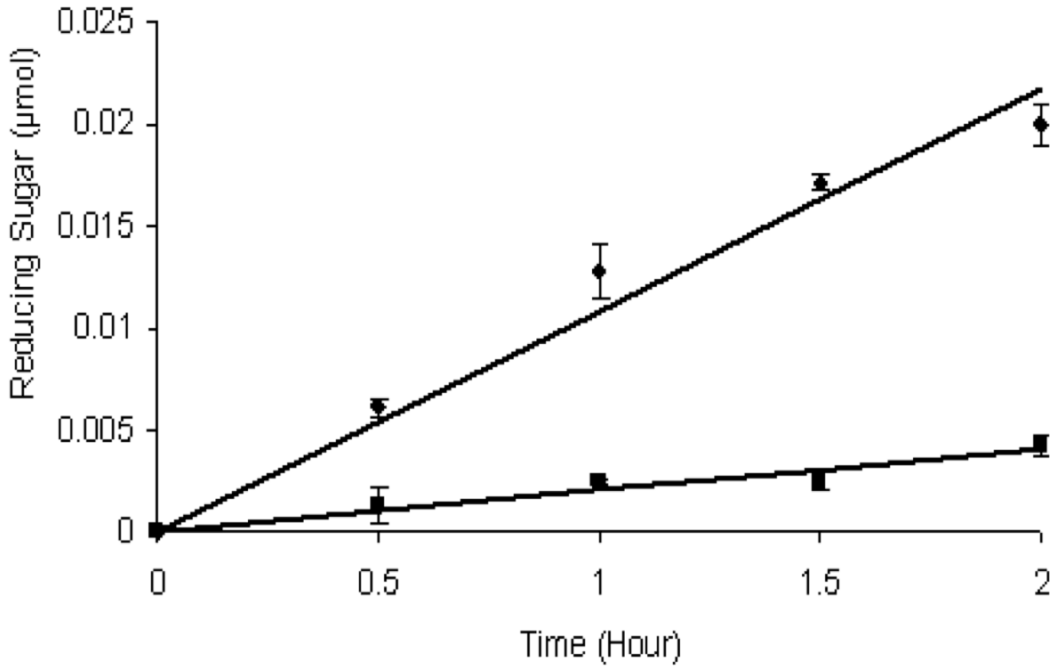

Diamonds (top line, ◆) indicate soluble reducing sugar detected (µmol cellobiose). Squares (bottom line, ■) indicate insoluble reducing sugar (µmol glucose). Linear trend lines were fitted using $y = mx$. For release of soluble reducing sugar, $m = 0.0108$, $R^2 = 0.97$. For formation of insoluble reducing sugar, $m = 0.0020$, $R^2 = 0.94$.

The contribution of the resident CBM6 of Cel5H to its activity and processivity was evaluated by comparing the activity of the full-length polypeptide to that of a truncated derivative consisting of the GH5 catalytic domain constructed by specific amplification (Cel5H'). For these experiments, the GH5 domain of Cel5H was amplified by PCR and ligated into pET28b as before (H. Zhang). Cel5H' was purified from Rossetta2™ (DE3) transformants. The specific activity of Cel5H' was 69 % that of Cel5H on near amorphous PASC and 78 % on soluble CMC. The ratio of soluble to insoluble products, however, remained indistinguishable from that of Cel5H (Table 3.5). Thus, the data suggests that processivity of the enzyme resides with the catalytic domain.

Table 3.5 – Properties of *S. degradans* Cel5H′

(A) Specific activity of *S. degradans* Cel5H′ on cellulosic substrates

Enzyme	Specific activity on the indicated substrate (μmol reducing sugar / minute / μmol enzyme [a,b])			
	CMC	Swollen Cellulose	Filter Paper	Avicel
Cel5H'	500 ± 10	545 ± 82	0.92 ± 0.1	0.66 ± 0.1

[a] Reducing sugar released from CMC and swollen cellulose was measured using a DNS assay relative to a cellobiose standard curve whereas cellobiose released from filter paper and avicel was measured using the glucose oxidase method after treatment with an excess of β-glucosidase. Mean and standard deviation are reported.

[b] μmol protein measured using BSA as the reference

(B) Processivity of *S. degradans* Cel5H′

Enzyme[a]	Specific Activity[b]	Processive Ratio[c]	Soluble Reducing Sugar[d]	Insoluble Reducing Sugar[d]
S. degradans Cel5H'	0.92 ± 0.01	4.42 ± 1.07	81.1%	18.9%

[a] 0.1 nmol of each endoglucanase was used in each 2 h degradation of filter paper.

[b] The specific activity is reported as μmol reducing sugar / minute / μmol enzyme.

[c] The processive ratio is defined as the μmol soluble reducing sugar (cellobiose standard) divided by μmol insoluble sugar (glucose standard)

Purification and properties of other GH5 endoglucanases

As before, each gene for the other GH5 glucanases of *S. degradans* was amplified by PCR and ligated into pET28 for expression in *E. coli* Rosetta™2 (DE3) (H. Zhang). Most of the expressed GH5 enzymes exhibited endoglucanase activity in β-glucan and HE cellulose zymograms consistent with their annotation as glucanases. Cel5B, Cel5D, Cel5F, and Cel5H were comparatively stable with a single full-length polypeptide of the expected size having glucanase activity. In contrast, Cel5E, Cel5G, and Cel5J were unstable, either producing multiple degradation products with activity or the active fragment migrated at a mass lower than expected. Full-length polypeptides as well as the fragments of Cel5D, Cel5G and Cel5J sufficient to carry the catalytic domain retained glucanase activity. None of the fragments derived from Cel5C or Cel5I exhibited evidence of glucanase activity on any substrate. Cel5A was not investigated due to the diversity of its multi-domain architecture.

Each polypeptide was purified to near homogeneity from Rosetta™2 (DE3) transformants as previously either as the full length polypeptide (Cel5B, Cel5E, Cel5F) or as an apparent catalytic domain (Cel5D, Cel5G, Cel5J) based upon the retention of activity and size correspondence with the structural predictions of each polypeptide (104, 105). The glucanase activity of the expressed enzymes had pH optima near 6.5, did not require salts and functioned up to 50 °C. In contrast to fungal endoglucanases (114), Cel5B, Cel5D, Cel5E, Cel5F, and Cel5G retained at least 60 % of the optimal activity at pH 8.0. The glucanase activity was inversely proportional to the crystallinity of the cellulose substrate with the highest activity observed on CMC (Table 3.6).

Table 3.6 – Specific activities of the *S. degradans* GH5 endoglucanases

Enzyme	Specific activity on the indicated substrate [a,b] (μmol reducing sugar / minute / mg protein)			
	CMC [c]	Swollen Cellulose [c]	Filter Paper [c]	Avicel [c]
Cel5B	2.23 ± 0.36	0.07 ± 0.02	(1.84 ± 0.01) x 10^{-3}	(1.44 ± 0.1) x 10^{-3}
Cel5D	(8.59 ± 2.23) x 10^{-4}	(1.13 ± 0.06) x 10^{-4}	(2.68 ± 0.75) x 10^{-5}	N/D[d]
Cel5E	0.05 ± 0.02	(5.96 ± 0.48) x 10^{-3}	(4.01 ± 0.76) x 10^{-6}	N/D[d]
Cel5F	0.37 ± 0.08	0.18 ± 0.04	(6.60 ± 0.46) x 10^{-4}	(6.26 ± 0.75) x 10^{-4}
Cel5G	4.62 ± 0.60	11.70 ± 1.75	(5.12 ± 0.20) x 10^{-3}	(4.88 ± 0.44) x 10^{-3}
Cel5H	9.61 ± 2.21	11.80 ± 1.77	(3.29 ± 1.64) x 10^{-2}	(2.18 ± 1.52) x 10^{-2}
Cel5J	6.97 ± 0.56	4.06 ± 0.61	(6.67 ± 0.40) x 10^{-3}	(2.18 ± 0.04) x 10^{-3}

[a] Reducing sugar released from CMC and swollen cellulose was measured using a DNS assay and a cellobiose standard curve. For activity on filter paper and avicel, released cellobiose was converted to glucose using an excess of β-glucosidase and the activity is calculated at 50 % the rate of glucose release as measured using the glucose oxidase method.

[b] milligrams of protein measured using BSA as the reference

[c] The approximate degree of crystallinity for each substrate (% crystallinity) (35): Carboxymethyl cellulose (CMC; 0 %), PASC (<10 %), filter paper (50 %), and Avicel™ (70 %).

[d] Activity not detected in a 15 h degradation period.

Although Cel5F is expressed at 46 % that of Cel5H, its specific activity on the tested substrates was significantly lower than that of Cel5H on the tested substrates, suggesting that this enzyme makes a minor contribution to the degradation of cellulose.

The activity of Cel5B, Cel5D, Cel5E and Cel5F formed products typical of classical endoglucanases with ratios of soluble to insoluble products similar to that of other endoglucanases (Table 3.7). The processivity ratios for Cel5G and Cel5J, however, were found to be significantly greater than 4 and each degraded filter paper and Avicel like Cel5H. Interestingly, the activity of these processive endoglucanases was not dependent upon the activity of classic endoglucanases. For example, Cel5H was not synergistic with Cel5D, Cel5F, and Cel5G at three different molar ratios (1:4, 1:1, and 4:1) (Table 3.8). This indicated that Cel5H does not recognize the free non-reducing ends of cellulose polymers like cellobiohydrolases (Table 3.8). The activity of Cel5G was also not dependent on the activity of other endoglucanases similar to Cel5H. This indicated that both Cel5H and Cel5G act as processive endoglucanases.

Table 3.7 – The processivity of *S. degradans* cellulases

Cellulase[a]	Processive Ratio[b]	Type of Endoglucanase[c]
Cel5B	1.42 ± 0.22	Classical
Cel5C[d]	N/T	Unknown
Cel5D	0.10 ± 0.02	Classical
Cel5E	0.096 ± 0.01	Classical
Cel5F	0.77 ± 0.22	Classical
Cel5G	4.59 ± 0.68	Processive
Cel5H	4.26 ± 0.70	Processive
Cel5I[d]	N/T	Unknown
Cel5J	4.04 ± 0.39	Processive

[a] Each GH5 cellulase of the *S. degradans* system except Cel5A (104).

[b] The processive ratio is defined as the μmol soluble reducing sugar (cellobiose standard) divided by μmol insoluble sugar (glucose standard). The error bars represent one standard deviation from triplicate trials.

[c] Classical endoglucanase was defined by a processive ratio of less than 2. A processive endoglucanase was defined by a processive ratio greater than 2.

[d] Cel5C and Cel5I did not show activity on the substrates used in this work.

Table 3.8 – Synergy within the *S. degradans* system

		Yield of Glucose (μg)[a]			
Cellulase	Nanomoles Cellulase	Independent Yield[b]	Theoretical Yield[c]	Observed Yield	DoS[d]
Cel5D	1	0.26 ± 0.15[e]			
Cel5F	1	1.64 ± 0.045			
	0.5	1.23 ± 0.081			
Cel5G	0.8	6.17 ± 0.33			
	0.5	4.92 ± 0.79			
	0.2	2.64 ± 0.09			
Cel5H	0.1[e]	20.4 ± 0.71[e]			
	0.8	18.7 ± 0.44			
	0.5	15.8 ± 2.27			
	0.2	11.1 ± 3.9			
Cel5D + Cel5H	1 + 0.1 (10:1)		20.7	12.2 ± 0.78	0.59
Cel5F + Cel5H	1 + 0.2 (5:1)		12.7	12.4 ± 0.44	0.98
Cel5G + Cel5H	0.8 + 0.2 (4:1)		17.3	12.0 ± 0.62	0.69
	0.5 + 0.5 (1:1)		20.7	16.9 ± 0.54	0.82
	0.2 + 0.8 (1:4)		21.3	19.3 ± 0.73	0.91
Cel5G + Cel5F	0.5 + 0.5 (1:1)		6.2	6.09 ± 0.27	0.98

[a] The yield of glucose is measured from a two hour filter paper assay as described

[b] The independent yield was measured from a two hour filter paper assay

[c] The sum of the μg glucose produced for both the *S. degradans* cellulases independently

[d] DoS: The degree of synergy: The actual yield divided by the theoretical yield

[e] Yield after 15 hours due to low activity of Cel5D

3.4 Discussion

The noncomplexed and complexed cellulolytic systems of microorganisms generally rely upon the activity of endoglucanases and cellobiohydrolases to solubilize cellulose. Some exceptions to this model had been noted in bacterial systems that appear to lack or have deficiencies in cellobiohydrolases (68). An example is the *S. degradans* cellulolytic system that is predicted to produce an unusual abundance of GH5 endoglucanases but has a comparative deficiency in annotated cellobiohydrolases (104, 105). Experimental analysis showed that the single annotated cellobiohydrolase was in fact a classic endoglucanase yet cellobiose was an early product of cellulose degradation by the *S. degradans* cellulolytic system. Thus, it was not apparent how the enzymes of the *S. degradans* cellulolytic system interact to produce cellobiose. The results presented here indicate that the *S. degradans* cellulolytic system utilizes a novel set of processive GH5 endoglucanases (Cel5G, Cel5H and Cel5J) to substitute for the apparent deficiency in cellobiohydrolase activity. These processive enzymes were not dependent on endoglucanases for activity, as unlike cellobiohydrolases, there was an absence of synergism with endoglucanases. Therefore, in contrast to other cellulolytic systems dependent upon endoglucanases and cellobiohydrolases, a processive endoglucanase coupled with the activity of β-glucosidases or a phosphorylase is sufficient for this bacterium to metabolize cellulose.

S. degradans Cel5G, Cel5H and Cel5J exhibit endoglucanase activity as indicated by the effect of these enzymes on the viscosity of CMC solutions and the synergisms detected with a known exoglucanase. The identification of Cel5G, Cel5H and Cel5J as processive endoglucanases acting on the β-1,4 bonds linking cellobiose units is supported

by the constant ratio of soluble to insoluble products formed during reaction time courses. Unlike classical endoglucanases that randomly cleave cellulose polymers to form a variety of degradation products, these enzymes appeared to primarily release cellobiose from a variety of cellulose substrates. Although this is not demonstrative of processivity due to the turnover rates of many endoglucanases (9), the processivity values for Cel5G, Cel5H and Cel5J exceeded 4, irrespective of the reaction time. The processivity values reported for *T. fusca* Cel9A, an extensively characterized processive endoglucanase, range from 3.1 to 7.0 under similar conditions (115, 116) as well as in our own experiments. In contrast, the *T. fusca* classic endoglucanase, Cel6A, only released twice as much soluble sugar as insoluble sugar (113). Therefore, the processivity values for *S. degradans* Cel5G, Cel5H and Cel5J were most similar to that of the processive *T. fusca* Cel9A. While a cloning artifact resulting in the observed processivity cannot be completely excluded, the cloning strategy was designed to take advantage of the enzyme modularity such that functional domains were retained in the expressed protein.

The processivity of most endoglucanases is dependent upon their associated CBM module. For example, the processivity of several bacterial GH9 endoglucanases is dependent upon the resident CBM3 module (117, 118). The processive GH5 endoglucanases identified in this study are all linked to CBM6 modules via flexible linkers (119). These CBM6 modules are expected to bind to individual polysaccharide polymers (120). The CBM6 of Cel5H or Cel5G, however, were not necessary for activity or processivity. A specifically designed derivative of Cel5H lacking the CBM6 as well as the expressed form of Cel5G that due to its size appeared to lack its CBM6

retained significant activity. The processivity ratio of either enzyme was not affected by the absence of the CBM6.

The processivity of the GH5 domains of *S. degradans* Cel5G, Cel5H and Cel5J is unusual. In bacterial systems, processive endoglucanases have almost exclusively been found in the GH9 family (68). Processive endoglucanase activity, however, has been reported for another member of the GH5 family, Cel5A produced by the brown rot basidiomycete *Gloeophyllum trabeum* (121). Because this is an atypical activity for GH5 enzymes, the processive endoglucanases of *S. degradans* should have distinctive structures. The catalytic sites of processive enzymes are typically associated with either tunnel conformations that enclose the substrate during catalysis or are located in deep clefts that partially enclose the substrate (122). The catalytic sites of GH5 enzymes are clefts and the 7 residues that form the active site and cleft of the GH5 domains of Cel5G, Cel5H and Cel5J are conserved (67, 123).

Other systems lacking obvious cellobiohydrolases have also been reported where the role of processive endoglucanases is not well understood (68). For example, the cellulolytic system of *Cytophaga hutchinsonii* appears to be composed of 9 candidate endoglucanases containing either a GH5 or GH9 domain and 4 candidate β-glucosidases (124). Cellobiohydrolases are not obvious in this system. A similar system appears to be found in *Fibrobacter succinogenes* that contains five endoglucanases including Cel9D (125, 126). Cel9D is interesting in that it exhibits a wide range of synergistic interactions with other members of its own family (126). *C. hutchinsonii*, *F. succinogenes*, and *S. degradans* all share the property of having a large number of predicted endoglucanases

with relatively few cellobiohydrolases. Processive enzymes would enable these organisms to more efficiently metabolize cellulose.

4. Influence of Organic Liquids on Cellulose Nanostructure

4.1 Introduction

The objective of this chapter is to understand how solvents can be used to disrupt cellulose nanostructure. The strong network of interactions in the nanostructure of cellulose poses an energy barrier to enzymatic degradation (2). In this work, phosphoric acid was used to solubilize the cellulose nanostructure to overcome this energy barrier. Phosphoric acid mixed with cellulose yields an acidic state (pH ≈ 1.5) which is not compatible with enzymatic degradation. In order for phosphoric acid solubilized cellulose (PAS cellulose) to be compatible with enzymes, the phosphoric acid must be removed. Washing PAS cellulose with a liquid dilutes the concentration of phosphate ions, which causes the cellulose polymers to precipitate (17). Through successive washes the phosphate is almost completely removed from the system. The relative fractions of amorphous and crystalline domains in the washed PAS cellulose nanostructure is dependent on the interactions between the wash liquid and the cellulose (82).

The material used to investigate the influence of organic wash liquids on cellulose nanostructure was microcrystalline cellulose, which is commonly marketed under the trade name: Avicel. Microcrystalline cellulose is the cellulose extracted from biomass in the crystalline state under controlled acid hydrolysis using sulfuric acid (127). The sulfuric acid solubilizes the biomass components such as hemicellulose and lignin while also dissolving amorphous regions in the cellulose. The sulfuric acid is diluted to prevent solubilization of the cellulose polymers in the crystal lattice, which yields microcrystalline cellulose that is ≈70 % crystalline (127). Avicel is a white powder with

spherical particles (diameter ≈ 50 μm). The spherical particles are aggregates of cellulose microfibrils which form micron scale structures (127).

Solvents such as methanol, ethanol, acetone, and ethylene glycol have been used in industrial processes. Ethanol has been shown to increase the degradability of biomass, but most studies have just focused on industrial aspects such as glucose yield and percent conversion of the material (99, 100). For example, *Miscanthus x giganteus* has been pretreated using ethanol organosolvent pretreatment as described by Brosse *et al.* (99). In the work of Brosse, using 60 % ethanol in water to wash acid solublized biomass increased the glucose yield by approximately 40 % relative to washing with pure water when pretreated at 170 °C and using 20 FPU per gram cellulose (99). Although solvents including ethanol have been shown to increase degradability, how they interact with cellulose and thus affect nano and molecular scale structures during pretreatment is not well understood (10, 12, 15).

Solution thermodynamics as summarized by the Flory Huggins theory, evaluates potential interactions between a liquid and polymer (20). In this theory, the free energy of liquid-polymer interactions is calculated from the sum of entropic and enthalpic contributions, where the Flory Huggins interaction parameter χ, largely determines the enthalpic interactions (20). χ is calculated, in part, using Hildebrand solubility parameters which represent the cohesive energy density of each polymer and liquid. The interaction parameter predicts the interactions to be either favorable ($\chi < 0.5$) or unfavorable ($\chi > 0.5$) (21, 34). A favorable interaction is defined in this work as one that disrupts the precipitation process of PAS cellulose, thus yielding increased amorphous content relative to water washed PAS cellulose. The activation of crystal formation is

driven largely by enthalpic contributions to the free energy, which indicates a thermodynamic activation barrier. Organic liquids including methanol, ethanol, and ethylene glycol were predicted to interact favorably with cellulose.

The solvents predicted by the Flory Huggins theory to interact both favorably and unfavorably with cellulose were used to precipitate PAS cellulose. Differences between favorable and unfavorable wash liquids were visually apparent in the form of semi-transparent cellulose gels and opaque white cellulose precipitates. Optical density was used to characterize the disruption in the washed PAS cellulose by quantifying the aggregation of the polymers. Optical density is a technique commonly used in the life sciences to measure cell density in liquid cultures (128). The optical density was reduced for the cellulose structures washed using ethanol, methanol and ethylene glycol relative to water washed PAS cellulose, which indicated the possibility of increased disruption.

The disruption to the washed cellulose nanostructures is an important factor in enzyme accessibility and degradability (22). The nanostructure of each washed PAS cellulose was characterized using small angle neutron scattering (SANS). SANS is commonly used to probe polymers in solution or suspension to determine trends in polymer configuration and aggregation (24, 25). SANS has been applied to characterize cellulose polymer properties in-situ during enzymatic polymerization and hydrolysis (129, 130). SANS has also been used recently to examine the effects of acid hydrolysis on the separation of biomass components. However, the effects solvent interactions have on the removal of acid has not been studied (18). In this work the fractal nature of the precipitates was characterized to assess trends in the polymer clustering and configuration and relative to the starting material and water washed cellulose.

Differences in the aggregation and morphology between PAS cellulose samples washed with different liquids suggests unique bonding networks on the molecular scale. The molecular structure of the washed PAS cellulose was characterized using Fourier transform infrared resonance (FTIR). FTIR measures the absorbance of infrared radiation over a range of wavenumbers, which yields information about the vibrations of each bond in the structure (131, 132). FTIR has been used to characterize interactions such as hydrogen bonding in the polymorphs of cellulose (133, 134). In this work, FTIR was used to characterize the hydrogen bonding and the carbon – oxygen interactions of the gel-like and opaque white washed materials to compare the bonding networks and relative properties of inter and intra molecular hydrogen bonds (Figure 4.1).

The gel-like material was more susceptible to enzyme degradation than water washed PAS cellulose. The Hildebrand solubility parameters used in the Flory Huggins theory do not explicitly predict the interactions caused by hydrogen bonding and polar interactions. Hansen solubility parameters were used to evaluate the contribution of hydrogen bonding and polarity during the washing of PAS cellulose (32). Hansen solubility parameters are calculated based on physical properties such as the dipole moment, whereas the Hildebrand solubility parameter is the cohesive energy density (34, 135). Understanding how solvent interactions can increase the degradability of cellulose relative to current water washing could lead to the discovery of the next generation of cellulose solvents.

Figure 4.1 – Hydrogen bonding interactions characterized in this chapter

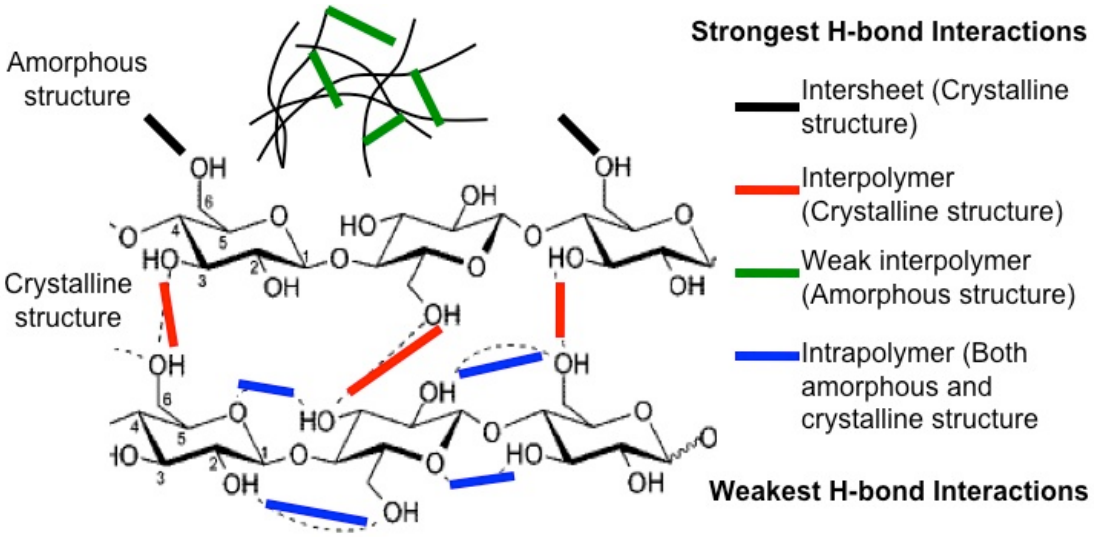

In an amorphous structure, interpolymer interactions are heterogeneous due to a range of bond distances and angles (21). In a crystalline structure, such as cellulose II, ordered intersheet and interpolymer interactions stabilize the lattice (29, 38). Intrapolymer interactions are common to both amorphous and crystalline cellulose structures (38).

4.2 Materials and Methods

Materials and chemicals: The cellulose used in all experiments was Avicel™ (PH-101) (Sigma Aldrich). The chemicals were obtained from Sigma Aldrich, Fisher Scientific, and VWR: phosphoric acid (85 % in water), methanol, ethanol, 1-propanol, 2-propanol, 1-butanol, 2-butanol, acetone, methyl ethyl ketone (MEK), ethylene glycol (EG) and glycerol.

Prediction of cellulose/wash liquid interactions: The Flory Huggins theory was used to predict interactions between liquids and cellulose that was solubilized in phosphoric acid. The Flory Huggins interaction parameter χ was calculated using equation (1) with Hildebrand solubility parameters and molar volumes from literature (Table 4.1) (20, 34). As cellulose is produced from a biosynthetic process, its chain length varies widely, which affects its cohesive energy density and thus Hildebrand solubility parameter. The χ parameter was calculated using a range of 25 – 30 $MPa^{1/2}$ for cellulose and the literature value for the wash liquid. The minimum value of χ was reported in Table 4.1. χ was calculated at 277 °K and R = 8.31 J/(mol x °K). The units of the solubility parameter, $MPa^{1/2}$ represent the square root of the energy per unit volume. Units of pressure are often expressed as energy per volume. One Pascal is equivalent to a joule per volume.

$$\chi = \frac{\left(\delta_{Cellulose} - \delta_{Solvent}\right)^2 V_M}{RT} \quad (1)$$

Table 4.1 – The Hildebrand solubility parameters and molar volumes of the liquids used to calculate the χ parameter (34).

Wash Liquid	Solubility Parameter ($MPa^{1/2}$)[a]	V_{Molar} (cm^3/mol)[a]	$\chi_{Minimum}$[a]
MEK	19.0	90.1	1.41
Acetone	20.3	74.0	0.71
2-Butanol	22.1	92.0	0.34
1-Butanol	23.3	91.5	0.11
2-Propanol	23.5	76.8	0.08
1-Propanol	24.3	75.2	0.02
Ethanol	26.0	58.5	0.00
Methanol	29.7	40.7	0.00
EG	29.9	55.8	0.00
Glycerol	33.8	73.8	0.46
Water	47.9	18.0	2.51

The boxes indicate the wash liquids predicted to be the most favorable, based on their calculated χ values.

[a] The values are from literature (34)

Preparation of washed PAS cellulose: Preparation followed the protocol for making phosphoric acid solubilized (PAS) cellulose as described by Zhang with minor modifications (17). Avicel (PH-101; 1 g) was added to 0.6 ml water to form a slurry (Figure 4.2). 100 ml of 85 % phosphoric acid was added to dissolve the cellulose and chilled (4 °C) to minimize formation of cellulose phosphate esters (electrostatic interaction). After 1 hour at 4 °C, 400 ml of cold liquid (4 °C) (Table 4.1) was added to wash the phosphate and precipitate the cellulose. After 30 minutes, the washed PAS cellulose was collected by centrifugation at 5000 RPM for 10 minutes. The wash process was repeated 4 times using 250 ml of fresh wash liquid each time. The concentration of liquid-washed cellulose was determined by drying 1 ml of the cellulose-liquid suspension and weighing the dried material.

Verification of removal of phosphate: FTIR was used to confirm the complete washing of phosphoric acid from the system. The spectra of liquid phosphoric acid was analyzed using attenuated total reflectance (ATR) to determine its unique peak locations (*see molecular characterization)*. The peak locations in the spectra of phosphoric acid and washed PAS cellulose cast as films *(see preparation of cellulose films)* were determined using the peak finder in Omnic 6.2 software with a sensitivity of 100. The removal of phosphate was defined as no detection of peaks at 944 and 873 cm^{-1} by the Omnic 6.2 peak finder (Figure 4.3 and Table 4.2).

Figure 4.2 – Preparation of washed PAS cellulose

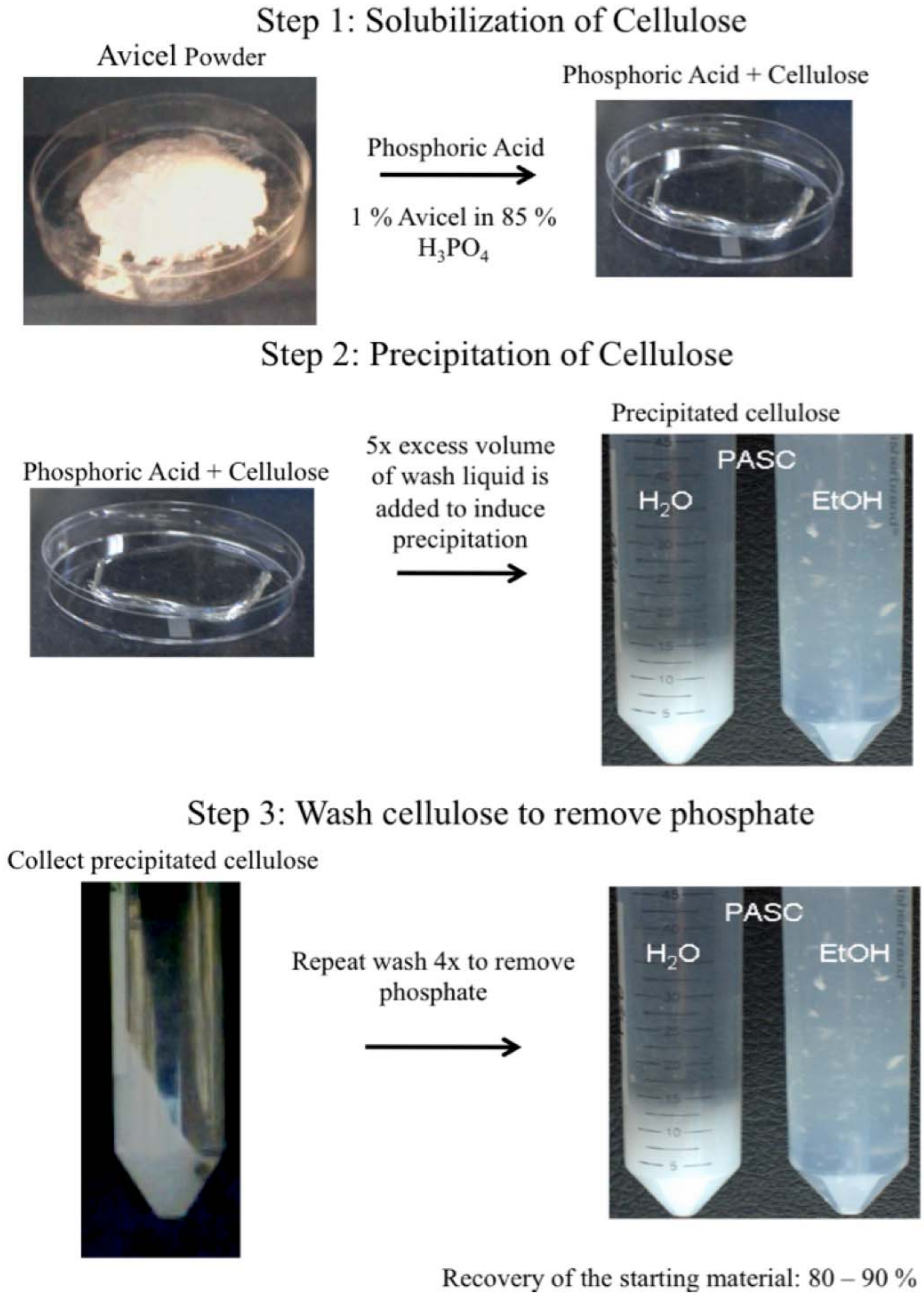

Figure 4.3 – FTIR spectra of liquid phosphoric acid control

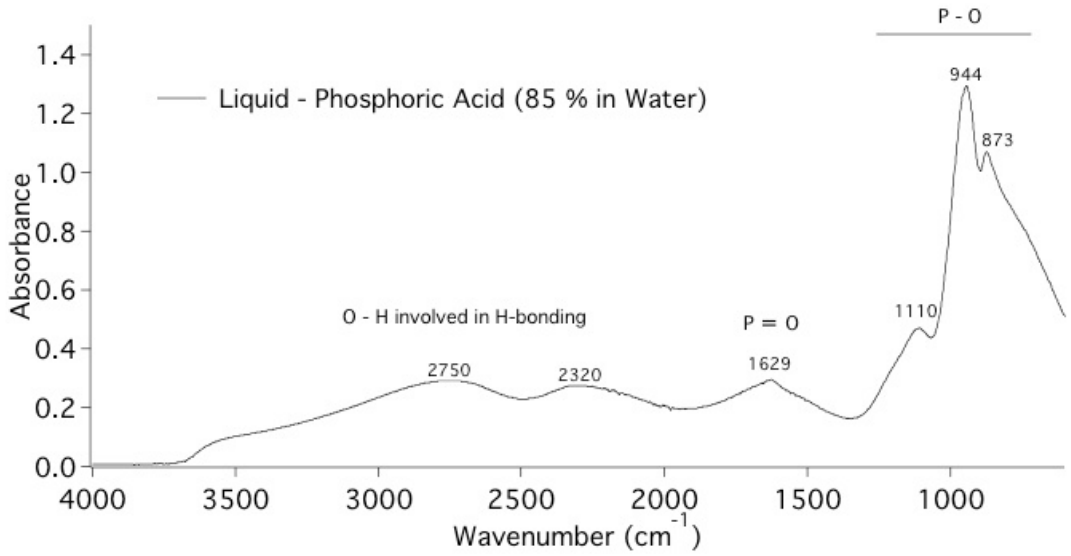

If residual phosphoric acid were present in the washed PAS cellulose samples, peaks would have been apparent in the region of 873 to 1110 cm^{-1}. *(See Table 4.2 below)*

Table 4.2 – Detection of phosphate in washed PAS cellulose samples

		Absorbance above baseline phosphate peaks (cm^{-1})[a]	
	Sample	944	867
Controls[b]	Starting Material	-	-
	Phosphate Control	1.29	1.07
Wash Liquid[c]	MEK	-	-
	Acetone	-	-
	2-propanol	-	-
	Butanol	-	-
	Ethanol	-	-
	Methanol	-	-
	Ethylene glycol	-	-
	Water	-	-

[a] The Omnic peak finder with a sensitivity of 100 was used to detect phosphate peaks

[b] The absorbance above the baseline, established by liquid phosphoric acid (85 % in water)

[c] Films of the washed PAS celluloses were cast and characterized in the region of the phosphate peaks determined from the controls.

Optical characteristics: The optical characteristics of the washed cellulose suspensions were measured 2 ways. First, the samples were examined visually noting opacity and settling volume. Then the optical density was measured using a Pharmacia Biotech spectrophotometer using a wavelength of 600 nm. The samples were suspended in quartz cuvettes with a 1 cm pathlength. The optical density was measured from suspensions with the cellulose concentration ≈ 5 mg/ml. The optical density was monitored over the course of 1 hour to ensure the suspended material did not settle.

Thermal analysis: The onset temperature of decomposition of the washed PAS cellulose was measured to assess trends in crystallinity. Thermal analysis was performed using a Shimadzu TGA-50 thermal gravimetric analyzer. The temperature range was 50 °C to 400 °C with a heating rate of 5 °C per minute in a nitrogen atmosphere. Approximately 5 mg of cellulose dried at room temperature were used in each trial. TA Universal Analysis 2000 software calculated the onset temperature of decomposition using tangents.

Nano scale characterization: The nanostructure of the washed PAS cellulose samples was characterized using small angle neutron scattering (SANS) at the 30 meter NG3 (neutron guide) beam line at the Center for Neutron Research at the National Institute of Standards and Technology, Gaithersburg, MD (136). Each sample contained a mass fraction of 0.5 % cellulose suspended in deuterated liquid obtained from Cambridge Isotope Laboratories: d-acetone (99.9 % D), d-ethanol (99 % D), d-ethylene glycol (98 % D), d-2-propanol (99 % D), d-methanol (99.5 % D), d-phosphoric acid (D_3) (85 % in D_2O) (99 % D), and d-water (99.9 % D). Three instrument configurations were used to yield a range of 0.001 $Å^{-1} < q = 4\pi/\lambda\sin(\theta/2) < 0.474$ $Å^{-1}$ with λ equal to the neutron

wavelength and θ equal to the scattering angle (Figure 4.4). Three scattering distances 13 m (λ = 8 Å), 7 m (λ = 6 Å), and 1 m (λ = 6 Å) were used for low q: 0.001 $Å^{-1}$ < q < 0.025 $Å^{-1}$, intermediate q: 0.006 $Å^{-1}$ < q < 0.077 $Å^{-1}$, and high q: 0.029 $Å^{-1}$ < q < 0.474 $Å^{-1}$ respectively. The sample thickness was 1 mm and the sample aperture diameter was 1.27 cm. The samples were allowed to settle for 24 hours before characterization to ensure no visual phase separation. Scattering was measured in the range of (10 to 140) °C dependent on the boiling point of the liquid to assess the thermal stability because disruption decreases stability. The low q configuration used a system of MgF_2 neutron focusing lenses that were inserted into the pre-sample neutron flight path to yield a lower q minimum and smaller beam spot on the detector.

Transmission and scattering runs from an empty and blocked beam were used for standard data correction using Igor Pro 6.11 (137). SANS data analysis was performed using a power law analysis. The scattering by each sample was divided by the contrast factor, ($\Delta\rho^2$), to normalize for contrast variations for comparison. The intensity of scattering is a function of the differential cross section per unit solid angle per unit volume: $d\Sigma(q)/d\Omega = I(q)$ (cm^{-1}) (25). To quantify the fractal nature of the washed PAS cellulose, the SANS data were fitted with a power law model. In the power law model, the fitted exponent, α, is representative of the polymer configuration on the nano scale (25, 27). The power law exponent was fitted in the range of 0.0010 $Å^{-1}$ < q < 0.15 $Å^{-1}$ with coefficient, A and background B.

$$\frac{d\Sigma}{d\Omega}(q) = Aq^{-\alpha} + B \qquad (2)(25)$$

Figure 4.4 – The experimental setup for small angle neutron scattering (SANS)

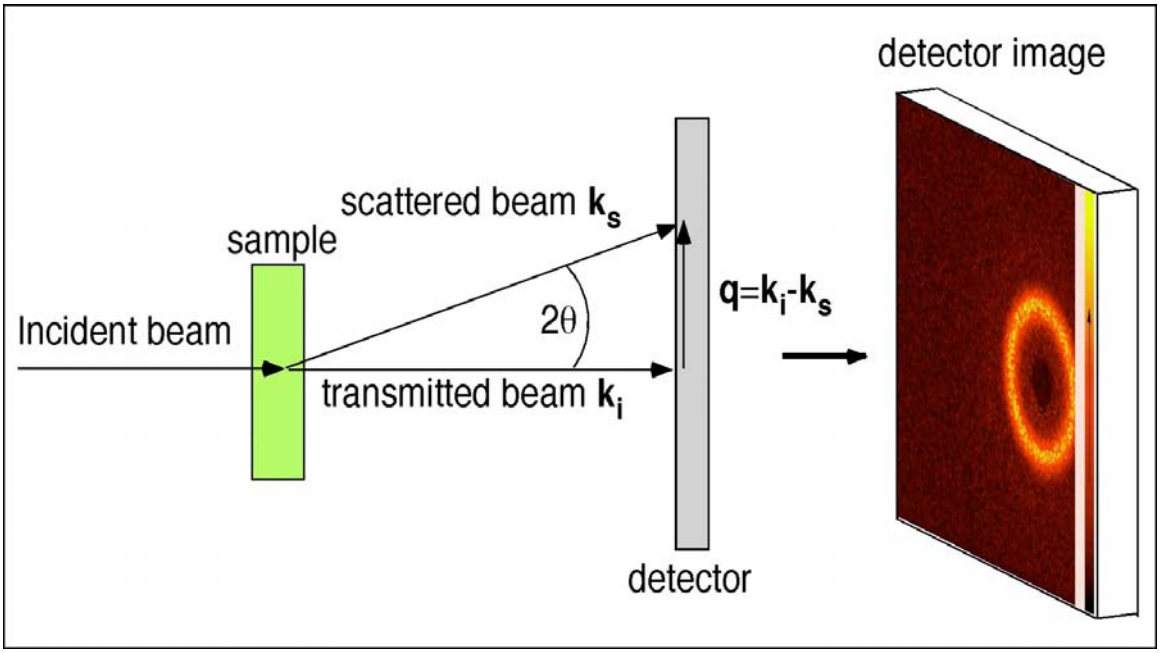

Figure obtained from Professor Robert Briber.

Degradability of cellulose by enzymes: Enzyme assays were performed as described previously in Chapter 2 and by Watson *et al* (128). Liquid-washed PAS cellulose was washed twice in aqueous assay buffer [20mM PIPES (piperazine-N,N'-bis(2-ethanesulfonic acid)), 1 % Instant Ocean, pH 6.5] by centrifugation at 5000 RPM for 10 minutes. 0.1 nmol of *Saccharophagus degradans* Cel5H were used in each assay. All assays were conducted at 50 °C. Reducing sugars were detected using the DNS (dinitrosalicylic acid) method (107), with the average ± one standard deviation reported.

The product yield as a function of time was measured using 2 mg of methanol, ethanol, ethylene glycol or water washed PAS cellulose in a total volume of 0.7 ml. *S. degradans* Bgl1A (0.1 nmol) was added to metabolize cellobiose to glucose. At periodic time points (0 to 24) hours, the samples were centrifuged at 8000 RPM for 15 seconds and 0.05 ml of the supernatant was removed to measure the glucose concentration. The substrate was then resuspended and placed back in the incubator.

Preparation of cellulose films for characterization

Films of washed PAS cellulose were cast by depositing 1 mg of washed PAS cellulose onto glass slides. To remove excess wash liquid the films were held at room temperature for 16 hours as described in literature with minor modifications (43, 138-141). Then the gelled films were removed from the glass using a razor blade (Figure 4.5).

Figure 4.5 – Preparation of cellulose films to partially separate the wash liquid

Step 1
≈1 mg of washed PAS cellulose is deposited onto a glass slide

Step 2
After 16 hours of drying at room temperature the cellulose forms a film which is removed from the glass

Step 3
The film is adhered to a sample holder card for FTIR characterization

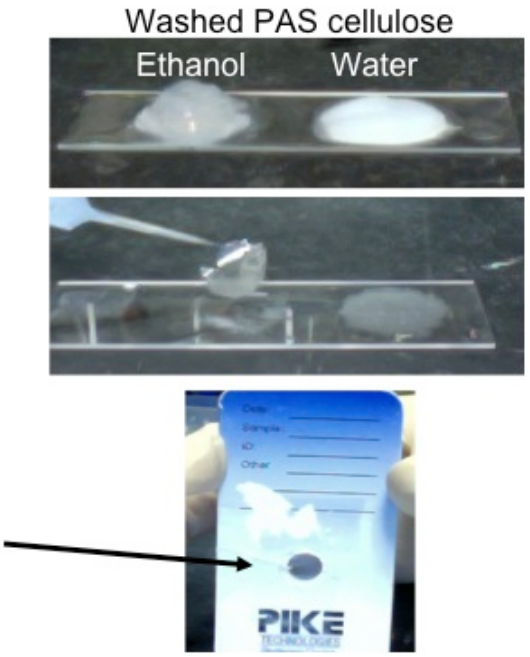

X-ray diffraction: The cast films of washed PAS cellulose were analyzed using a Rigaku x-ray diffraction instrument to assess crystallinity. Avicel powder (included as a control) and cellulose films of water washed and ethanol washed cellulose were characterized over the range of 10 to 40 ° 2θ. The voltage was 40 kV and the current was 40 mA. The crystallinity of the cellulose samples was calculated from equation 3 (96, 142).

$$Crystallinity\ Index = 100 \times \left(\frac{I_{(200)} - I_{(amorphous)}}{I_{(200)}} \right) \quad (3)$$

Molecular characterization: The hydrogen bonding of the washed cellulose was characterized using a Nexus 670 Fourier transform infrared spectrometer with a deuterated triglycine sulfate (DTGS) detector (Figure 4.6A). Liquid samples were characterized using attenuated total reflectance (ATR) with a thermo scientific ATR accessory with a diamond interface (Figure 4.6B). Spectra were collected with a resolution of 4 cm^{-1} using 64 scans in the range of (400 to 4000) cm^{-1} using transmission geometry in a nitrogen atmosphere at room temperature. The automatic peak finder in Omnic 6.2 with a sensitivity of 100 was used to detect peak location and absorbance of peaks in the range of 970 to 1190 cm^{-1}, which represents C – O interactions and greater then 2900 cm^{-1}, which represents O – H interactions (58). Difference spectra were processed using the subtraction function in Omnic 6.2. The spectra of water washed PAS cellulose was subtracted from the spectra of ethanol washed PAS cellulose to yield differences in the pattern of hydrogen bonding between the two washed PAS materials. The peak absorbance values were analyzed from at least 5 unique batches of washed cellulose to calculate the instrument and experimental error (reported as one standard deviation).

Control experiments for molecular characterization

Detection limit of ethanol: The sensitivity of the FTIR to ethanol and water in the system is critical to establishing that cellulose/cellulose interactions and not solvent/cellulose interactions were being characterized. Mixtures of ethanol and water were prepared with volume fractions of ethanol ranging from 1 to 0.5 % vol. The Thermo Scientific ATR accessory was used to characterize the liquid mixtures. The peak finder with a sensitivity of 100 was used to detect the characteristic peaks of ethanol at 1046 and 1085 cm^{-1}. The sensitivity limit was determined when the peak finder was not able to detect the peak of ethanol at 1046 cm^{-1}.

Verification that casting of the films did not alter the degree of crystallinity: Crystalline cellulose (I and II) were used as controls in the analysis of the spectra of washed PAS cellulose. The native cellulose (cellulose I) control was Avicel. The spectra of Avicel was collected using between 1 to 8 mg of Avicel pressed into a potassium bromide (KBr) pellet with a total mass of 100 mg. Cellulose II was prepared using the Mercer process (48). Cellulose II was prepared by suspending 1 g of Avicel in 25 % sodium hydroxide in water. The caustic suspension of Avicel was stirred for 24 hours at 4 °C. The sodium hydroxide was separated from the suspension by centrifugation at 5,000 RPM for 10 minutes. The supernatant was decanted and 250 mls of fresh water was added. This process was repeated 4 times.

Figure 4.6 – Process diagram for Fourier transform infrared resonance (FTIR)

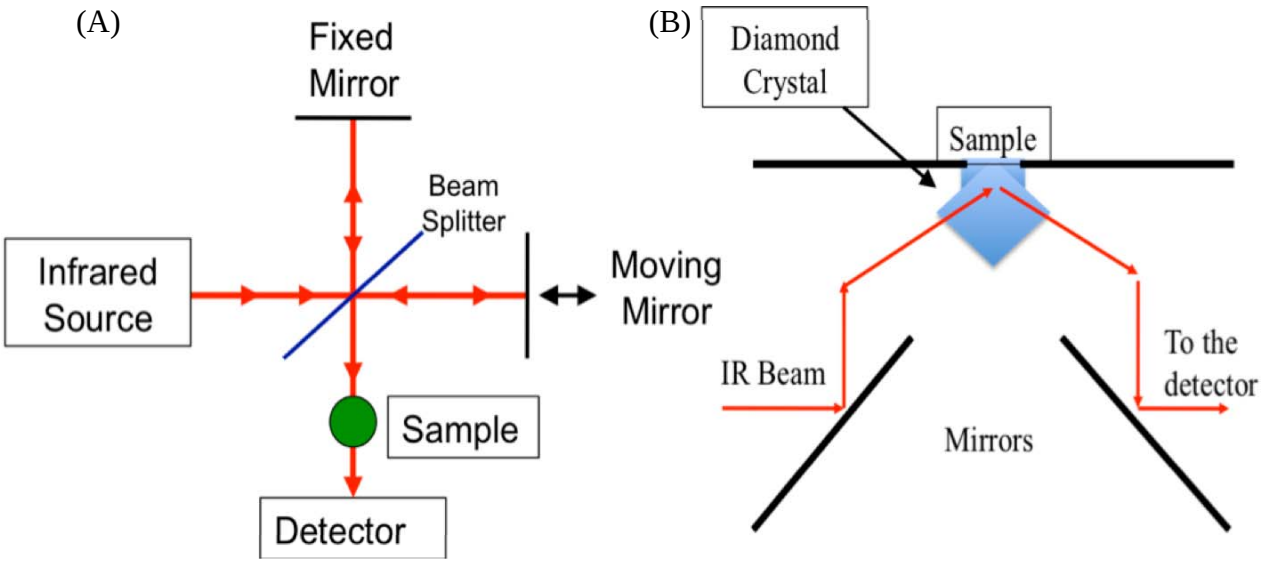

(A) FTIR process diagram (132, 143). (B) Attenuated total reflectance (ATR) is an accessory that is mounted into the IR beam, to characterize liquid samples (132).

4.3 Results

Identification of candidate cellulose precipitation liquids

To understand how organic liquids interact with cellulose, liquids predicted to have favorable interactions with cellulose were first identified. To do this, the Flory Huggins interaction parameter was calculated for selected cellulose/liquid pairs using the published Hildebrand solubility parameters for liquids (34), an estimate of 25 to 30 $MPa^{1/2}$ for cellulose (34, 144, 145), and eqn. 1. As cellulose contains multiple hydroxyl groups per monomer, the primary focus in these evaluations was alcohols, glycols and ketones with electronic structures most likely to interact with glucose. The liquids with the most favorable potential interactions with cellulose ($\chi = 0.00$) were methanol, ethanol, and ethylene glycol (Table 4.1). It is important to note that these methanol, ethanol, and ethylene glycol have been incorporated into pretreatments, and this work seeks to understand how they influence the cellulose nanostructures. Other liquids predicted to have favorable interactions with cellulose included 2-propanol and 1-butanol. Water, methyl ethyl ketone, and acetone were predicted to have unfavorable interactions with cellulose.

Influence of organic liquids on the precipitation of cellulose

To determine the effects of the wash liquids on PAS cellulose, samples were washed with each liquid in Table 4.1. Each washed PAS cellulose sample was poured into a test tube and allowed to settle overnight. Then the samples were characterized visually and by optical density measurements. Figure 4.7 shows that the most favorable wash liquids yielded the largest settling volumes and least opaque systems. The least favorable liquids produced the most opaque systems and the smallest settling volumes.

The optical density of the favorable liquids was less than that of the control, water washed PAS cellulose. Complete washing was confirmed by Fourier transform infrared resonance (FTIR) that showed the absence of peaks at 944 cm^{-1} and 873 cm^{-1}.

Figure 4.7 – Effect of selected liquids on washing of phosphoric acid solubilized cellulose (PAS cellulose)

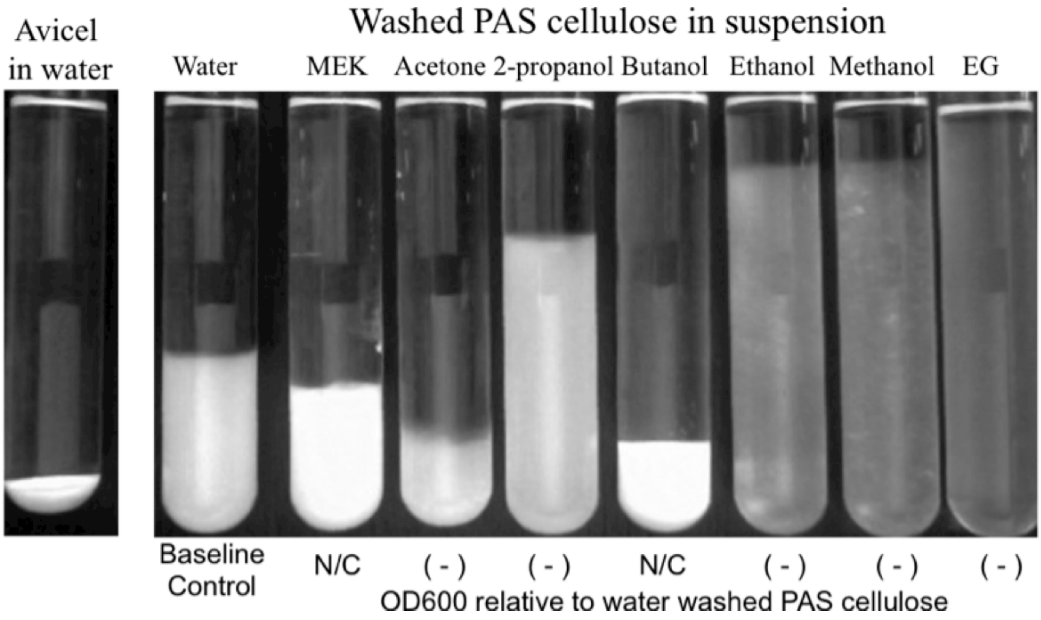

Each test tube was filled with approximately 100 mg of washed PAS cellulose in a volume of approximately 30 ml and allowed to settle overnight. The OD600 evaluated the opacity of washed PAS cellulose that was well dispersed in the suspension. The OD600 was measured on the 5 mg/ml suspensions of washed material in the respective solvent and reported relative to water washed PAS cellulose as no change (N/C) or decrease in OD600 (-).

The optical density (OD600) of each washed sample was measured to evaluate the number density. A suspension of 5 mg/ml of water washed PAS cellulose was used as the baseline to compare the washed PAS cellulose samples. The OD600 of washed PAS cellulose in suspensions was stable for greater than 1 hour. The OD600 of suspensions of PAS cellulose washed with methanol, ethanol, 2-propanol, acetone and ethylene glycol, was reduced relative to the water washed PAS material (Figure 4.7). In contrast, PAS cellulose washed with butanol and methyl ethyl ketone showed no significant decrease in OD600 relative to water washed PAS cellulose (significance determined by one standard deviation from the baseline control). The reduced optical densities of several of the washed PAS cellulose materials indicated increased disruption relative to the water washed PAS cellulose.

Thermal characterization of washed PAS cellulose

Decreased optical densities of the liquid-washed PAS celluloses suggest disruption to the nanostructure. If such a change occurred, the thermal stability of celluloses washed with favorable liquids should decrease (34, 146). The onset temperature for thermal decomposition of Avicel and water-washed PAS cellulose was 309 ± 5 °C and 281 ± 14 °C, respectively, as indicated by the loss of mass (Figure 4.8). The onset temperature of thermal decomposition for PAS cellulose washed with acetone, 2-propanol, ethanol and methanol was 195 - 210 °C suggesting increased disruption relative to the water washed and starting material. PAS cellulose washed with ethylene glycol decomposed at 251 ± 2 °C. As there were similar onset temperatures of decomposition for acetone and the alcohols, significant differences in disruption between the PAS celluloses washed with favorable liquids could not be resolved further.

Figure 4.8 – Thermal characterization of washed PAS cellulose

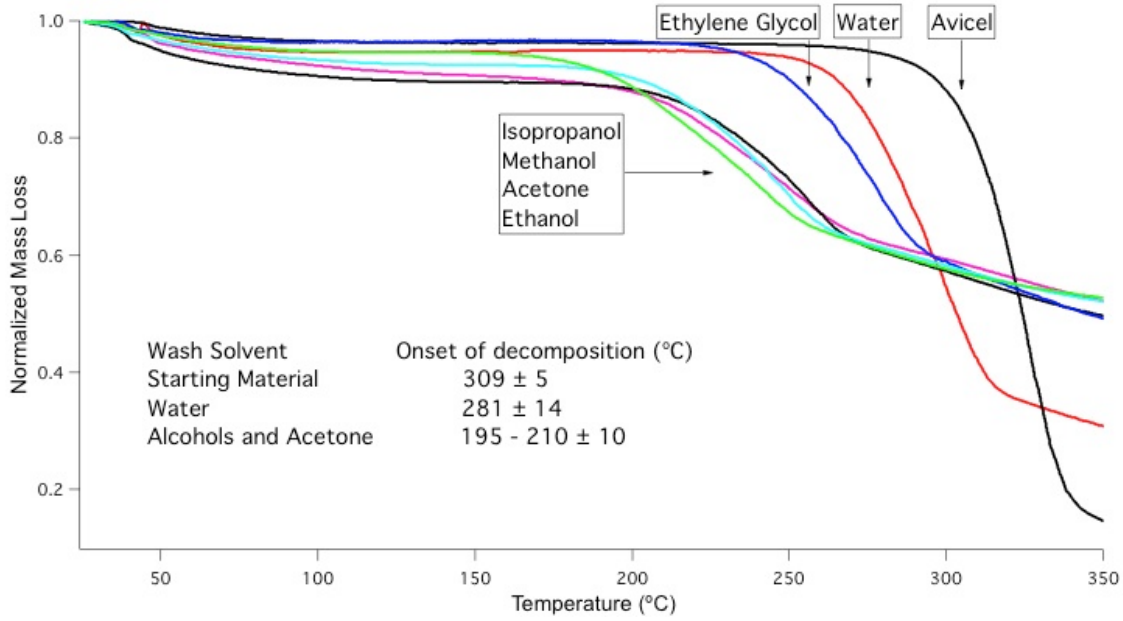

The disruption to the nanostructure was characterized using thermal gravimetric analysis (TGA). The onset of thermal decomposition was determined by the intersection of tangent lines drawn from the initial flat slope and the slope during mass loss. Each onset temperature was measured in at least duplicate trials and the error is reported as one standard deviation.

Nano scale characterization of washed PAS cellulose

To evaluate disruption of cellulose nanostructure, the liquid washed PAS celluloses were analyzed in a suspension with deuterium-substituted liquid by small angle neutron scattering (SANS). The relative scattering intensity at low q is one indication of polymer solvation since intensity decreases as solvation increases due to a reduction in concentration fluctuations (25). The scattering intensity at low q ($q = 0.0013$ $Å^{-1}$) corresponds to scattering from cellulose bundles on the length scale of 483 nm ($d = 2\pi/q$) (Figure 4.9). PAS cellulose washed using methanol, ethanol, and ethylene glycol, forming apparent gel-like material, had the lowest SANS intensity at low q relative to the suspensions of starting material and water washed PAS cellulose.

Figure 4.9 – Small angle neutron scattering from cellulose washed with selected liquids.

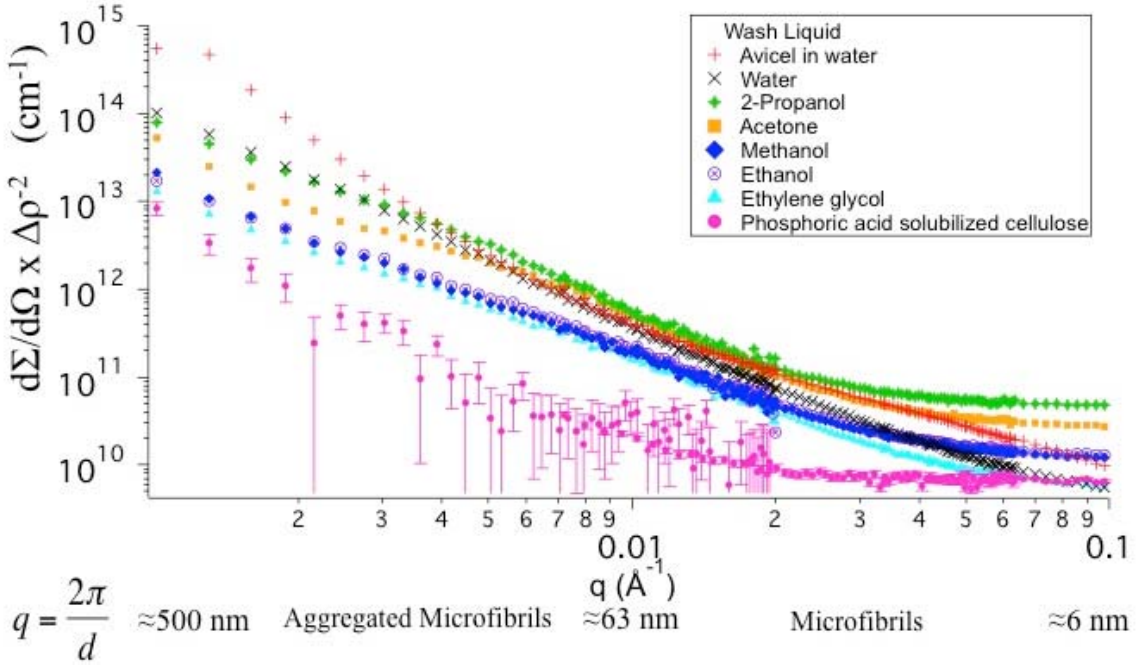

The Y-axis represents the SANS intensity. Liquid-washed PAS cellulose was re-suspended in the same deuterated liquid for contrast with cellulose. The decrease in scattering at low q relative to the starting material, and the slope of the low q region were used to compare cellulose disruption and fractal nature. The error bars represent the instrument error and are too small to be shown outside the data point except for PAS cellulose.

The linear region of the SANS data was fitted using a power law to quantify the fractal nature of each washed PAS cellulose. The fitted power law exponent, α, is the slope of the linear section of the scattering curve log(I) vs. log(q) at low to intermediate q and provides a fractal representation of the material (25). The slopes for low q ($q < 0.01$) and intermediate q ($0.005 < q < 0.1$) were not statistically different within instrument and experimental error. Thus, the average power law was fitted for each sample over the range of $0.0010\ Å^{-1} < q < 0.15\ Å^{-1}$. Table 4.4 shows the fitted power law exponents for the washed PAS cellulose samples. The fitted α of the starting Avicel material was -3.56 whereas the α of PAS cellulose in D_3-phosphoric acid increased to -1.89 (Table 4.3). PAS cellulose washed with water exhibited an α of -2.40 consistent with partial reformation of cellulose nanostructure relative to PAS cellulose. The α's of the gel-like PAS cellulose washed in methanol, ethanol, or ethylene glycol were -2.10, -2.17, and -2.09 respectively. In contrast, the fitted α's of acetone- and 2-propanol-washed cellulose were closer to that of the water washed PAS material.

The power law was used to fit scattering data from unique batches of cellulose to determine the reproducibility. Duplicate trials of water, methanol and ethylene glycol washed PAS cellulose yielded an average power law exponent ± one standard deviation of -2.40 ± 0.01, -2.10 ± 0.06 and -2.09 ± 0.02 respectively and triplicate trials for ethanol washed material, yielded -2.17 ± 0.06. This indicated that the results were reproducible.

Table 4.3 – Fitted power law exponents of liquid washed PAS cellulose as determined by SANS.

Wash Liquid	Fitted Power Law Exponent[a]
Avicel in water	-3.56 ± 0.02
Water	-2.40 ± 0.01
Acetone	-2.39 ± 0.01
2-propanol	-2.26 ± 0.01
Ethanol	-2.17 ± 0.01
Ethylene Glycol	-2.09 ± 0.01
Methanol	-2.10 ± 0.01
Phosphoric Acid	-1.89 ± 0.03

[a] The statistical error is reported for each power law fit.

Thermal stability of washed PAS cellulose characterized by SANS

Weakened polymer interactions are also apparent in the thermal stability of washed cellulose samples. The rate of change in the power law exponent, dα/dT, was calculated to evaluate the thermal stability of the washed PAS cellulose samples by characterizing the scattering at elevated temperatures (Figure 4.10). The dα/dT of water washed PAS cellulose was $(2.6 \pm 0.3) \times 10^{-4}$ °K^{-1}. PAS cellulose washed with methanol, ethanol, or ethylene glycol yielded significantly lower calculated values of dα/dT: $(-7.3 \pm 2.7, -9.8 \pm 2.1$, and $-3.1 \pm 0.8) \times 10^{-4}$ °K^{-1}, respectively. This trend suggests ethanol washing yielded the least thermally stable and thus the most disrupted cellulose nanostructure.

Figure 4.10 – Thermal stability of gel-like washed PAS cellulose samples as characterized by SANS

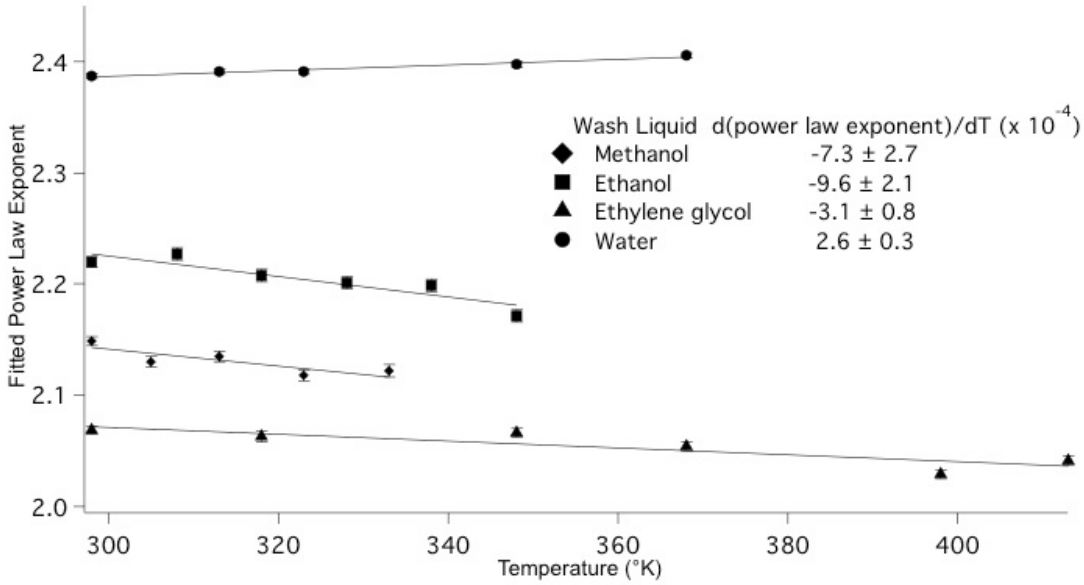

Degradability of washed PAS cellulose

The disruption of cellulose structure after washing with the selected alcohols and glycols suggests that these materials should be more degradable by enzymes. *S. degradans* Cel5H, which is highly biased toward amorphous cellulose (128), was used to compare the glucose yield from organic liquid and water washed PAS cellulose. The washed PAS cellulose samples were re-equilibrated in aqueous assay buffer, which may have caused a partial reversal in the gel-like properties. Ethanol washed PAS cellulose yielded ≈30 % more glucose than water-washed PAS cellulose (Figure 4.11). The glucose product was also measured from methanol and ethylene glycol washed PAS cellulose, but the yield was not significantly different than water washed PAS material.

A CMC assay was used as a control to evaluate if the leveling of the product as a function of time was due to material properties or reduced enzyme activity, which could be caused by thermal or solvent effects. To evaluate if Cel5H was still active after 20 hours, aliquots from the water and ethanol washed PAS cellulose samples were used as the enzyme source for a CMC assay. Positive activity on CMC relative to a negative control was observed which suggested that the maximum product concentration was due to material properties and was not caused by thermal or solvent inactivation of the enzyme. The increased degradability suggests that ethanol washed PAS cellulose has the most disrupted structure of the washed PAS cellulose samples characterized.

Figure 4.11 – The degradation of washed PAS cellulose samples by *S. degradans* Cel5H

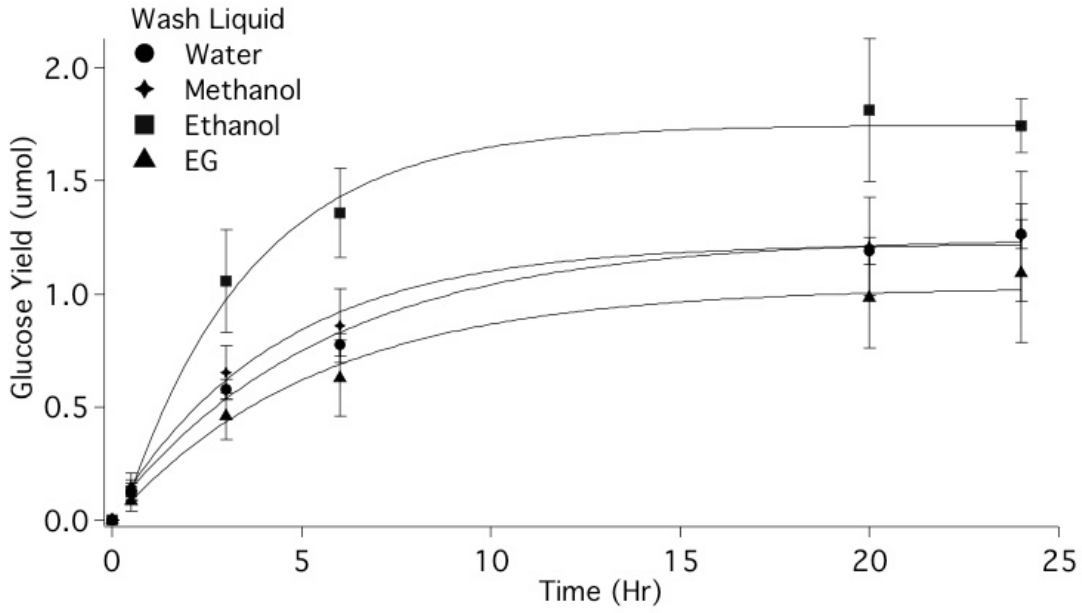

The error bars represent one standard deviation from triplicate trials.

Molecular scale characterization of washed PAS cellulose

The formation of a gel when PAS cellulose is washed by ethanol suggests the presence of unique structural features at the molecular scale. Fourier transform infrared resonance (FTIR) was used to characterize the hydrogen bonding networks to determine why PAS cellulose washed with ethanol yielded a gel-like material, whereas PAS cellulose washed with water yielded an opaque white precipitate. Due to the limit of instrument resolution, this analysis is not meant to be a crystallographic representation of bonding, but rather an analysis of the patterns of hydrogen bonding contributing to the formation of gel-like material and opaque white precipitate.

Water washed PAS cellulose was initially characterized in suspension with the wash liquid to determine patterns in bonding. To collect spectra of the washed PAS cellulose suspended in its wash liquid, attenuated total reflectance (ATR) was used with the spectra of the pure liquid used as the background. The spectra were very noisy. In an effort to reduce the background contributed by free wash liquid, the wash liquid was exchanged for deuterated wash liquid. This is advantageous because the IR absorbance of deuterium occurs at ≈2500 cm^{-1} compared to ≈3400 cm^{-1} for hydrogen so O – D bonds in the wash liquid could be distinguished from O – H bonds in the cellulose (41). A signal to noise ratio (SNR) greater than 3 is necessary to quantitatively analyze FTIR spectra (132). However, the SNR for water washed PAS cellulose suspended in D_2O was calculated to be 1.55 (Figure 4.12). Thus, further sample preparation was necessary.

Figure 4.12 – The FTIR-ATR spectra of water washed PAS cellulose in suspension of D_2O

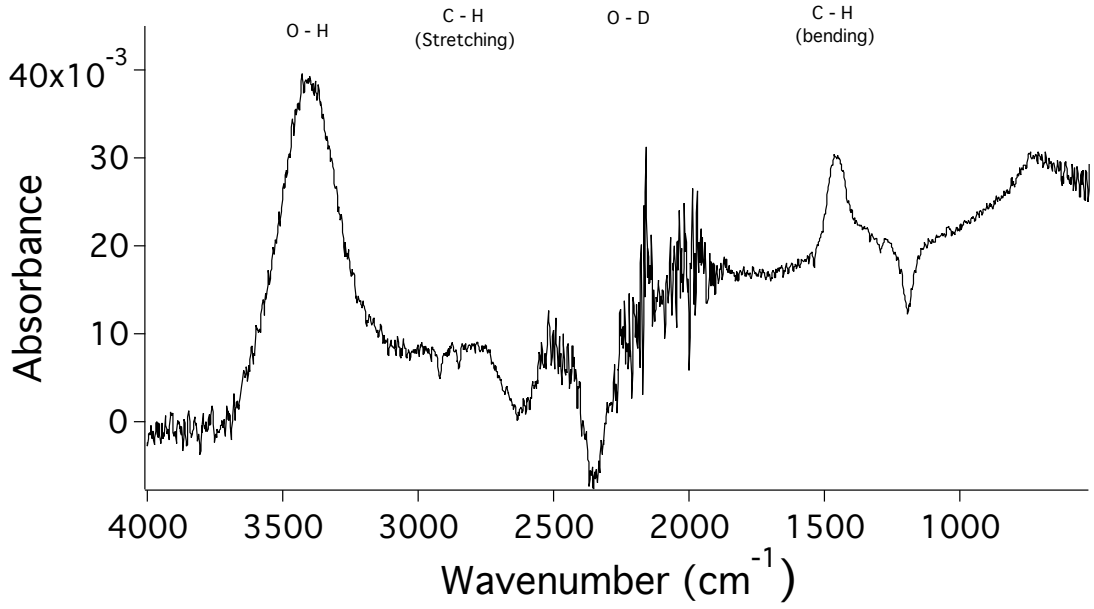

Note: The peak absorbance was evaluated at ≈ 3450 and was 0.04 and the noise was evaluated at ≈2200 cm^{-1} and was 0.025. Therefore the signal to noise ratio was 1.55.

The high background level from the wash liquid indicated that it needed to separated from the washed PAS cellulose. To determine the volume fraction of wash liquid that had to be separated from the washed PAS cellulose suspension, the sensitivity of the FTIR to ethanol in water was evaluated. ATR was used to determine the lowest detectable volume fraction of ethanol in liquid ethanol/water mixtures. Liquid ethanol has peaks at 1046 cm^{-1} and 1086 cm^{-1} characteristic of C – O and C – C interactions (41, 131). The peak finder in Omnic 6.2 with a sensitivity of 100 was used to determine if the peak at 1046 cm^{-1} was present. The peak finder was not able to detect ethanol in volume fractions less than 0.75 %, which indicated that greater than 99.25 % of the wash liquid had to be separated (Figure 4.13). This suggested films cast to separate the liquid would be required.

The cellulose films were first characterized to determine if the spectra reflected cellulose/cellulose interactions or retained solvent/cellulose interactions. The spectra of water and ethanol washed PAS cellulose films were analyzed in the region of covalent C – O interactions in cellulose near the locations of the C – O and C – C interactions in ethanol. Because FTIR cannot resolve individual covalent interactions, the region of the C – O interactions of cellulose is an average of interactions with discrete peaks for the most occurring bonds. This means that if ethanol/cellulose interactions were being detected the cellulose peaks would shift towards the characteristic peak of ethanol (1046 cm^{-1}). The peak locations of the ethanol washed PAS cellulose at ≈1022 cm^{-1} and 1060 cm^{-1} were either farther from the standard location of the ethanol peak or not significantly different from the peak locations of water washed PAS cellulose, which indicated cellulose/cellulose interactions were being characterized (Figure 4.14).

Figure 4.13 – FTIR detection of ethanol in ethanol/water liquid mixtures

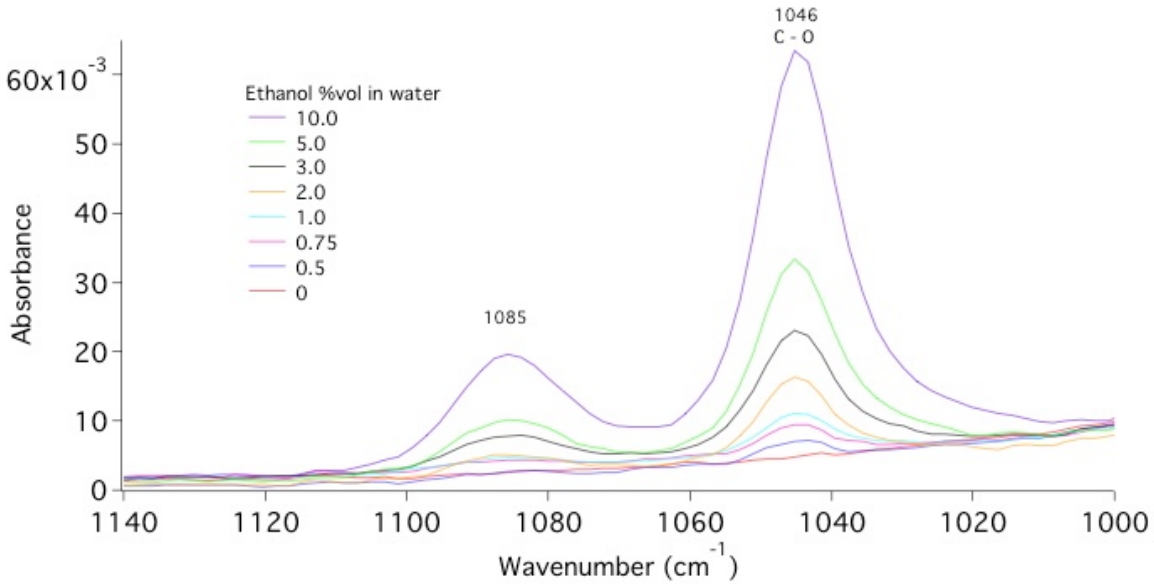

The baseline spectra (red) is pure water.

Figure 4.14 – FTIR analysis of C – O interactions in washed PAS cellulose suspensions after partial separation of the wash liquid. The locations of the C – O bonds in cellulose are indicated.

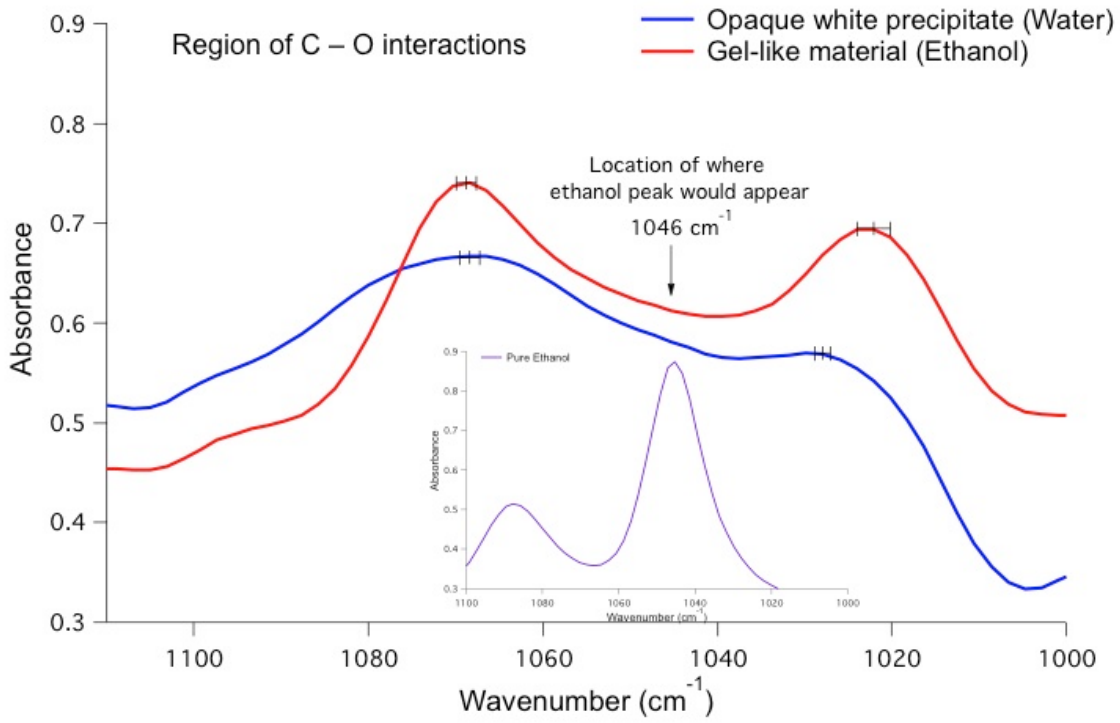

Note: The peak location of the ethanol washed PAS cellulose at ≈1022 cm^{-1} was farther away from the location of where pure ethanol would be detected relative to water washed PAS cellulose.

The impact of partial separation of the wash liquid on the cellulose crystal structure was evaluated to verify that the cellulose films were representative of the interactions in the suspensions of washed PAS cellulose. Native cellulose (Avicel: cellulose I) and crystalline cellulose II were used as controls to determine if partial separation of the wash liquid altered the crystal structure in the cellulose films. Peaks representing crystalline cellulose were identified at 3345 cm^{-1} (cellulose I), 3450 cm^{-1} (cellulose II), and 3494 cm^{-1} (cellulose II) (Figure 4.15). These peaks were largely absent in both water and ethanol washed PAS cellulose. This suggested both samples remained in the amorphous state after partial separation of the wash liquid and thus were not significantly affected.

X-ray diffraction was used to confirm the amorphous character of the PAS cellulose films after partial separation of the wash liquid. Native cellulose in the form of Avicel: cellulose I was used as the positive control to detect peaks from crystalline cellulose. The crystallinity index of Avicel was calculated using equation 3 to be 73 %. The x-ray diffraction spectra for both water and ethanol washed PAS cellulose was in the form of broad peaks in the region of ≈15 to 25 ° 2θ (Figure 4.16). This confirmed both PAS cellulose films were amorphous after partial separation of the wash liquid.

Figure 4.15 – FTIR was used to determine the impact of partial separation of the wash liquid on the crystalline structure of the cellulose films

(A)

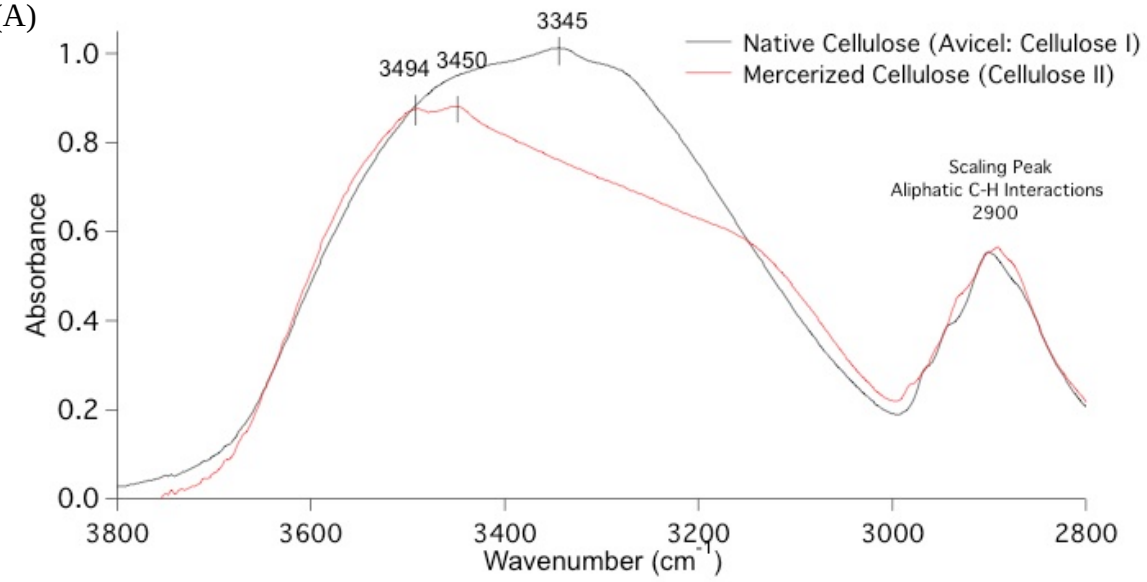

Native cellulose (Avicel: cellulose I) and Mercerized cellulose II were used as controls to show both possible crystalline structures.

Figure 4.16 – XRD characterization of the crystallinity of cellulose films of washed PAS cellulose after partial separation of the wash liquid

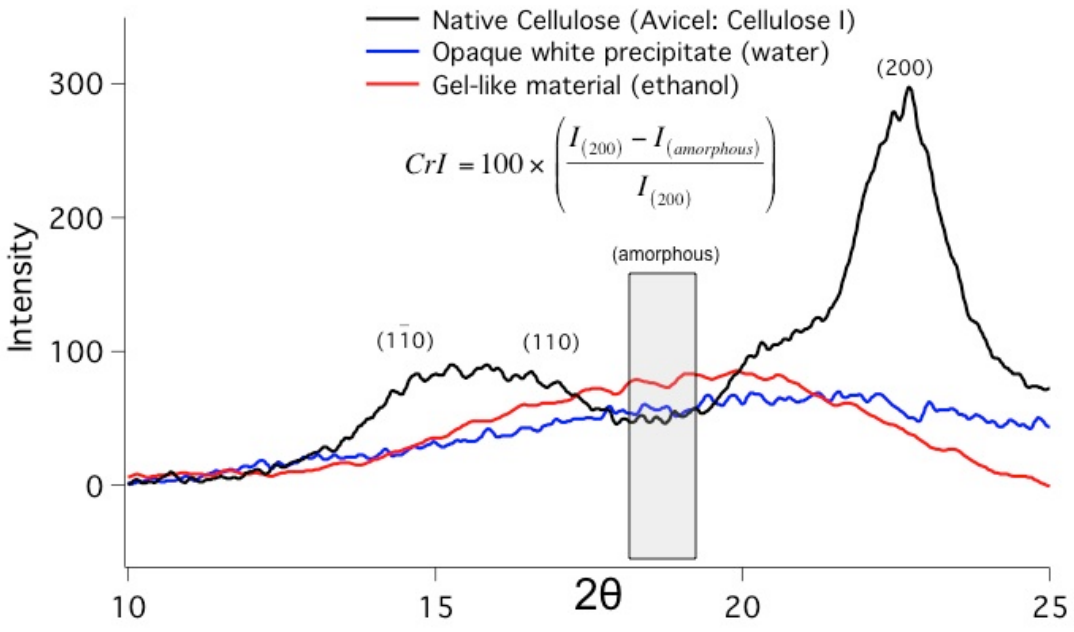

The washed PAS cellulose was characterized to determine if reformation of the crystal structure occurred. Native cellulose (Avicel: cellulose I) was used as the control to demonstrate the ability to detect crystalline peaks.

Characterization of O – H bonds

Differences in the fitted power law exponents suggest the gel-like and white precipitate have distinct hydrogen bonding networks. The covalent O – H bonds in cellulose absorb IR at ≈3600 cm^{-1} (41, 131). When the hydrogen atom of a cellulose hydroxyl group forms a hydrogen bond, the vibrational energy of the covalent O – H bond is reduced. Decreasing vibrational energy decreases the wavenumber of the absorbance to the region of 3000 to 3600 cm^{-1}. This broad peak represents the average absorbance by the O – H groups of cellulose involved in hydrogen bonding (41, 131). The peak at ≈2900 cm^{-1} corresponds to C – H bonds in the glucosyl ring structure and was used to scale the spectra (58). A discrete peak in the spectra of water washed PAS cellulose was observed at 3442 ± 2 cm^{-1} which indicated a preference for intrapolymer bonding similar to cellulose II (133, 147, 148) (Figure 4.17). Only a broad peak at 3402 ± 8 cm^{-1} was observed in the spectra of ethanol washed PAS cellulose. The lack of a discrete spectral feature at ≈3440 cm^{-1} in the hydrogen bonding region of ethanol washed PAS cellulose indicated a diverse collection of hydrogen bonds.

Figure 4.17 – FTIR characterization of the hydrogen bonding network of washed PAS cellulose

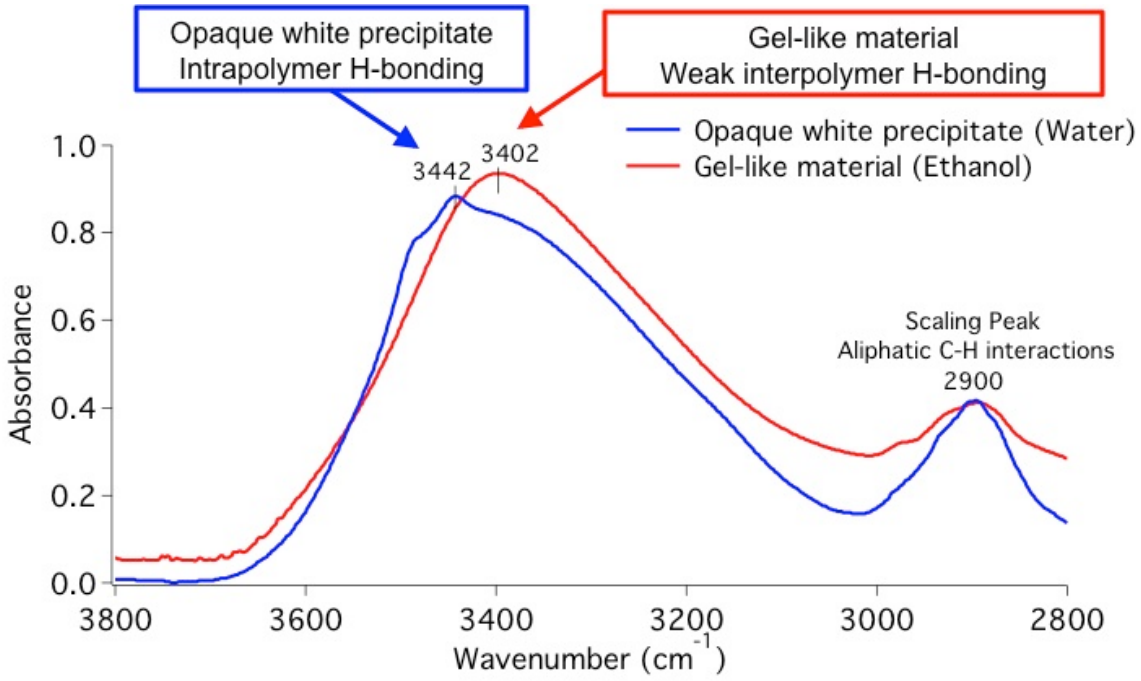

Measurement of 5 of unique batches of washed PAS cellulose were used to determine the experimental error of the peak locations reported as one standard deviation. The error bars are too small to be visible at this scale.

Characterization of hydrogen bonding through spectral subtraction

A linear trend in the FTIR absorbance characteristics of hydrogen and covalent bonding in cellulose was observed (Figure 4.18). This shows Beer's Law was satisfied so spectral subtraction could be used to evaluate the relative contributions of the hydrogen bonding in cellulose as a function of the wash liquid (132). The spectra of water washed PAS cellulose was subtracted from the spectra of ethanol washed PAS cellulose to yield differences in the pattern of hydrogen bonding between the two washed PAS materials. The difference spectra indicated a minimum peak at 3488 cm^{-1} with a shoulder at 3452 cm^{-1}. This suggests greater intrapolymer bonding in water washed PAS cellulose (Figure 4.19). The maximum peaks in the difference spectra at 3380 and 3220 cm^{-1} indicated increased interpolymer interactions in ethanol washed PAS cellulose. The broad peak at 3045 cm^{-1} indicated greater possible intersheet interactions in ethanol washed PAS cellulose. The difference spectra indicated that intrapolymer interactions are dominant in water washed PAS cellulose. Whereas interpolymer and intersheet interactions are more significant in the structure of ethanol washed PAS cellulose.

Figure 4.18 – FTIR absorption as a function of mass of cellulose showing Beer's Law behavior

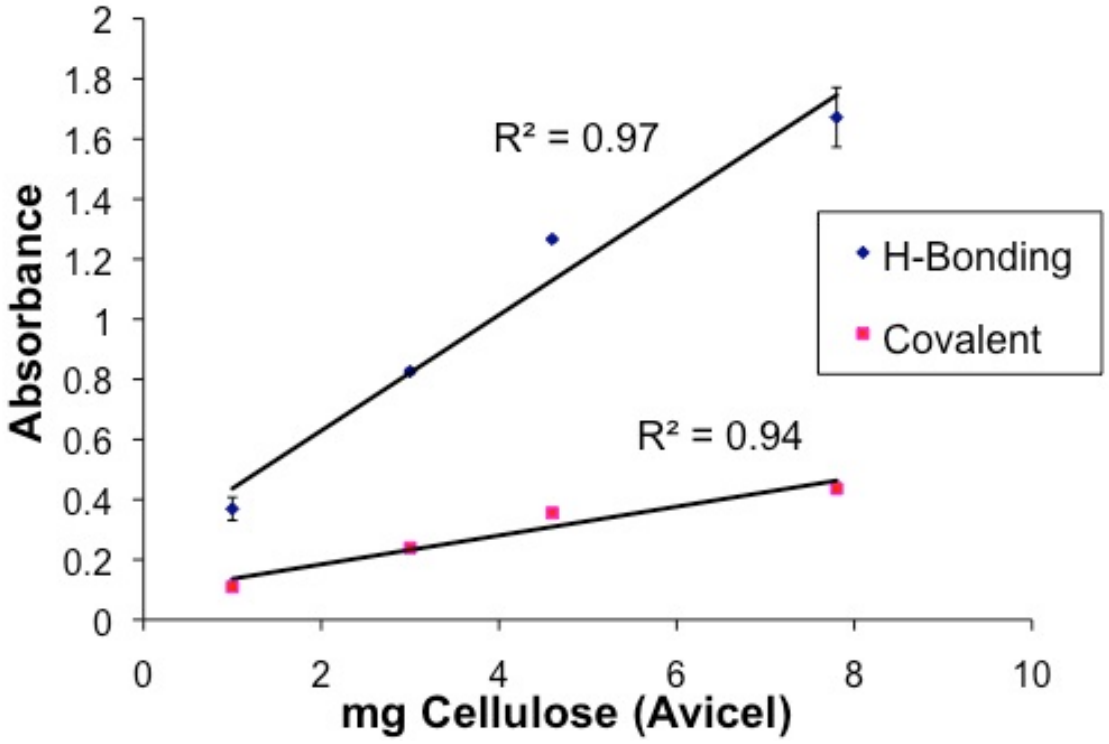

The absorbance of the peaks at 2900 cm^{-1} (C – H bonds) and 1160 cm^{-1} (β-1,4 linkage) are nearly constant regardless of disruption to the structure. The absorbance was measured in triplicate with the average absorbance ± one standard deviation reported.

Figure 4.19 – Difference spectra of water washed PAS cellulose subtracted from ethanol washed cellulose

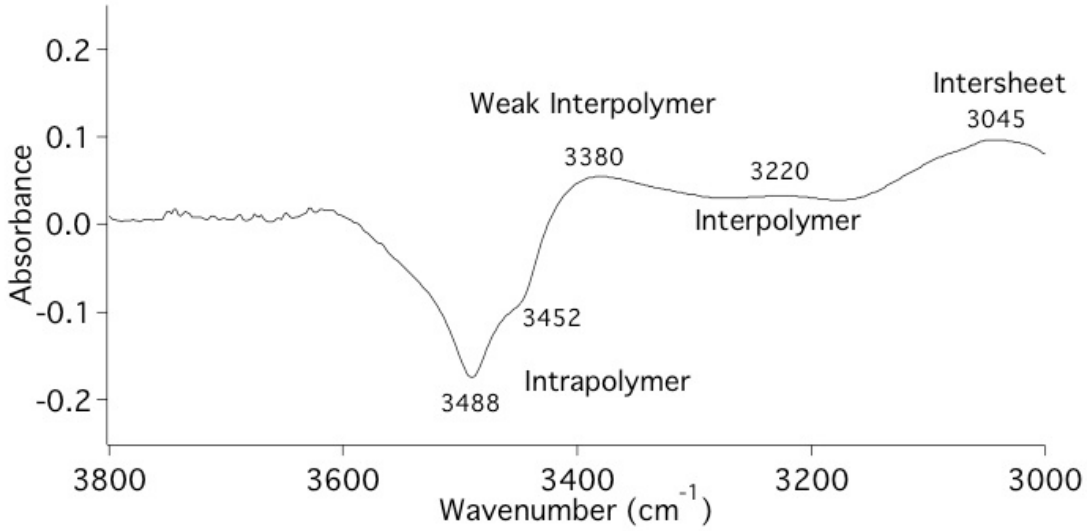

Maximum peaks indicate bonds favored in ethanol washed PAS cellulose, while minimum peaks indicate bonds favored in water washed PAS cellulose.

Characterization of C – O interactions

The spectral region of 950 to 1200 cm^{-1} represents covalent C – O interactions in cellulose, which are affected by hydrogen bonding (58). When hydrogen bonding is present the C – O vibrational energy is altered depending on the bond angle and distance. This creates a diverse set of environments which yields peak broadening. The C3 – O3 is important because it can form an intrapolymer hydrogen bonds to the O6 or O5 of the same polymer or it can form interpolymer and intersheet interactions to the O6 of neighboring polymers. The peak width was measured from the base of the peak (inflection point in the slope) at ≈1040 cm^{-1} to the corresponding horizontal wavenumber of the other side (significance determined by one standard deviation from at least 3 unique batches of material) (Figure 4.20). The peak width of the water washed PAS cellulose was 53 ± 5 while ethanol washed PAS cellulose was 31 ± 5. This indicated greater hydrogen bonding at the C3 – O3 in water washed PAS cellulose.

The hydroxymethyl group is important because it can be involved in intersheet, interpolymer and intrapolymer interactions (42). The absorbance was scaled to the β-1,4 linkage (≈1160 cm^{-1}) and was used to compare bond formation of water and ethanol washed PAS cellulose. When the conformation of the hydroxymethyl group is out of the cellulose plane in either *gg* or *gt*, a peak is observed at ≈995 cm^{-1} (42, 58). A discrete peak was detected in the spectra of water washed PAS cellulose at 997 cm^{-1}, where the scaled absorbance ratio was calculated, 0.96 ± 0.03 (Figure 4.20). This peak was not detected in the spectra of ethanol washed PAS cellulose by the peak finder in Omnic 6.2 although the calculated scaled absorbance was 1.10 ± 0.08. The lack of detection of a discrete peak in the spectra of ethanol washed PAS cellulose indicated the presence of a

shoulder and thus less ordered intersheet interactions relative to water washed PAS cellulose. The increased scaled absorbance in ethanol washed PAS cellulose, indicated numerous intersheet interactions consistent with the difference spectra relative to water washed PAS cellulose.

The hydroxymethyl group can also have the *tg* conformation in the cellulose plane which yields a peak at ≈1030 cm^{-1} (42, 58). The scaled absorbance for ethanol washed PAS cellulose, 1.34 ± 0.05, was significantly greater than that calculated for water washed PAS cellulose, 1.19 ± 0.07, which was an indication of a broad shoulder at 1030 cm^{-1} in water washed PAS cellulose. The broad shoulder in the spectra of water washed PAS cellulose indicated greater in-plane hydrogen bonding relative to ethanol washed PAS cellulose. There were not significant differences in the scaled absorbance's for the C3 – O3 and C2 – O2 bonds between water and ethanol washed PAS cellulose.

Figure 4.20 – FTIR characterization of the covalent interactions in washed PAS cellulose samples

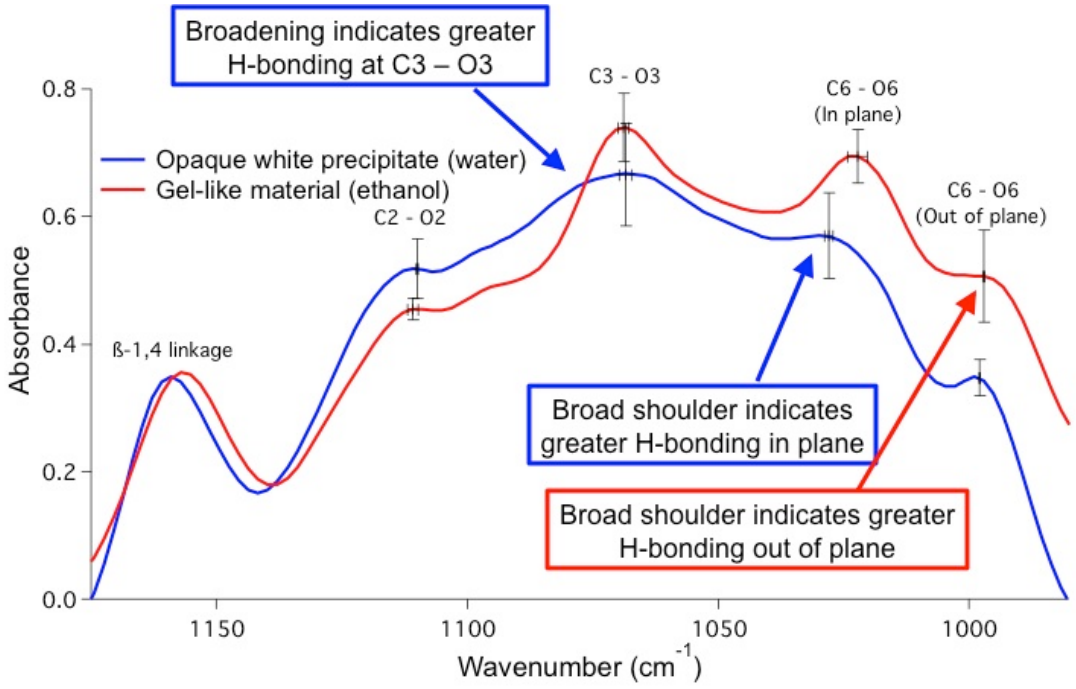

The spectra were scaled to the peak at ≈1160 cm^{-1} which represents the β-1,4 linkage of cellulose. The vertical error bars represent one standard deviation of the peak absorbance divided by the absorbance of the scaled peak for 5 unique batches of material. The horizontal error bars represent one standard deviation in the peak location.

Summary of FTIR characterization

1. *Characterization of O – H interactions*
    a. Discrete peak observed in the hydrogen bonding region of the spectra of water washed PAS cellulose suggesting intrapolymer hydrogen bonding.
    b. No discrete peak observed in the hydrogen bonding region of the spectra of ethanol washed PAS cellulose. The peak of the broad hydrogen bonding region indicated heterogeneous interpolymer interactions.
2. *Characterization of C – O interactions*
    a. C3 – O3 peak broader in the spectra of water washed PAS cellulose relative to ethanol washed PAS cellulose. Indicated greater hydrogen bonding at the C3 – O3 in water washed PAS cellulose relative to ethanol washed PAS cellulose.
    b. Broad shoulder at 995 cm^{-1} in the spectra of ethanol washed PAS cellulose suggesting diverse intersheet interactions relative to water washed PAS cellulose.
    c. Discrete peak at 995 cm^{-1} in the spectra of water washed PAS cellulose, which was an indication of cellulose II structure.
    d. Broad shoulder at 1030 cm^{-1} in the spectra of water washed PAS cellulose indicated more hydrogen bonding in plane at the C6 relative to ethanol washed PAS cellulose.

4.4 Discussion

To facilitate the development of advanced pretreatments, the interaction of individual organic liquids with cellulose was characterized in the attempt to understand at the nano scale the interactions of selected organic solvents with cellulose during a pretreatment. Uniform starting conditions of PAS cellulose enabled the disruption to the cellulose nanostructure caused by washing with organic liquids to be investigated. PAS cellulose washed with selected thermodynamically favorable liquids, as determined by Flory Huggins theory, formed partially transparent gels with increased disruption and altered hydrogen bonding networks. The main effect of the favorable liquids was the apparent disruption of the hydrogen bonds linked to the C6 hydroxyl of each sugar in the cellulose structure. Favorable cellulose/organic liquid interactions at the C6 hydroxyl increased heterogeneous interpolymer hydrogen bond cross-links which may have contributed to the gel-like qualities of the material. Unfavorable interactions that increased intrapolymer interactions and ordered interplaner interactions were associated with the formation of an opaque white precipitate. The results indicate that solvent properties such as the tendency to form hydrogen bonds and polar interactions, likely associated with ethanol and acetone, disrupt cellulose nanostructure which improves accessibility for enzymes to digest the material. The results provide a molecular explanation for the effects of some organic liquids in pretreatments and should lead to the development of advanced pretreatment technologies involving solvent mixtures.

Initially, the Flory Huggins theory for solution thermodynamics of polymers was used to predict potential organic liquids with favorable interactions with cellulose. Selection of the liquids to be evaluated was further refined by their potential affinity to

interact with hydrogen bonding and hydrophobic regions of the glucose units in cellulose and their impact on the efficacy of pretreatments. Alcohols were selected based on their ability to form hydrogen bonds with the hydroxyls of glucose that would disrupt hydrogen bonding interactions between cellulose polymers. This was supported by prior work showing that alcohols have improved the degradability of biomass (98, 99). Based on the SANS fractal analysis the wash liquids that yielded the lowest χ parameters, (methanol, ethanol, and ethylene glycol) yielded the most disrupted cellulose, while the least favorable, water, yielded the least disrupted cellulose. The calculated χ parameters for 2-propanol and acetone were in between the alcohols/glycol and the result was intermediate disruption. The calculated χ parameter was determined to scale inversely proportional to increased disruption in agreement with theory. The $\chi = 0.5$ boundary for favorable/unfavorable interaction often given in literature was not consistent with the results, since 2-propanol and butanol did not follow predictions.

To reduce the impact of the energy barrier to solubilization and to simply focus on solvent-cellulose interactions, a two step process was employed in which cellulose was first solubilized in phosphoric acid (17) and then a second liquid was used to wash the solubilized PAS cellulose. Solvent-polymer interactions were explored in the second liquid in which retained phosphate was not apparent. When the tested liquids were used to wash PAS cellulose, two types of material were observed: a semi-transparent gel or an opaque white precipitate. The wash liquids predicted to have unfavorable interactions with cellulose (methyl ethyl ketone and water) yielded an opaque dense white precipitate whose physical properties were consistent with minimal disruption of the cellulose nanostructure. The liquids predicted to have the most favorable interactions (methanol,

ethanol, and ethylene glycol), formed a partially transparent gel with properties consistent with increased disruption.

The washed PAS cellulose had distinct structures and morphologies. The fitted power law exponent (α) of the SANS data represents the fractal dimension of the cellulose nanostructure on the length scale of 6 to 483 nanometers ($d = 2\pi/q$) (24, 27). The α of Avicel was -3.56 which represented a fractal surface, with unsmooth edges (24, 25). After Avicel was solubilized in phosphoric acid the α was -1.89 which indicated disruption to the fractal surface to yield swollen polymers. Water washed PAS cellulose had an α of -2.40 consistent with the disruption of the cellulose nanostructure relative to Avicel (18, 129, 130). The increased value of α for PAS cellulose washed with methanol, ethanol or ethylene glycol relative to water washed PAS cellulose indicated increased disruption of the cellulose nanostructure (18, 24, 149) (Figure 4.21). The $\alpha \approx -2$ indicated the cellulose nanostructures still formed rod-like aggregates, which could be caused by hydrogen bonding cross-links in cellulose. PAS cellulose washed with acetone and 2-propanol had values of α similar to that of water, which indicated these liquids did not improve disruption. The fitted power law exponent indicated the nanostructures of PAS cellulose washed with methanol, ethanol and ethylene glycol were the most disrupted of the washed structures characterized.

Figure 4.21 – Possible interpretation of the fitted power law exponent applied to disrupted cellulose

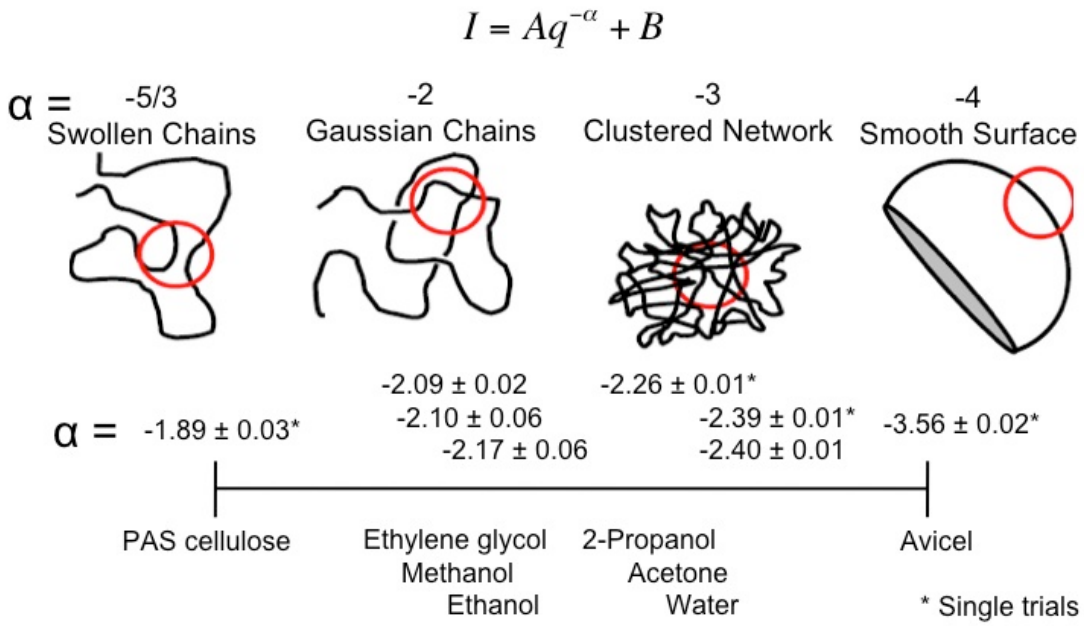

The fitted power law exponent, α, represents trends in the polymer clustering. The black bar represents the range of α's from the starting material Avicel, α = -3.56, to phosphoric acid solubilized (PAS) cellulose, α = -1.89. Polymer figures reproduced with permission (24).

To verify the trend in disruption of cellulose the rate of change of the fitted power law exponent with respect to temperature, dα/dT, was calculated to evaluate thermal stability. Hydrogen bonding is highly influenced by temperature (34, 131), with disrupted cellulose structures becoming increasingly unstable at higher temperatures. dα/dT indicated that ethanol washed PAS cellulose was the most disrupted relative to water washed PAS cellulose.

The thermal stability of the washed PAS celluloses was also measured by TGA and was reported as the onset temperature of thermal degradation. Avicel was used as negative control to show the thermal stability of a crystalline material. Water washed PAS cellulose was used as a positive control to establish a baseline for disruption. The material washed with acetone, methanol, ethanol, 2-propanol, and ethylene glycol all had reduced thermal stabilities relative to water washed PAS cellulose, which suggested increased disruption. However, inconsistencies were observed in that the onset temperature of ethylene glycol washed PAS cellulose was greater than PAS cellulose washed with the other organic liquids, and acetone and 2-propanol washed PAS cellulose had onset temperatures similar to those of ethanol and methanol washed PAS cellulose. It is possible that variation in the film thickness and the rate of drying of ethylene glycol may have adversely affected the characterization (39, 146). For these reasons the thermal stability of the organic liquid washed samples could not be resolved. The most important conclusion was that the thermal stability of the organic liquid washed material was reduced relative to the Avicel and water washed PAS cellulose controls.

The degradability of washed PAS cellulose by Cel5H was consistent with disruption of the cellulose nanostructure. This enzyme is strongly biased towards

amorphous cellulose (disrupted cellulose) (128). The activity of Cel5H after 20 hours in the assay was verified using a CMC assay, which indicted significant activity relative to a control. The CMC control was essential because it showed the enzyme was still active and not denatured by residual solvent or heat of the assay. The washed PAS cellulose was equilibrated in aqueous buffer, which most likely caused a partial reversal of the disruption as cellulose is insoluble in water (82). An increase in the glucose yield, even with a partial reversal in the properties, represents the minimum increase to degradability. While methanol, ethanol, and ethylene glycol washed PAS cellulose gels indicated disrupted structure, only ethanol yielded a more degradable material compared to water washed PAS cellulose. The increased degradability of ethanol washed PAS cellulose was consistent with the SANS temperature analysis which indicated ethanol washed material to be the most disrupted.

The purpose of characterizing the molecular structure of washed PAS cellulose was to determine patterns in the hydrogen bonding networks that led to gel-like and opaque white precipitate formation. Due to low signal to noise ratio caused by the wash liquid, the characterization could not be completed in suspension, but after partial separation of the wash liquid, acceptable spectra were obtained from the washed PAS cellulose. While partial separation of the wash liquid could have altered the aggregation of the micro and nano-scale structure, comparison with crystalline cellulose controls was used to ensure the molecular scale interactions represented the patterns of bonding.

Networks of cellulose polymers are held together at the molecular level by a complex network of hydrogen bonding. Resolution of individual hydrogen bonds is difficult due to the disorder of the amorphous regions and 11 possible hydrogen bonds

which have similar vibrational energies (57, 150). The absorbance of the broad peak in the hydrogen bonding region of the spectra is affected by the heterogeneity of bonding. The peak wavenumber of the hydrogen bonding region is effected by bond distance and angle (131, 143). Thus the location of the peak in the hydrogen bonding region is an indicator of which type of bonds (e.g. intra vs. inter) were favored in the structure. In PAS cellulose washed with water, a discrete peak was observed in the hydrogen bonding region. This was interpreted to mean there is more ordered intrapolymer bonding in water washed PAS cellulose relative to ethanol washed PAS cellulose (58, 134).

The conformation of the hydroxymethyl group influences the ordering of hydrogen bonding. In water washed PAS cellulose a discrete peak was detected at ≈995 cm^{-1} for the hydroxymethyl group out to the cellulose plane in either the *gt or gg* conformations. This indicated ordered intersheet interactions similar to the structure of cellulose II in water washed PAS cellulose relative to ethanol washed PAS cellulose. The scaled absorbance was greater near ≈995 cm^{-1} in the spectra of ethanol washed PAS cellulose, but was only detected as a broad shoulder, suggesting intersheet or interpolymer interactions with a diverse set of distances and angles consistent with amorphous structure. The broad shoulder in water washed PAS cellulose at 1030 cm^{-1} indicates greater hydrogen bonding in plane relative to ethanol washed PAS cellulose, which likely forms intrapolymer hydrogen bonds to the O3 as suggested by the broadening of the C3 – O3 peak. In water washed PAS cellulose the increased ordering of intersheet interactions and intrapolymer hydrogen bonding was similar to the cellulose II control which suggests ordered packing of cellulose polymers. The increased ordering in water washed PAS cellulose likely explains the white precipitate (Figure 4.22).

Figure 4.22 – The hydrogen bond networks favored in the gel-like and opaque white precipitate

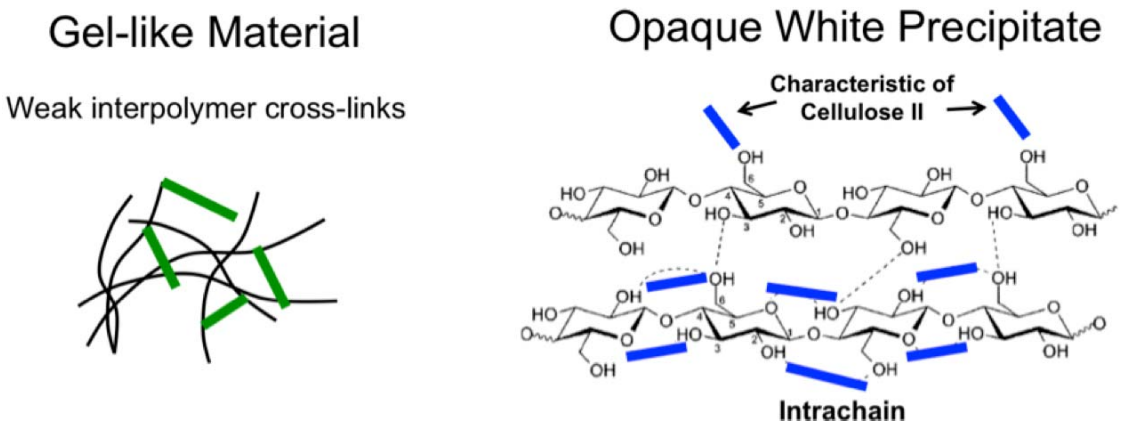

Summary of the hydrogen bonding networks in the gel-like and opaque white precipitated materials

Left: The gel-like material is composed of increased heterogeneous interpolymer hydrogen bond cross-links relative to the opaque white precipitate. The heterogeneous interpolymer bonds indicate a diverse set of bond distances and angles, which suggests increased amorphous content relative to the opaque white precipitate. **Right:** The opaque white precipitate has a tendency to form relatively more ordered intrapolymer hydrogen bonds compared to the gel-like material. The discrete peak at 995 cm^{-1} indicated ordering of the hydroxymethyl groups similar to cellulose II. Both the intrapolymer and the hydroxymethyl group suggest a relatively greater fraction of cellulose II in the opaque white precipitate relative to the gel-like material.

Although favorable liquids were identified using the Flory-Huggins theory, exceptions to the predictions were noted. A shortcoming of the Hildebrand solubility parameter used initially to evaluate compatibility of these liquids with cellulose is that it does not take into account polar and hydrogen bonding interactions (32). It is clear that polar and hydrogen bonding properties of these wash liquids are important in the disruption of cellulose because of the presence of hydroxyl groups in cellulose. Water, which easily forms hydrogen bonds with many substances including cellulose, is a poor solvent of cellulose (82). Short alcohols that can also form hydrogen bonds, but also disrupt polar interactions, increased the solvation of celluloses but longer chain alcohols with the similar properties were less effective. This argues that a balance between the disruption of polarity and hydrogen bonding is necessary to disrupt the cellulose nanostructure.

Hansen solubility parameters for dispersion, polarity and hydrogen bonding, can be used to quantify the polar and hydrogen bonding properties of the wash liquids (32, 34). Hansen solubility parameters are calculated in literature for the interactions of dispersion, polarity and hydrogen bonding (32, 135). As dispersion is nearly constant for the wash liquids, only the interactions for polarity and hydrogen bonding were evaluated (32). The polar and hydrogen bonding Hansen solubility parameters of each wash liquid were plotted to identify the contributions of each interaction in precipitation (Figure 4.23) (32, 151). The plot of the polar vs. hydrogen bonding solubility parameters (32, 135, 152) hypothesized that a region of gel-like structures is indicated. Hansen solubility parameters were not available for phosphoric acid (32, 34). It suggests a ratio of polar and hydrogen bonding interactions is required to yield gel-like material.

Figure 4.23 – The Hansen solubility parameters for each wash liquid

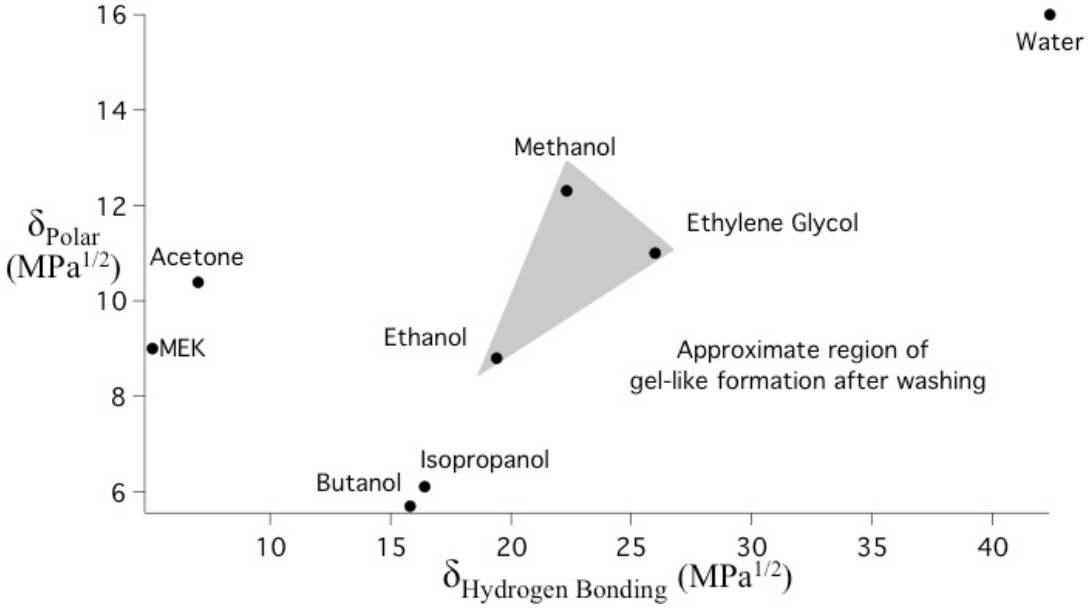

The characterization of PAS cellulose washed with organic liquids yielded information on how cellulose/solvent interactions affects the disruption of cellulose nanostructure after cellulose has been solubilized using phosphoric acid. Understanding cellulose/solvent interactions during pretreatment will enable the development of new solvent based pretreatments that could yield cellulose with disrupted nanostructure, which will ultimately increase degradability. The increase in digestibility was similar to other ethanol organosolvent processes in literature such as the work by Brosse *et al.* The work in this dissertation obtained a similar increase in glucose conversion when using ethanol in the wash, but at lower temperature and reduced enzyme loading. By increasing degradability, the required enzyme loading will be reduced yielding potential cost savings.

Favorable wash liquids formed a reversible gel-like material that by definition indicates that some hydrogen bonds and/or van der Waals interactions reformed to generate cross-linking between cellulose polymers as indicated by SANS. The cellulose/liquid interaction affected the orientation of the C6 hydroxyl which disrupted both inter and intrasheet interactions as indicated by FTIR. Retention of the ability to form some hydrogen bonds for interpolymer interactions could allow the formation of the observed gels. By incorporating non-aqueous liquids into pretreatments to disrupt cellulose structure, increased degradability could be accomplished with lower associated costs.

5. Optimization of Wash Liquids and Application to Municipal Office Waste

5.1 Introduction

The objective of this chapter is to apply the investigation of fundamental wash liquid/cellulose interactions from Chapter 4 to make wash liquids more effective through the formulation of mixtures, and applicable to real materials. None of the pure wash liquids in this dissertation were able to completely solubilize cellulose. When a single solvent is unable to dissolve a polymer, often using a mixture of at least two solvents can yield increased solubilization (153). Mixtures are generally most beneficial when the polymer is stabilized by multiple forces such as in cellulose (153). The solvent mixture can be formulated to interact with properties of the polymer such as hydrogen bonding, to more effectively solubilize its structure. It is hypothesized that mixtures of wash liquids could increase the disruption of PAS cellulose. This could also be applied to process diverse biomass feedstocks to make biofuels more economical.

Of the pure wash liquids studied, ethanol was found to have the greatest impact on the disruption of PAS cellulose. Thus, ethanol was included in all mixtures with other liquids added to differ the hydrogen bonding and polar interactions. These mixtures were examined to determine if such wash liquid mixtures could increase the disruption in the cellulose structure. Ethanol/water mixtures were determined to yield the most disrupted cellulose of the blends investigated. The most effective ethanol/water mixture was defined as the mixture with the lowest volume fraction of ethanol (V_{EtOH}) required to yield a gel-like material. The most effective ethanol/water mixture was applied to wash phosphoric acid solubilized (PAS) recycled municipal office waste.

Municipal office waste (MOW) is composed of waste office paper and newsprint and is currently under consideration for use a feedstock for biofuels production (154). MOW is a near ideal feedstock because it is generally rich in cellulose, abundant, low cost, and non-edible (87, 154). MOW is advantageous because it is processed to remove lignin and hemicellulose when first made into paper (155, 156). One of the most common methods of producing paper is the Kraft process in which wood chips are heated in an alkali solution of sodium hydroxide and sodium sulfide (155, 156). This solubilizes and separates most of the hemicellulose and lignin from the cellulose pulp (155, 156). The processed cellulose pulp is washed with water and dried prior to being milled into paper (155, 156). Coatings containing calcium carbonate are often applied to paper to enhance texture and are often found on MOW (87). The degradability of the PAS MOW was improved by ≈30 % when washed with the most effective ethanol/water mixture (V_{EtOH} = 0.4) compared to conventional water washing which demonstrated the applicability of this approach. By increasing the degradability of a recycled feedstock biofuels processing could become commercially viable.

5.2 Materials and Methods

Materials and chemicals: The cellulose used in all experiments was Avicel™ (PH-101) (Sigma Aldrich). MOW was obtained from the Washington DC metropolitan area in the form of an ink free dried solid. The chemicals were obtained from Sigma Aldrich, Fisher Scientific and VWR: phosphoric acid (85 % in water), ethanol, 1-butanol, and acetone.

Calculation of the Hansen solubility parameters for binary wash liquid mixtures

The Hansen solubility parameters for polarity ($\delta_{Polarity}$) and hydrogen bonding ($\delta_{hydrogen\ bonding}$) were used from literature (Table 5.1) (32, 34). A simple mass balance was used to

calculate the Hansen solubility parameters for each binary mixture. Each binary mixture contained ethanol, with a mass fraction of 0, 0.25, 0.5, 0.75 or 1.

Preparation of disrupted cellulose: Preparation of phosphoric acid solubilized cellulose followed the protocol reported by Zhang with minor modifications as described in Chapter 4 (17). *Please see Figure 4.1 for the process diagram.*

Small angle neutron scattering was conducted at the Center for Neutron Research at the National Institute of Standards and Technology, Gaithersburg, MD using the NG3 (neutron guide) and NG7 beam lines. Minor modifications to the protocol reported in Chapter 4 were used since most of the work was performed using NG7. Each sample contained a mass fraction of 0.5 % cellulose suspended in deuterated liquid obtained from Cambridge Isotope Laboratories: d-ethanol (99 % D) and d-water (99.9 % D). Three instrument configurations were used to yield a range of $0.0009\ Å^{-1} < q = 4\pi/\lambda\sin(\theta/2) < 0.474\ Å^{-1}$ with λ equal to the neutron wavelength and θ equal to the scattering angle. Three scattering distances 13 m (λ = 8 Å), 7 m (λ = 6 Å), and 1 m (λ = 6 Å) were used for low q: $0.0009\ Å^{-1} < q < 0.025\ Å^{-1}$, intermediate q: $0.006\ Å^{-1} < q < 0.077\ Å^{-1}$, and high q: $0.029\ Å^{-1} < q < 0.474\ Å^{-1}$ respectively. The SANS data analysis was performed as reported in Chapter 4.

Table 5.1 – The Hansen solubility parameters of solvents evaluated

Wash Liquid	$\delta_{Polarity}$	$\delta_{hydrogen\ bonding}$
Acetone	10.4	7.0
1-Butanol	5.7	15.8
Ethanol	8.8	19.4
Water	16.0	42.3

These values were taken from literature (32, 34).

Composition analysis of MOW was performed using FTIR. The FTIR settings are described in Chapter 4. The potassium bromide (KBr) pellet technique was used in which a powder mixture of 99 % KBr and 1 % MOW was mixed and pressed at 8,000 lbs of pressure (132). The spectra were recorded in units of absorbance in transmission geometry in a nitrogen atmosphere. Control samples of pure Avicel, xylan, lignin, and calcium carbonate were used to determine the source of each peak in the MOW spectra. The peaks unique to each component were: cellulose, 1060 cm^{-1}; hemicellulose, 1465 cm^{-1}; lignin, 1510 cm^{-1}; and calcium carbonate, 875 cm^{-1} (58, 157). The peak height tool in Omnic 6.2 was used to determine the peak height relative to the baseline, which was used to calculate the ratios of each component.

Degradability of MOW was assessed using the protocol described in Chapter 4 and by Watson *et al*. (128).

5.3 Results

Prediction of mixtures to increase the disruption of washed PAS cellulose

Wash liquids with polar and hydrogen bonding interactions were mixed with ethanol in an attempt to increase the disruption of washed PAS cellulose. The plot of the Hansen solubility parameters for polarity and hydrogen bonding was used to predict wash liquid mixtures that could potentially expand the region of gel-like precipitation, and thus identify a more effective mixture. A mass balance was used to calculate the δ_{Polar} and $\delta_{Hydrogen\ bonding}$ for each binary ethanol mixture. Acetone was used to test the effect of increasing polar interactions, water was used to increase polar and hydrogen bond interactions and butanol was used to reduce polarity (Figure 5.1).

Figure 5.1 – The contributions of the polar and hydrogen bonding interactions for the wash liquid mixtures examined represented by Hansen solubility parameters.

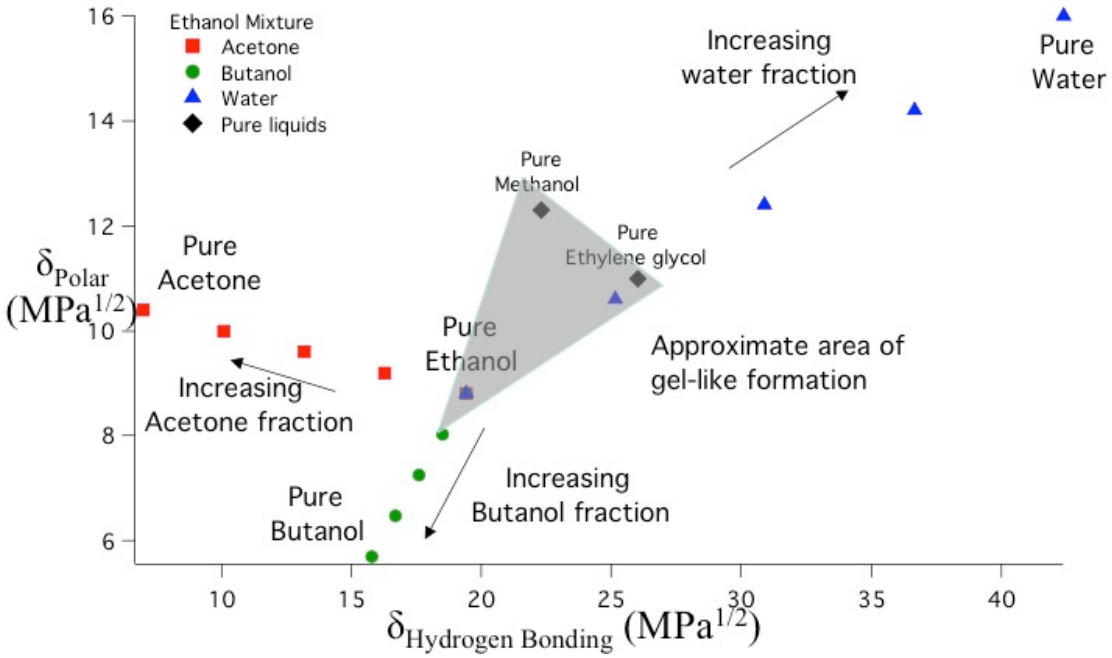

The approximate area of gel-like formation was determined from the behavior area of pure liquids that yielded disrupted PAS cellulose. Each point on the chart corresponds to a binary ethanol wash liquid mixture.

Effect of mixtures on the disruption of washed PAS cellulose

PAS cellulose was washed with mixtures of liquids with varying degrees of hydrogen bonding and polar interactions to explore how to produce the maximum possible disruption of cellulose nanostructure. The apparent disruption caused by each mixture was characterized by measuring the optical density of each suspension of washed PAS cellulose. The ratio of Hansen solubility parameters, $\delta_{\text{Hydrogen Bonding}}/\delta_{\text{Polar}}$, was used to quantify the contributions of hydrogen bonding and polar interactions during washing of PAS cellulose. When acetone and butanol were added to ethanol as the 2nd wash liquid, PAS cellulose formed an opaque white precipitate with opacity greater than or equal to that of ethanol washed PAS cellulose (Figure 5.2). This indicated no improvement to the disruption of cellulose nanostructure.

Mixtures of ethanol and water yielded washed PAS cellulose with gel-like properties when the volume fraction of ethanol (V_{EtOH}) was $\geq$ 50 %. The formation of a gel-like precipitate using ethanol/water wash mixtures was consistent with the triangle of gel-like precipitate in Figure 5.1. This suggested mixtures of ethanol and water may more effectively disrupt cellulose nanostructure relative to water or ethanol washed PAS cellulose. Other process conditions such as washing with liquids with increased pH, elevated temperature, or residual phosphate did not yield material with increased disruption.

Figure 5.2 – Optical density (opacity) of PAS cellulose washed with ethanol mixtures as a function of Hansen solubility parameters, $\delta_{\text{Hydrogen Bonding}}/\delta_{\text{Polar}}$.

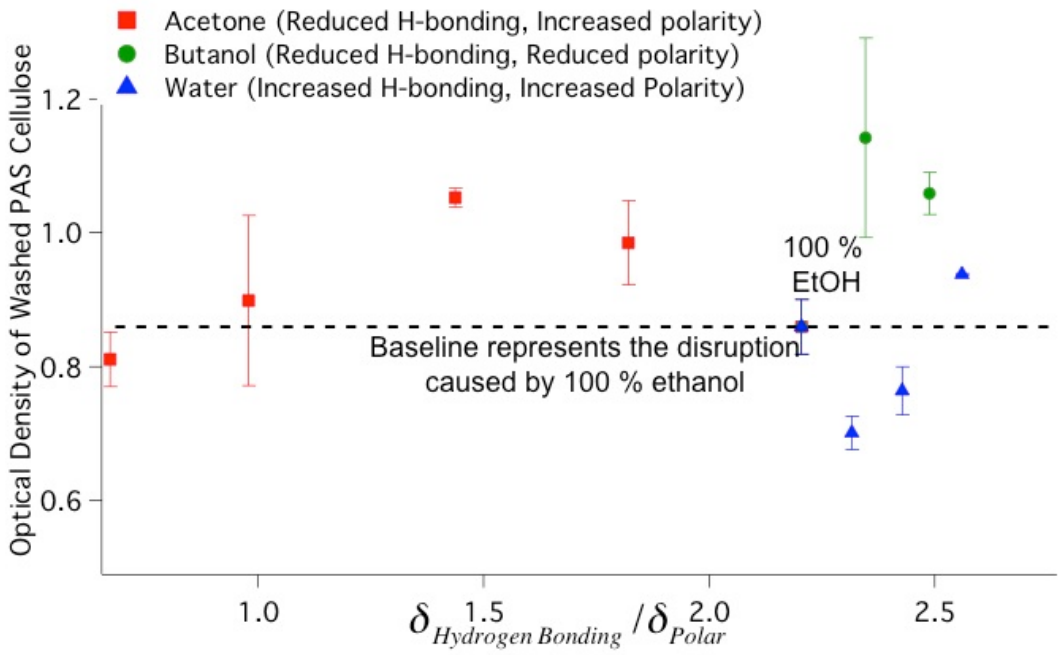

The dashed line represents the optical density of samples washed with pure ethanol. Samples with optical densities below the dashed line indicate mixtures that were less opaque and likely more disrupted than samples washed with pure ethanol. The error bars represent the standard deviation of triplicate measurements of each material.

Effect of ethanol/water mixtures on the disruption of washed PAS cellulose

Ethanol/water mixtures appeared to yield washed PAS cellulose with gel-like properties that was at least as disrupted as material washed with pure ethanol or pure water. PAS cellulose washed with ethanol/water mixtures was initially characterized using OD600 to determine the apparent number density, which is indicative of polymer aggregation. The OD600 reading was stable for greater than 1 hour. The OD600 of PAS cellulose washed with pure ethanol was 0.86 ± 0.04 and was used as a control to determine if washing with mixtures yielded washed material with increased disruption. When PAS cellulose was washed with V_{EtOH} in the range of 0.4 to 0.75, the OD600 of the washed PAS cellulose was statistically significantly lower relative to that of the PAS cellulose washed with pure ethanol as defined by one standard deviation (Figure 5.3). This indicated that the combination of hydrogen bonding and polar interactions of ethanol/water mixtures may increase the disruption of PAS cellulose relative to washing using only pure liquids.

Figure 5.3 – Optical density as an indicator of the apparent disruption of washed PAS cellulose in ethanol/water mixtures

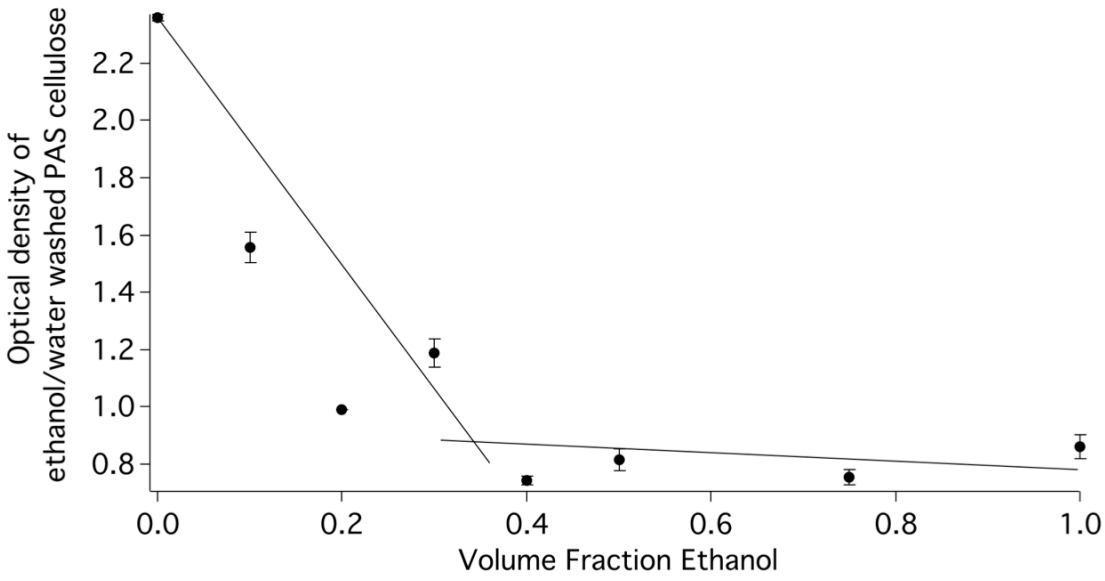

The trend lines was drawn by hand. The error bars represent the standard deviation calculated from duplicate measurements of each material.

Effect of ethanol/water wash mixtures on the cellulose nanostructure

The apparent increased disruption to the cellulose nanostructure of PAS cellulose washed with ethanol/water mixtures was characterized and was compared relative to PAS cellulose washed with pure liquids. SANS was used to characterize suspensions of disrupted PAS cellulose washed with ethanol/water mixtures. The relative scattering intensity at low q is one indication of disruption since scattering intensity decreases as disruption increases due to a reduction in concentration fluctuations (24, 25) (Figure 5.4).

The scattering from suspensions of PAS cellulose washed with ethanol/water mixtures exhibited fractal behavior indicative of the level of clustering in the cellulose nanostructure (24, 25). To quantify the clustering of washed PAS cellulose, the average power law exponent, α, was fitted in the range of $0.0030\ Å^{-1} < q < 0.18\ Å^{-1}$ using equation 2 from Chapter 4. There was not a significant difference in the slope between the low q and intermediate q range due to instrument error. The fitted α was analyzed as a function of V_{EtOH} (Figure 5.5). The R^2 values of linear fits in the region of V_{EtOH} =0 to 0.4 and 0.5 were assessed to determine at which point increasing V_{EtOH} did not further decrease the fitted power law exponent. Consistent with the R^2 value for the SANS scattering intensity, the highest value was 0.99 for the range of V_{EtOH} =0 to 0.4. The disruption of washed PAS cellulose was similar between V_{EtOH} = 0.4 (α = -2.21 ± 0.01) and V_{EtOH} = 1 (α of -2.17 ± 0.01) which suggests PAS cellulose forms gel-like nanostructures when V_{EtOH} = 0.4 or greater.

Figure 5.4 – SANS characterization of washed PAS cellulose using ethanol/water mixtures

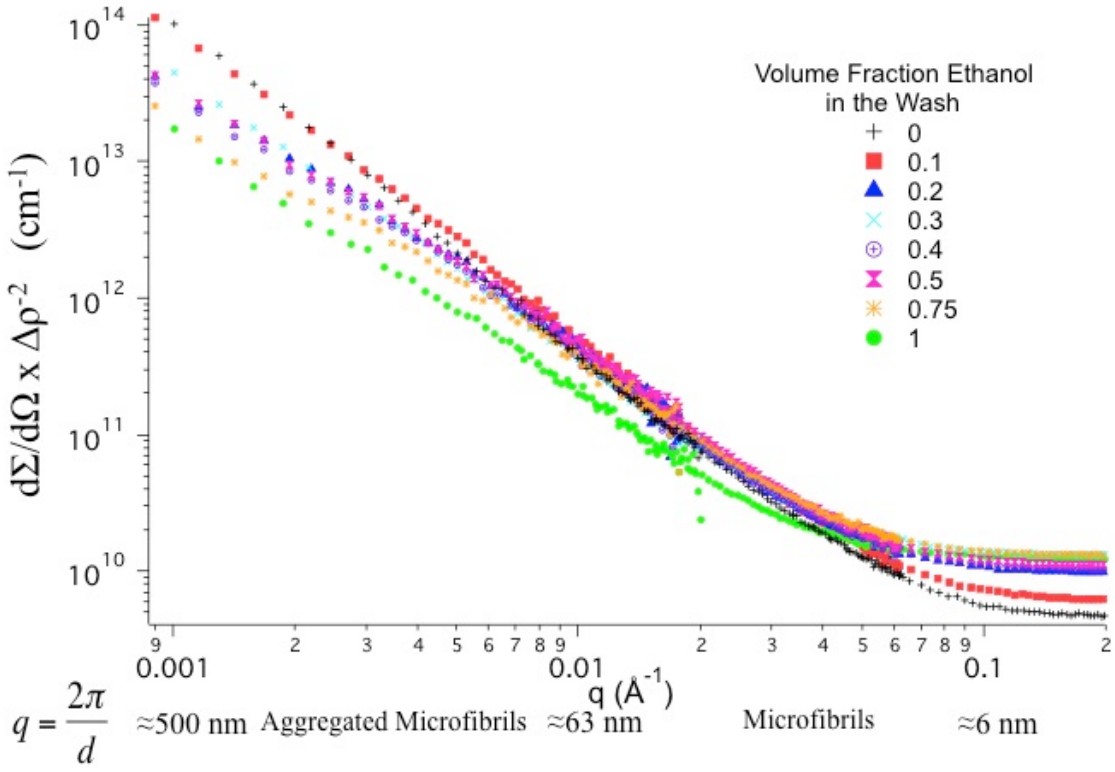

The y-axis represents the scattering intensity corrected for the contrast factor. The error bars are sufficiently small to be shown at this scale.

Figure 5.5 – Fitted α's of ethanol/water washed PAS cellulose

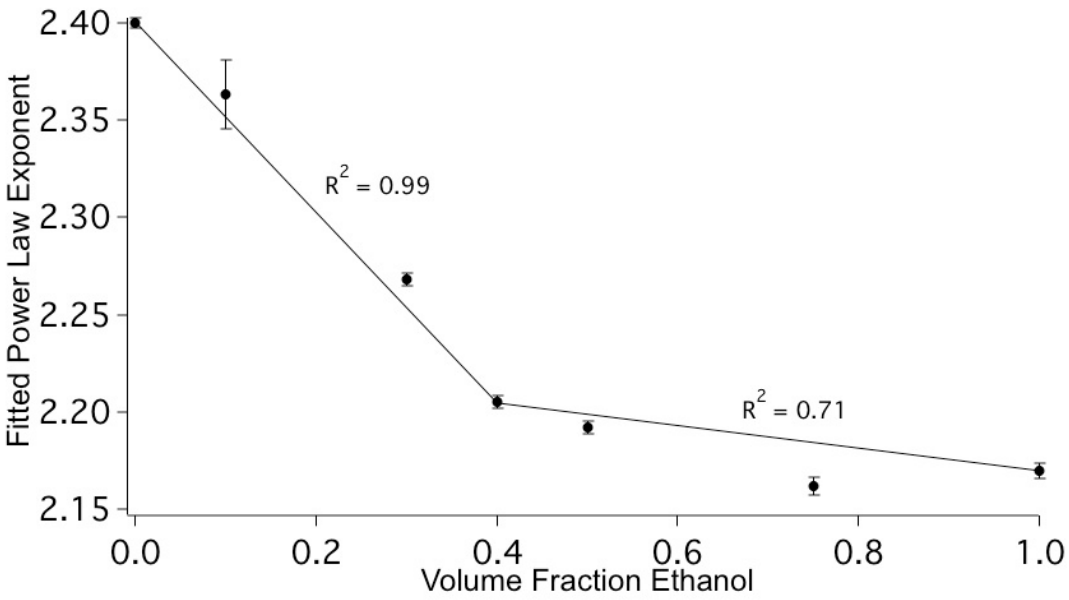

The error bars represent the statistical fitting error calculated using Igor Pro 6.11. Each value of α on the y-axis represents the (-) value. The R^2 values represent the goodness of fit of the linear trend lines. The trend line was drawn by hand to guide the eye.

Application to real biomass: processing municipal office waste (MOW)

To further the development of biofuels processing, the most effective ethanol/water mixture (V_{EtOH} = 0.4) was applied to washing acid solubilized MOW. FTIR was used to evaluate the composition of the MOW to determine the cellulose content. The composition of MOW was calculated to be approximately 66 % cellulose, 15 % xylan, and 19 % calcium carbonate (instrument and experimental error were approximately 8 %) (Figure 5.6). Since cellulose was calculated to be the dominant component, MOW is likely a feasible feedstock for biofuels applications.

Demonstration of Principle with MOW

To determine the feasibility of applying ethanol/water mixtures to actual recycled biomass to yield digestible material, the effects to the nanostructure of MOW from washing were compared to that of Avicel prepared under identical conditions. The MOW was solubilized using phosphoric acid and was washed using V_{EtOH} = 0.4 in water. SANS was used to compare the disruption to the cellulose nanostructure of PAS MOW to that water washed PAS cellulose (Figure 5.7). The fitted power law exponent, α, of the PAS cellulose washed with V_{EtOH} = 0.4 was -2.21 ± 0.004 whereas the α of the washed PAS MOW was -2.26 ± 0.004. The minimal difference indicated the ethanol/water mixture could be applied to disrupting the nanostructure of cellulose in MOW.

Figure 5.6 – FTIR composition analysis of as received MOW

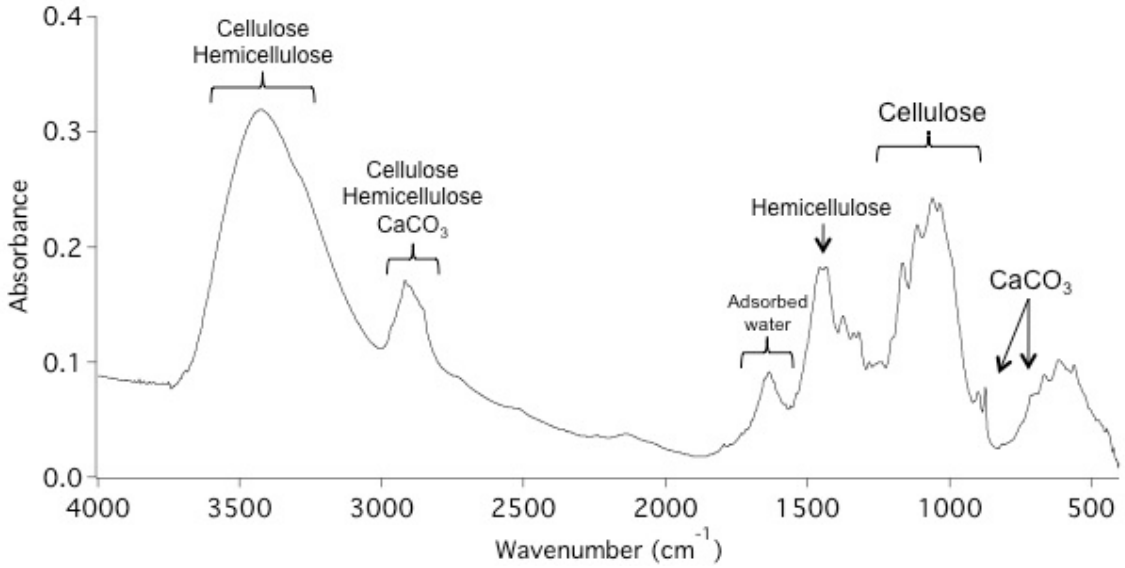

The composition of MOW was analyzed to determine if there was sufficient glucose content to be used as a feedstock for biofuels. Each region of the spectra is labeled to show the absorbance contributed by each component (58, 157, 158).

Figure 5.7 – Comparison of SANS data for PAS cellulose and PAS MOW washed with a V_{EtOH} = 0.4

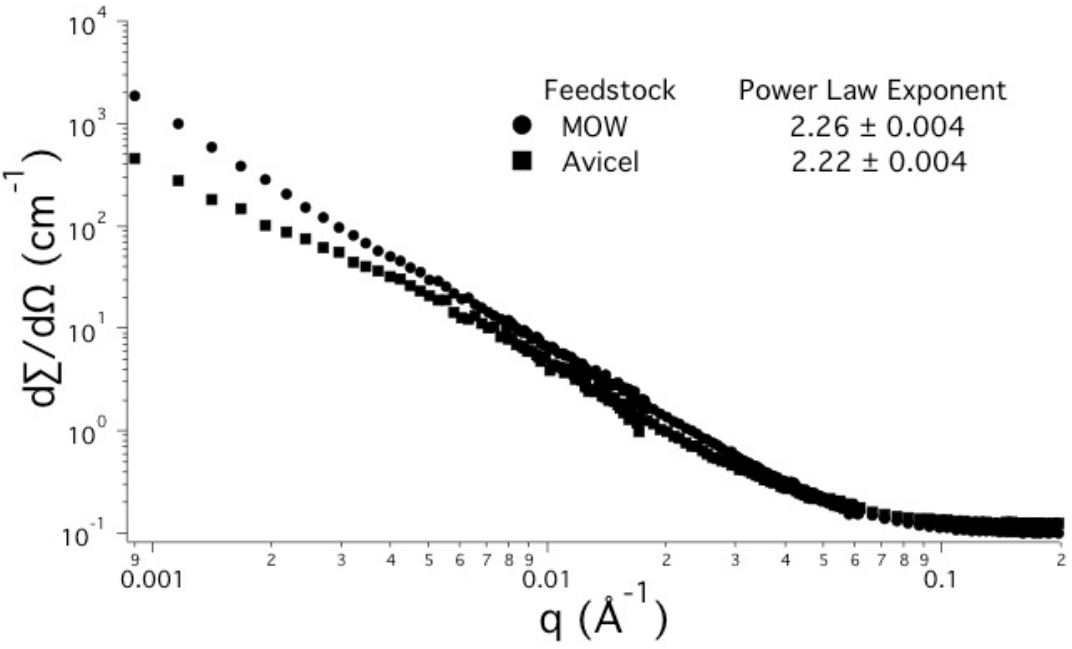

The applicability of the acid solubilization protocol was determined by comparing PAS cellulose and PAS MOW side by side. Error bars were too small to be shown at this length scale.

Degradability of washed PAS MOW

The degradability of PAS MOW washed with V_{EtOH} = 0.4 in water was compared to that of PAS MOW washed with water (conventional process) to assess the benefit of using ethanol in the wash. Each PAS washed material was equilibrated in aqueous enzyme assay buffer. While this may have caused a partial reversal in the gel-like properties, it was necessary to create optimal assay conditions for the enzyme and was common to both washed samples. The degradability was measured from the glucose yield produced by *S. degradans* Cel5H, which preferentially acts on amorphous cellulose (128). After 20 hours the glucose product concentration from MOW pretreated with V_{EtOH} = 0.4 was 0.64 ± 0.02 μmol/ml compared to 0.44 ± 0.03 μmol/ml for water washed PAS MOW (Figure 5.8). This indicated that PAS MOW washed with V_{EtOH} = 0.4 increased enzyme accessibility to the substrate and thus by inference, disruption of the material relative to PAS MOW washed with water.

Figure 5.8 – The degradability of PAS MOW by *S. degradans* after washing with V_{EtOH} = 0.4 in water

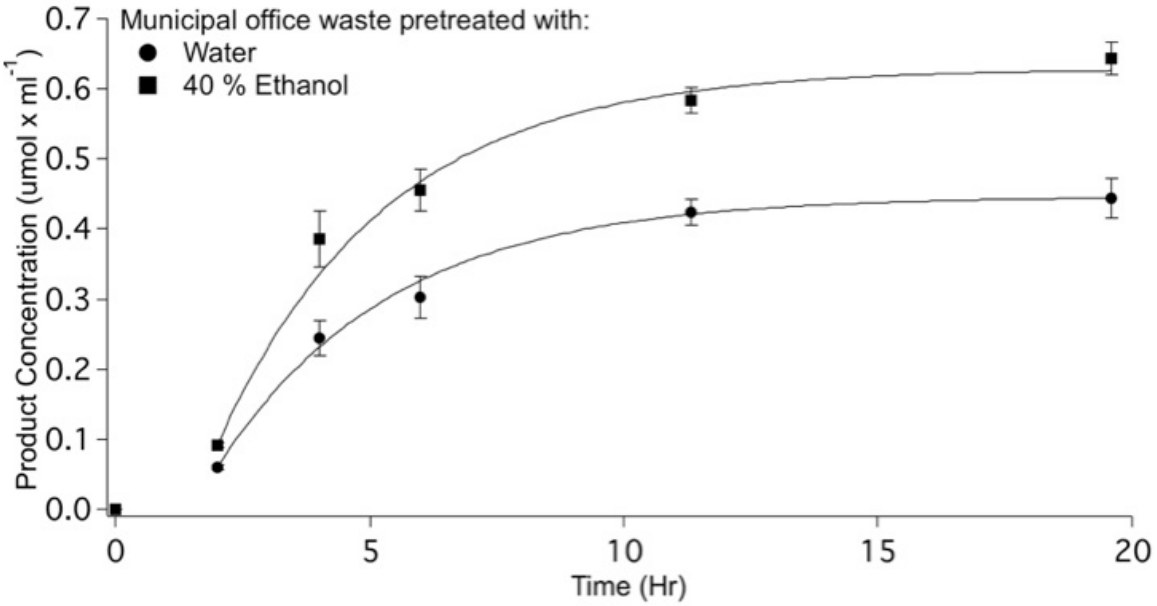

The error bars represent one standard deviation calculated from triplicate trials.

5.4 Discussion

Ethanol was previously determined to produce the least stable and most degradable PAS cellulose nanostructure, due in part, to its hydrogen bonding to hydroxyl groups and aliphatic methyl groups. Other wash liquids were mixed with ethanol to vary the hydrogen bonding and polar interactions of the wash liquid to disrupt the cellulose nanostructure in the washed PAS material. The significant finding was that mixtures of ethanol and water were the most effective in producing washed PAS cellulose. It is hypothesized that the ethanol moderated the high polar and hydrogen bonding interactions of water. The addition of polar (acetone) and less polar (butanol) liquids did not increase disruption relative to PAS cellulose washed with pure liquids. Using a 40 % ethanol/water mixture the degradability of MOW was improved by ≈30 % which demonstrates the potential to yield sugars from recycled materials for subsequent biofuels production.

Ethanol was included in all mixtures examined because it increased the degradability and reduced the thermal stability (SANS) of the washed PAS cellulose the most relative to the other wash liquids investigated in Chapter 4. Ethanol has also been found to increase the degradability of cellulose in industrial pretreatments (99). Ethanol is advantageous because it has a hydroxyl group capable of hydrogen bonding and two methyl groups that can interact with the face of the glucosyl ring of cellulose (34). The polarity of the wash mixture was varied by adding acetone, which has a highly polar double bonded oxygen, and butanol which has reduced polarity compared to ethanol due to the increased number of methyl groups (34). The hydrogen bonding character of the wash mixture was varied by adding water which has a strong tendency to form hydrogen

bonding (also highly polar) (34). Increased polar interactions contributed by acetone in ethanol mixtures did not increase the observed disruption relative to PAS cellulose washed with pure ethanol or acetone. The increase in hydrogen bonding interactions from water was the most effective in increasing the region of gel-like structures in washed PAS treated cellulose (Figure 5.9). By identifying the region of polar and hydrogen bonding interactions that yielded gel-like disrupted cellulose, mixtures of wash liquids could be tailored to individual applications. Although the region of gel-like formation was constructed using several different pure liquids and mixtures, it was not universally applicable to the washing of PAS cellulose. For example, acetone/water mixtures in this range were not able to yield gel-like material, which suggests other factors such as molecular size and functional groups must be considered.

Figure 5.9 – The mixtures of wash liquids that yielded washed PAS cellulose with gel-like properties as a function of Hansen solubility parameters

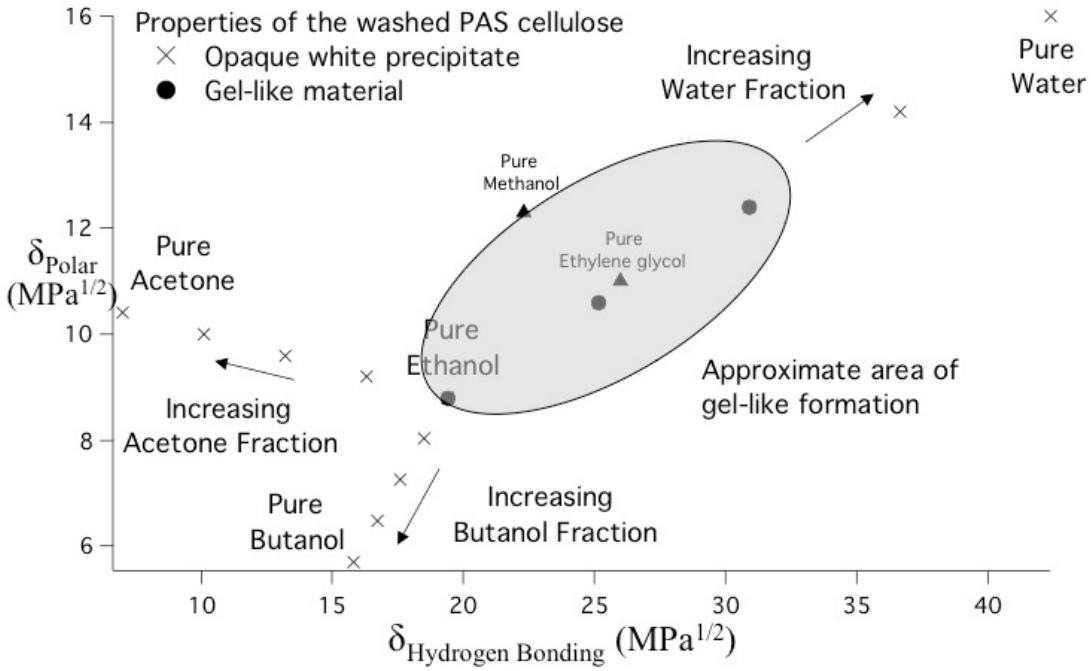

The shaded area is the approximate region where each ethanol/water mixture as well as pure methanol and ethylene glycol (triangles) yielded gel-like precipitates.

The scattering at low q of the mixture washed PAS cellulose could be described using fractals. The power law model was used, in which the exponent α, represents the fractal dimension of the cellulose nanostructure (24, 25, 27). The fitted power law exponent, α, represents an average of clustered swollen polymers α = -2 and clustered networks when α = -3 (24, 25). The increase in α from -2.40 to -2.21 as V_{EtOH} was increased from 0 to 0.4 indicated increased disruption to the cellulose nanostructure. This corresponds to a transition in the washed material from an opaque white precipitate to gel-like formation. The disruption to PAS cellulose when $V_{EtOH} > 0.4$, α = -2.20, only improved to α = -2.17 for $V_{EtOH} = 0.75$ and 1 which was consistent with the SANS intensity at low q which indicated that increasing $V_{EtOH} > 0.4$ did not change disruption. Both the SANS intensity and fitted α indicated that after the washed PAS cellulose has undergone the gel-like transition near $V_{EtOH} = 0.4$, increasing V_{EtOH} did not further disrupt the nanostructure and was thus the most effective wash liquid mixture.

Further analysis of this phase transition was attempted through SANS at different temperatures. Initial experiments attempted to determine the transition temperature by analyzing the inverse SANS intensity at low q as a function of inverse temperature (159). However, since the cellulose polymers were in suspension and not solution, it is unclear what physical significance this transition temperature represented.

The ultimate goal of cellulose materials research is to develop a solvent system, to fully solubilize cellulose in conditions suitable for enzymatic degradation. The interactions of ethanol and water indicated that both polar and non-polar functional groups are required to disrupt cellulose. The non-polar groups are required to interact with the glucopyranose ring, while the polar group is required to interact with the

hydroxyl groups of cellulose. Further research is necessary to determine how the electronic structure of the molecule affects interactions with cellulose. By completely solubilizing cellulose, increased enzyme accessibility would likely yield a dramatic increase in degradability, which could make cellulosic biofuels commercially viable.

In order for any feedstock to be commercially viable it must contain a high fraction of cellulose. In this study, the cellulose fraction of MOW was evaluated through a composition analysis using FTIR. The finger print region of cellulose (900 to 1200 cm^{-1}) clearly indicated the presence of cellulose in the MOW spectra (58). The broad peak in the region of 1430 to 1460 cm^{-1} indicated crosslinking of the cellulose and xylan polymers which suggested the presence of hemicellulose (157). Discreet peaks for calcium carbonate were observed at 875 cm^{-1} and 775 cm^{-1}. The absence of lignin was obvious due to the lack of an aromatic signature in the region of ≈1510 cm^{-1} (158). The relative amount of cellulose was 66 % so the composition analysis established MOW is rich in cellulose and is thus a suitable feedstock.

Acid pretreatment is widely applicable to a variety of biomass feedstocks, but the use of V_{EtOH} = 0.4 in water for washing PAS treated recycled MOW is novel and had to be demonstrated to show applicability of the method. Avicel and MOW were pretreated side by side using the protocol to prepare PAS cellulose. SANS was used to compare the effects to the disruption of the cellulose nanostructure of washed PAS cellulose (Avicel) to washed PAS MOW. Comparing the SANS intensity directly was not appropriate because the MOW contained additional phases (contaminants). Thus, the SANS power law exponent fitted to the scattering from both materials was compared. The values of α

only varied by 0.05, which indicated the protocol to prepare PAS cellulose (Avicel) could be applied to MOW.

The degradability of cellulose structure to enzymatic degradation is a critical barrier to the efficient release of sugars (2). The glucose yield is the best measure to compare the degradability of two materials, because the data are taken over a time course which provides numerous points for statistical analysis. The conversion of material is also important because higher material conversion translates to lower cost. The ≈30 % increase in degradability of the PAS MOW washed with V_{EtOH} = 0.4 relative to water washed PAS MOW demonstrated the application of non-aqueous liquids in wash mixtures to a real material.

Ethanol/water mixtures were determined to cause similar disruption to cellulose nanostructure compared to pure ethanol washed PAS cellulose and were successfully applied to increase the degradability of MOW. The combination of hydrogen bonding and polar interactions in the wash mixtures induced disruption of washed PAS cellulose to form a gel-like material. The transition from an opaque white precipitate to gel-like material was investigated which determined that increasing V_{EtOH} after the transition to gel-like material only marginally enhanced disruption. The ethanol/water mixture that produced the most disrupted washed PAS cellulose using the least ethanol was applied to processing MOW. The application to MOW represents how fundamental thermodynamic interactions can be applied to diverse and especially, commercial materials.

6. Conclusion

The objective of this dissertation was to develop an understanding of how solvents could be used to disrupt cellulose nanostructure to improve degradability by enzymes. The most effective pure wash liquid was ethanol, which after washing PAS cellulose yielded a gel-like material. The properties of the gel-like material were characterized on both the nano and molecular scale to understand how the interactions of the wash liquid affected the polymer structure in terms of the state of aggregation of the cellulose nanostructures and in particular, the relative fractions of inter and intrapolymer hydrogen bonds.

Specifically, the gel-like material indicated there was increased disruption of the cellulose nanostructure as indicated by the SANS results (α = -2.17) relative to the opaque white precipitate (α = -2.40). The increased α of the gel-like material indicated reduced polymer clustering of the rod-like cellulose polymers relative to the opaque white precipitate. Hydrogen bonding is the force binding the cellulose nanostructures characterized by SANS. The gel-like material has a network of heterogeneous interpolymer cross-links which likely prevented ordering of the system, which was evident by the increased SANS α (α = -2.17) relative to the opaque white precipitate (α = -2.40). The hydrogen bonding of the opaque white precipitate showed ordered intrapolymer hydrogen bonding and a hydroxymethyl group conformation similar to that of cellulose II relative to the gel-like material. The increased crystallinity of the opaque white precipitate is believed to be a result of increased clustering of the cellulose polymers relative to the gel-like material, which is consistent with the reduced α (α = -2.40). Understanding the influence hydrogen bonding and polar interactions have on the

washing of PAS cellulose, enabled the formulation of wash mixtures that were as effective as pure ethanol but more appropriate for enzymatic degradation due to decreased ethanol content.

Reducing the polymer clustering and increasing the amorphous content of the gel-like material relative to the opaque white precipitate improved enzyme accessibility. This was evident by the 30 % increase in the glucose yield of Cel5H acting on the gel-like material relative to the opaque white precipitate. Since the substrate material was re-equilibrated in aqueous assay buffer, this represents the minimum possible increase to degradability.

Wash liquid mixtures were formulated to increase the disruption to the material. The most effective wash mixture was 40 % ethanol in water, which was the lowest volume fraction of ethanol required to yield a gel-like material. The efficacy of this wash mixture was tested using municipal office waste (MOW). The pretreated MOW was characterized using SANS, which had an $\alpha = -2.26$ compared to $\alpha = -2.21$ for PAS cellulose washed under identical conditions. Since the α's only varied by 0.05 the wash protocol was applicable to MOW. As with pure Avicel, the cellulose nanostructure of PAS MOW was disrupted and had the morphology of a gel-like structure after washing with 40 % ethanol in water. Cel5H acting on gel-like PAS MOW yielded a similar 30 % increase in glucose yield which indicated increased enzyme accessibility. This work has the potential to enhance the commercial viability of cellulosic biofuels production by using a common solvent to disrupt the cellulose nanostructure of a recyclable biomass feedstock.

The main contributions of this dissertation are:

1. Identification of novel processive enzymes, which enable *S. degradans* to degrade cellulose independent of cellobiohydrolase activity. The processive ratios of Cel5G, Cel5H and Cel5J were greater than 4, which indicated multiple rounds of cleavage before dissociation from the substrate. By utilizing enzymes with characteristics of both an endoglucanase and a cellobiohydrolase only one enzyme is required to degrade cellulose directly to cellobiose, which reduces the required enzyme loading.
2. The gel-like cellulose nanostructures observed in ethanol washed cellulose were related to heterogeneous interpolymer hydrogen bonded cross-links. The formation of the opaque white precipitate for water washed materials was the result of more highly ordered intrapolymer and hydroxymethyl groups in a structure similar to crystalline cellulose II.
3. Hansen solubility parameters were used to identify ethanol/water mixtures as having the best potential to interact through hydrogen bonding and polar forces. SANS characterization indicated the most effective wash liquid mixture was 40% ethanol in water. This mixed wash liquid yielded gel-like cellulose structures while minimizing the amount of ethanol in the mixture. This is important because the enzymes denature in pure ethanol and ethanol is more expensive than water.
4. Application of the 40 % ethanol in water wash liquid mixture to disrupt the cellulose nanostructure of MOW. This suggests a pathway to an economical recyclable feedstock for the production of cellulosic biofuels.

7. Future Directions

The work of this dissertation examined the intermolecular interactions that yield material with increased disruption relative to the conventional water washing process. Future research should work to synthesize new wash liquids that have both polar and hydrogen bonding properties on the same molecule. By increasing the electrostatic interactions between the solvent and cellulose the driving force to keep the polymers soluble will become greater. To achieve this objective several questions related to the pretreatment and enzymology processes could be addressed:

1. Use of favorable liquids to lower the concentration of cellulose solvent

   One of the most costly steps of the bioconversion process is solubilization of cellulose using 85 % phosphoric acid. It is likely the favorable liquids could be added to reduce the acid concentration. Because phosphoric acid is soluble in ethanol/water mixtures a potential future experiment could evaluate more dilute phosphoric acid solutions in the ethanol/water solvents. If favorable interactions reduce the amount of phosphoric acid required, cost and negative environmental impacts would be reduced.

2. Using glucose to increase disruption to cellulose nanostructure

   Cellulose chains reform structures through hydrogen bonding, after washing PAS cellulose. Cellulose/solvent hydrogen bonds with a pure solvent such as ethanol were not strong enough to completely disorder the structure, but a molecule capable of increased hydrogen bonding could increase disorder. By adding a molecule to the wash that the cellulose can form increased hydrogen bonding with, such as glucose could disorder the cellulose nanostructure.

3. Investigation of the phase transition that occurs during washing to yield a gel-like material or opaque white precipitate

   Understanding how the material can be transformed into a more degradable state is important because the thermodynamics could be used to predict even more favorable liquids. The research question could ask: What is the mechanism of the phase transition? To address this question analyzing material washed with ethanol/water mixtures using SANS at elevated temperatures could be insightful. Initial SANS analysis at varying temperatures of solubilized cellulose washed with ethanol/water mixtures suggested the presence of a critical temperature. However, the nature of the critical temperature was unclear and should be investigated further. To further investigate this transition, analyzing SANS under pressure could be used to define the thermodynamics using an added state. Understanding the contributions to the energy of the transition, would guide the development of new solvents.

4. The Flory Huggins interaction χ parameter and Hansen solubility parameters were effective in predicting favorable interactions. Figure 5.9 indicated the contributions to the hydrogen bonding and polar interactions of the liquid, which can be predicted for new solvents prior to synthesis. Group contributions to each polar and hydrogen bonding interactions could be used to estimate the properties of new synthetic solvents. This would yield the architecture of functional groups that would be required in a new solvent molecule. By predicting polar and hydrogen bonding groups, on the same molecule, it maybe possible to increase disruption.

Several research questions on *S. degradans* could address the following:

1. Several cellulases (Cel5D, Cel5I, Cel6A and Cel9B) have carbohydrate binding modules belonging to families 2 and 10 which bind specifically to crystalline cellulose. What role do these CBMs play in the degradation of crystalline regions?
2. The processivity was measured on insoluble filter paper by taking the ratio of soluble to insoluble sugar. How does the processivity of Cel5H vary between insoluble and soluble substrates? How do the different binding interactions in solution versus on the surface of the substrate affect the processive mechanism?

8. References

1. Rubin EM (2008) Genomics of cellulosic biofuels. *Nature* 454:841-845.

2. Himmel ME (2007) Biomass recalcitrance: engineering plants and enzymes for biofuels production. *Science* 316:982-982.

3. Burton RA, Gidley MJ, & Fincher GB (2010) Heterogeneity in the chemistry, structure and function of plant cell walls. *Nat Chem Biol* 6:724-732.

4. Saxena IM & Brown RM (2005) Cellulose biosynthesis: Current views and evolving concepts. *Ann Bot-London* 96:9-21.

5. Cosgrove DJ (2005) Growth of the plant cell wall. *Nat Rev Mol Cell Bio* 6:850-861.

6. Koyama M, Helbert W, Imai T, Sugiyama J, & Henrissat B (1997) Parallel-up structure evidences the molecular directionality during biosynthesis of bacterial cellulose. *P Natl Acad Sci USA* 94:9091-9095.

7. Dumitriu S (2005) *Polysaccharides : structural diversity and functional versatility* (Marcel Dekker, New York); Polysaccharides : structural diversity and functional versatility 2nd Ed pp xvii, 1204 p.

8. Jarvis M (2003) Chemistry - Cellulose stacks up. *Nature* 426:611-612.

9. Horn SJ, *et al.* (2006) Costs and benefits of processivity in enzymatic degradation of recalcitrant polysaccharides. *P Natl Acad Sci USA* 103:18089-18094.

10. Zhang YHP, *et al.* (2007) Fractionating recalcitrant lignocellulose at modest reaction conditions. *Biotechnol Bioeng* 97:214-223.

11. Mosier N, *et al.* (2005) Features of promising technologies for pretreatment of lignocellulosic biomass. *Bioresource Technol* 96:673-686.

12. Moxley G, Zhu ZG, & Zhang YHP (2008) Efficient sugar release by the cellulose solvent-based lignocellulose fractionation technology and enzymatic cellulose hydrolysis. *J Agr Food Chem* 56:7885-7890.

13. Sathitsuksanoh N, *et al.* (2009) Saccharification of a Potential Bioenergy Crop, Phragmites australis (Common Reed), by Lignocellulose Fractionation Followed by Enzymatic Hydrolysis at Decreased Cellulase Loadings. *Ind Eng Chem Res* 48:6441-6447.

14. Zhu ZG, *et al.* (2009) Comparative Study of Corn Stover Pretreated by Dilute Acid and Cellulose Solvent-Based Lignocellulose Fractionation: Enzymatic Hydrolysis, Supramolecular Structure, and Substrate Accessibility. *Biotechnol Bioeng* 103:715-724.

15. Zhao XB, Cheng KK, & Liu DH (2009) Organosolv pretreatment of lignocellulosic biomass for enzymatic hydrolysis. *Appl Microbiol Biot* 82:815-827.

16. Bergenstrahle M, Wohlert J, Himmel ME, & Brady JW (2010) Simulation studies of the insolubility of cellulose. *Carbohyd Res* 345:2060-2066.

17. Zhang YHP, Cui JB, Lynd LR, & Kuang LR (2006) A transition from cellulose swelling to cellulose dissolution by o-phosphoric acid: Evidence from enzymatic hydrolysis and supramolecular structure. *Biomacromolecules* 7:644-648.

18. Pingali SV, *et al.* (2010) Breakdown of Cell Wall Nanostructure in Dilute Acid Pretreated Biomass. *Biomacromolecules* 11:2329-2335.

19. Gavillon R & Budtova T (2007) Kinetics of cellulose regeneration from cellulose-NaOH-water gels and comparison with cellulose-N-methylmorpholine-N-oxide-water solutions. *Biomacromolecules* 8:424-432.

20. Flory PJ (1965) Statistical Thermodynamics of Liquid Mixtures. *J Am Chem Soc* 87:1833-&.

21. Graessley WW (2003) *Polymeric liquids and networks* (Taylor & Francis, New York ; London); Polymeric liquids and networks p 576 p.

22. Arantes V & Saddler JN (2010) Access to cellulose limits the efficiency of enzymatic hydrolysis: the role of amorphogenesis. *Biotechnol Biofuels* 3:-.

23. Jeoh T, *et al.* (2007) Cellulase digestibility of pretreated biomass is limited by cellulose accessibility. *Biotechnol Bioeng* 98:112-122.

24. Hammouda B (2008) *Probing Nanoscale Structures: The SANS Toolbox* (NIST: National Center for Neutron Research); Probing Nanoscale Structures: The SANS Toolbox.

25. Higgins JS & Benoît H (1994) *Polymers and neutron scattering* (Clarendon Press, Oxford); Polymers and neutron scattering pp xix, 436 p.

26. Melnichenko YB & Wignall GD (2007) Small-angle neutron scattering in materials science: Recent practical applications. *J Appl Phys* 102:-.

27. Beaucage G (1995) Approximations leading to a unified exponential power-law approach to small-angle scattering. *J Appl Crystallogr* 28:717-728.

28. Henrissat B & Davies G (1997) Structural and sequence-based classification of glycoside hydrolases. *Current Opinion in Structural Biology* 7:637-644.

29. Langan P, Nishiyama Y, & Chanzy H (2001) X-ray structure of mercerized cellulose II at 1 angstrom resolution. *Biomacromolecules* 2:410-416.

30. Nishiyama Y, Langan P, & Chanzy H (2002) Crystal structure and hydrogen-bonding system in cellulose 1 beta from synchrotron X-ray and neutron fiber diffraction. *J Am Chem Soc* 124:9074-9082.

31. Nishiyama Y, Sugiyama J, Chanzy H, & Langan P (2003) Crystal structure and hydrogen bonding system in cellulose 1(alpha), from synchrotron X-ray and neutron fiber diffraction. *J Am Chem Soc* 125:14300-14306.

32. Hansen CM (2007) *Hansen solubility parameters : a user's handbook* (CRC Press, Boca Raton); Hansen solubility parameters : a user's handbook 2nd Ed p 519 p.

33. Hansen NML & Plackett D (2008) Sustainable films and coatings from hemicelluloses: A review. *Biomacromolecules* 9:1493-1505.

34. Brandrup J, Immergut EH, & Grulke EA (2004) *Polymer handbook, 4th edition* (Wiley, New York ; Chichester); Polymer handbook, 4th edition 4th Ed p 2 v. (2336 p.).

35. Zhang YHP, Himmel ME, & Mielenz JR (2006) Outlook for cellulase improvement: Screening and selection strategies. *Biotechnology Advances* 24:452-481.

36. Cousins SK & Brown RM (1997) Photoisomerization of a dye-altered beta-1,4 glucan sheet induces the crystallization of a cellulose-composite. *Polymer* 38:903-912.

37. Santa-Maria M & Jeoh T (2010) Molecular-Scale Investigations of Cellulose Microstructure during Enzymatic Hydrolysis. *Biomacromolecules* 11:2000-2007.

38. Wada M, Nishiyama Y, Chanzy H, Forsyth T, & Langan P (2008) The structure of celluloses. *Powder Diffraction* 23:92-95.

39. Lin YC, Cho J, Tompsett GA, Westmoreland PR, & Huber GW (2009) Kinetics and Mechanism of Cellulose Pyrolysis. *J Phys Chem C* 113:20097-20107.

40. Nishiyama Y, Johnson GP, French AD, Forsyth VT, & Langan P (2008) Neutron Crystallography, Molecular Dynamics, and Quantum Mechanics Studies of the Nature of Hydrogen Bonding in Cellulose I-beta. *Biomacromolecules* 9:3133-3140.

41. Lide DR (2010) *CRC handbook of chemistry and physics* (CRC Press, Boca Ratón (Florida)); CRC handbook of chemistry and physics 90th Ed.

42. Mazeau K & Heux L (2003) Molecular dynamics simulations of bulk native crystalline and amorphous structures of cellulose. *J Phys Chem B* 107:2394-2403.

43. Kontturi E, Tammelin T, & Oesterberg M (2007) Cellulose—Model Films and the Fundamental Approach. *ChemInform* 38:no-no.

44. Cousins SK & Brown RM (1995) Cellulose-I Microfibril Assembly - Computational Molecular Mechanics Energy Analysis Favors Bonding by Vanderwaals Forces as the Initial Step in Crystallization. *Polymer* 36:3885-3888.

45. Cousins SK & Brown RM (1997) X-ray diffraction and ultrastructural analyses of dye-altered celluloses support van der Waals forces as the initial step in cellulose crystallization. *Polymer* 38:897-902.

46. Kobayashi S (2005) Challenge of synthetic cellulose. *J Polym Sci Pol Chem* 43:693-710.

47. Cullity BD & Stock SR (2001) *Elements of x-ray diffraction* (Prentice Hall, Upper Saddle River, NJ); Elements of x-ray diffraction 3rd Ed pp xviii, 664 p.

48. Dinand E, Vignon M, Chanzy H, & Heux L (2002) Mercerization of primary wall cellulose and its implication for the conversion of cellulose I -> cellulose II. *Cellulose* 9:7-18.

49. Nishiyama Y, Kuga S, & Okano T (2000) Mechanism of mercerization revealed by X-ray diffraction. *J Wood Sci* 46:452-457.

50. Kim NH, Imai T, Wada M, & Sugiyama J (2006) Molecular directionality in cellulose polymorphs. *Biomacromolecules* 7:274-280.

51. Okano T & Sarko A (1985) Mercerization of Cellulose .2. Alkali Cellulose Intermediates and a Possible Mercerization Mechanism. *J Appl Polym Sci* 30:325-332.

52. KroonBatenburg LMJ, Bouma B, & Kroon J (1996) Stability of cellulose structures studied by MD simulations. Could mercerized cellulose II be parallel? *Macromolecules* 29:5695-5699.

53. Wada M, *et al.* (2001) Improved structural data of cellulose IIII prepared in supercritical ammonia. *Macromolecules* 34:1237-1243.

54. Wada M, Chanzy H, Nishiyama Y, & Langan P (2004) Cellulose IIII crystal structure and hydrogen bonding by synchrotron X-ray and neutron fiber diffraction. *Macromolecules* 37:8548-8555.

55. Wada M (2002) Lateral thermal expansion of cellulose I-beta and IIII polymorphs. *J Polym Sci Pol Phys* 40:1095-1102.

56. Wada M, Heux L, & Sugiyama J (2004) Polymorphism of cellulose I family: Reinvestigation of cellulose IV. *Biomacromolecules* 5:1385-1391.

57. Sturcova A, His I, Wess TJ, Cameron G, & Jarvis MC (2003) Polarized vibrational Spectroscopy of fiber polymers: Hydrogen bonding in cellulose II. *Biomacromolecules* 4:1589-1595.

58. Marechal Y & Chanzy H (2000) The hydrogen bond network in I-beta cellulose as observed by infrared spectrometry. *J Mol Struct* 523:183-196.

59. Perrin CL & Nielson JB (1997) "Strong" hydrogen bonds in chemistry and biology. *Annu Rev Phys Chem* 48:511-544.

60. Li J, Du L, & Wang L (2010) Glycosidic-Bond Hydrolysis Mechanism Catalyzed by Cellulase Cel7A from Trichoderma reesei: A Comprehensive Theoretical Study by Performing MD, QM, and QM/MM Calculations. *The Journal of Physical Chemistry B* 114:15261-15268.

61. Heiner AP, Sugiyama J, & Teleman O (1995) Crystalline Cellulose I-Alpha and I-Beta Studied by Molecular-Dynamics Simulation. *Carbohyd Res* 273:207-223.

62. Nishiyama Y (2009) Structure and properties of the cellulose microfibril. *J Wood Sci* 55:241-249.

63. Qian XH, Ding SY, Nimlos MR, Johnson DK, & Himmel ME (2005) Atomic and electronic structures of molecular crystalline cellulose I beta: A first-principles investigation. *Macromolecules* 38:10580-10589.

64. Gusakov AV, *et al.* (2005) Purification, cloning and characterisation of two forms of thermostable and highly active cellobiohydrolase I (Cel7A) produced by the industrial strain of Chrysosporium lucknowense. *Enzyme Microb Tech* 36:57-69.

65. Zechel DL & Withers SG (2001) Dissection of nucleophilic and acid-base catalysis in glycosidases. *Curr Opin Chem Biol* 5:643-649.

66. White A & Rose DR (1997) Mechanism of catalysis by retaining beta-glycosyl hydrolases. *Current Opinion in Structural Biology* 7:645-651.

67. Ducros V, *et al.* (1995) Crystal-structure of the catalytic domain of a bacterial cellulase belonging to family-5. *Structure* 3:939-949.

68. Wilson DB (2008) Three microbial strategies for plant cell wall degradation. *Annals of the New York Academy of Sciences* 1125:289-297.

69. Bayer EA, Chanzy H, Lamed R, & Shoham Y (1998) Cellulose, cellulases and cellulosomes. *Current Opinion in Structural Biology* 8:548-557.

70. Wilson DB (2004) Studies of Thermobifida fusca plant cell wall degrading enzymes. *The Chemical Record* 4:72-82.

71. Zhang S, Irwin DC, & Wilson DB (2000) Site-directed mutation of noncatalytic residues of Thermobifida fusca exocellulase Cel6B. *European Journal of Biochemistry* 267:3101-3115.

72. Gross AS & Chu JW (2010) On the Molecular Origins of Biomass Recalcitrance: The Interaction Network and Solvation Structures of Cellulose Microfibrils. *J Phys Chem B* 114:13333-13341.

73. Carroll A & Somerville C (2009) Cellulosic Biofuels. *Annu Rev Plant Biol* 60:165-182.

74. Langan P, Sukumar N, Nishiyama Y, & Chanzy H (2005) Synchrotron X-ray structures of cellulose I-beta and regenerated cellulose II at ambient temperature and 100 K. *Cellulose* 12:551-562.

75. Porro F, Bedue O, Chanzy H, & Heux L (2007) Solid-state C-13 NMR study of Na-cellulose complexes. *Biomacromolecules* 8:2586-2593.

76. Marzialetti T, *et al.* (2008) Dilute acid hydrolysis of Loblolly pine: A comprehensive approach. *Ind Eng Chem Res* 47:7131-7140.

77. Wada M, Nishiyama Y, & Langan P (2006) X-ray structure of ammonia-cellulose I: New insights into the conversion of cellulose I to cellulose III. *Macromolecules* 39:2947-2952.

78. Nishiyama Y, Langan P, Wada M, & Forsyth VT (2010) Looking at hydrogen bonds in cellulose. *Acta Crystallogr D* 66:1172-1177.

79. Lau MW & Dale BE (2009) Cellulosic ethanol production from AFEX-treated corn stover using Saccharomyces cerevisiae 424A(LNH-ST). *P Natl Acad Sci USA* 106:1368-1373.

80. Kobayashi K, Kimura S, Togawa E, & Wada M (2011) Crystal transition from Na-cellulose IV to cellulose II monitored using synchrotron X-ray diffraction. *Carbohyd Polym* 83:483-488.

81. Huebner A, Ladisch MR, & Tsao GT (1978) Preparation of Cellodextrins - Engineering Approach. *Biotechnol Bioeng* 20:1669-1677.

82. Lindman B, Karlstrom G, & Stigsson L (2010) On the mechanism of dissolution of cellulose. *Journal of Molecular Liquids* 156:76-81.

83. Horvath AL (2006) Solubility of structurally complicated materials: I. Wood. *J Phys Chem Ref Data* 35:77-92.

84. Foston M & Ragauskas AJ (2010) Changes in the Structure of the Cellulose Fiber Wall during Dilute Acid Pretreatment in Populus Studied by H-1 and H-2 NMR. *Energ Fuel* 24:5677-5685.

85. Kumar R, Mago G, Balan V, & Wyman CE (2009) Physical and chemical characterizations of corn stover and poplar solids resulting from leading pretreatment technologies. *Bioresource Technol* 100:3948-3962.

86. Kim TH, Kim JS, Sunwoo C, & Lee YY (2003) Pretreatment of corn stover by aqueous ammonia. *Bioresource Technol* 90:39-47.

87. Wyman C (1996) *Handbook on bioethanol : production and utilization* (Taylor & Francis, Washington, DC); Handbook on bioethanol : production and utilization pp xvii, 424 p.

88. Fink HP, Weigel P, Purz HJ, & Ganster J (2001) Structure formation of regenerated cellulose materials from NMMO-solutions. *Prog Polym Sci* 26:1473-1524.

89. Shao Q, *et al.* (2010) Enzymatic digestibility and ethanol fermentability of AFEX-treated starch-rich lignocellulosics such as corn silage and whole corn plant. *Biotechnol Biofuels* 3:-.

90. Pinkert A, Marsh KN, Pang SS, & Staiger MP (2009) Ionic Liquids and Their Interaction with Cellulose. *Chem Rev* 109:6712-6728.

91. El Seoud OA, Koschella A, Fidale LC, Dorn S, & Heinze T (2007) Applications of ionic liquids in carbohydrate chemistry: A window of opportunities. *Biomacromolecules* 8:2629-2647.

92. Gorke J, Srienc F, & Kazlauskas R (2010) Toward Advanced Ionic Liquids. Polar, Enzyme-friendly Solvents for Biocatalysis. *Biotechnol Bioproc E* 15:40-53.

93. Bose S, Armstrong DW, & Petrich JW (2010) Enzyme-Catalyzed Hydrolysis of Cellulose in Ionic Liquids: A Green Approach Toward the Production of Biofuels. *The Journal of Physical Chemistry B.*

94. Kumar P, Barrett DM, Delwiche MJ, & Stroeve P (2009) Methods for Pretreatment of Lignocellulosic Biomass for Efficient Hydrolysis and Biofuel Production. *Ind Eng Chem Res* 48:3713-3729.

95. Mansfield SD, Mooney C, & Saddler JN (1999) Substrate and enzyme characteristics that limit cellulose hydrolysis. *Biotechnol Progr* 15:804-816.

96. Park S, Baker JO, Himmel ME, Parilla PA, & Johnson DK (2010) Cellulose crystallinity index: measurement techniques and their impact on interpreting cellulase performance. *Biotechnol Biofuels* 3:-.

97. Park S, Johnson DK, Ishizawa CI, Parilla PA, & Davis MF (2009) Measuring the crystallinity index of cellulose by solid state C-13 nuclear magnetic resonance. *Cellulose* 16:641-647.

98. Li B, Asikkala J, Filpponen I, & Argyropoulos DS (2010) Factors Affecting Wood Dissolution and Regeneration of Ionic Liquids. *Ind Eng Chem Res* 49:2477-2484.

99. Brosse N, Sannigrahi P, & Ragauskas A (2009) Pretreatment of Miscanthus x giganteus Using the Ethanol Organosolv Process for Ethanol Production. *Ind Eng Chem Res* 48:8328-8334.

100. Hallac BB, *et al.* (2010) Effect of Ethanol Organosolv Pretreatment on Enzymatic Hydrolysis of Buddleja davidii Stem Biomass. *Ind Eng Chem Res* 49:1467-1472.

101. Sun FB & Chen HZ (2008) Enhanced enzymatic hydrolysis of wheat straw by aqueous glycerol pretreatment. *Bioresource Technol* 99:6156-6161.

102. Martinez D, *et al.* (2008) Genome sequencing and analysis of the biomass-degrading fungus Trichoderma reesei (syn. Hypocrea jecorina) (vol 26, pg 553, 2008). *Nat Biotechnol* 26:1193-1193.

103. Doi RH & Kosugi A (2004) Cellulosomes: Plant-cell-wall-degrading enzyme complexes. *Nat Rev Microbiol* 2:541-551.

104. Taylor LE, *et al.* (2006) Complete cellulase system in the marine bacterium Saccharophagus degradans strain 2-40(T). *Journal of Bacteriology* 188:3849-3861.

105. Weiner RM, *et al.* (2008) Complete genome sequence of the complex carbohydrate-degrading marine bacterium, Saccharophagus degradans strain 2-40(T). *Plos Genetics* 4:-.

106. Suvorov M, Kumar, R, Zhang, H, Hutcheson, S (2011) Novelties of the cellulolytic system of a marine bacterium applicable to cellulosic sugar production. *Biofuels* 2:xxx-xxx.

107. Ghose TK (1987) Measurement of Cellulase Activities. *Pure Appl Chem* 59:257-268.

108. Park JK, Wang LX, Patel HV, & Roseman S (2002) Molecular cloning and characterization of a unique beta-glucosidase from Vibrio cholerae *J Biol Chem* 277:29555-29560.

109. Kang MS, Kang IC, Kim SM, Lee HC, & Oh JS (2007) Effect of Leuconastoc spp. on the formation of Streptococcus mutans biorilm. *Journal of Microbiology* 45:291-296.

110. Doner LW & Irwin PL (1992) Assay of reducing end-groups in oligosaccharide homologs with 2,2'-bicinchoninate. *Anal Biochem* 202:50-53.

111. Lo Leggio L & Larsen S (2002) The 1.62 angstrom structure of Thermoascus aurantiacus endoglucanase: completing the structural picture of subfamilies in glycoside hydrolase family 5. *Febs Letters* 523:103-108.

112. Jeoh T, Wilson DB, & Walker LP (2006) Effect of cellulase mole fraction and cellulose recalcitrance on synergism in cellulose hydrolysis and binding. *Biotechnol Progr* 22:270-277.

113. Zhang S, Barr BK, & Wilson DB (2000) Effects of noncatalytic residue mutations on substrate specificity and ligand binding of Thermobifida fusca endocellulase Cel6A. *European Journal of Biochemistry* 267:244-252.

114. Kumar R, Singh S, & Singh OV (2008) Bioconversion of lignocellulosic biomass: biochemical and molecular perspectives. *Journal of Industrial Microbiology & Biotechnology* 35:377-391.

115. Irwin DC, Spezio M, Walker LP, & Wilson DB (1993) Activity Studies of 8 Purified Cellulases - Specificity, Synergism, and Binding Domain Effects. *Biotechnol Bioeng* 42:1002-1013.

116. Li YC, Irwin DC, & Wilson DB (2007) Processivity, substrate binding, and mechanism of cellulose hydrolysis by Thermobifida fusca Ce19A. *Appl Environ Microb* 73:3165-3172.

117. Gilad R, *et al.* (2003) Ce1I, a noncellulosomal family 9 enzyme from Clostridium thermocellum , is a processive endoglucanase that degrades crystalline cellulose. *Journal of Bacteriology* 185:391-398.

118. Sakon J, Irwin D, Wilson DB, & Karplus PA (1997) Structure and mechanism of endo/exocellulase E4 from Thermomonospora fusca *Nature Structural Biology* 4:810-818.

119. Howard MB, Ekborg NA, Taylor LE, Hutcheson SW, & Weiner RM (2004) Identification and analysis of polyserine linker domains in prokaryotic proteins with emphasis on the marine bacterium Microbulbifer degradans. *Protein Science* 13:1422-1425.

120. Boraston AB, Bolam DN, Gilbert HJ, & Davies GJ (2004) Carbohydrate-binding modules: fine-tuning polysaccharide recognition. *Biochemical Journal* 382:769-781.

121. Cohen R, Suzuki MR, & Hammel KE (2005) Processive endoglucanase active in crystalline cellulose hydrolysis by the brown rot basidiomycete Gloeophyllum trabeum *Appl Environ Microb* 71:2412-2417.

122. Breyer WA & Matthews BW (2001) A structural basis for processivity. *Protein Science* 10:1699-1711.

123. Violot S, *et al.* (2005) Structure of a full length psychrophilic cellulase from Pseudoalteromonas haloplanktis revealed by x-ray diffraction and small angle x-ray scattering. *Journal of Molecular Biology* 348:1211-1224.

124. Xie G, *et al.* (2007) Genome sequence of the cellulolytic gliding bacterium Cytophaga hutchinsonii *Appl Environ Microb* 73:3536-3546.

125. Qi M, Jun HS, & Forsberg CW (2007) Characterization and synergistic interactions of Fibrobacter succinogenes glycoside hydrolases. *Appl Environ Microb* 73:6098-6105.

126. Qi M, Jun HS, & Forsberg CW (2008) Cel9D, an atypical 1,4-beta-D-glucan glucohydrolase from Fibrobacter succinogenes : characteristics, catalytic residues, and synergistic interactions with other cellulases. *Journal of Bacteriology* 190:1976-1984.

127. Elazzouzi-Hafraoui S, *et al.* (2008) The shape and size distribution of crystalline nanoparticles prepared by acid hydrolysis of native cellulose. *Biomacromolecules* 9:57-65.

128. Watson BJ, Zhang HT, Longmire AG, Moon YH, & Hutcheson SW (2009) Processive Endoglucanases Mediate Degradation of Cellulose by Saccharophagus degradans. *Journal of Bacteriology* 191:5697-5705.

129. Kent MS, *et al.* (2010) Study of Enzymatic Digestion of Cellulose by Small Angle Neutron Scattering. *Biomacromolecules* 11:357-368.

130. Koizumi S, *et al.* (2008) Bacterium organizes hierarchical amorphous structure in microbial cellulose. *Eur Phys J E* 26:137-142.

131. McQuarrie DA & Simon JD (1997) *Physical chemistry : a molecular approach* (University Science Books, Sausalito, Calif.); Physical chemistry : a molecular approach pp xxiii, 1270 p.

132. Smith BC (1996) *Fundamentals of Fourier transform infrared spectroscopy* (CRC Press, Boca Raton); Fundamentals of Fourier transform infrared spectroscopy p 202 p.

133. Oh SY, Yoo DI, Shin Y, & Seo G (2005) FTIR analysis of cellulose treated with sodium hydroxide and carbon dioxide. *Carbohyd Res* 340:417-428.

134. Schwanninger M, Rodrigues JC, Pereira H, & Hinterstoisser B (2004) Effects of short-time vibratory ball milling on the shape of FT-IR spectra of wood and cellulose. *Vib Spectrosc* 36:23-40.

135. Hansen CM (1969) Universality of Solubility Parameter. *Ind Eng Chem Prod Rd* 8:2-&.

136. Glinka CJ, *et al.* (1998) The 30 m small-angle neutron scattering instruments at the National Institute of Standards and Technology. *J Appl Crystallogr* 31:430-445.

137. Kline SR (2006) Reduction and analysis of SANS and USANS data using IGOR Pro. *J Appl Crystallogr* 39:895-900.

138. Gunnars S, Wagberg L, & Stuart MAC (2002) Model films of cellulose: I. Method development and initial results. *Cellulose* 9:239-249.

139. Kadokawa JI, Murakami MA, & Kaneko Y (2008) A facile preparation of gel materials from a solution of cellulose in ionic liquid. *Carbohyd Res* 343:769-772.

140. Edgar CD & Gray DG (2003) Smooth model cellulose I surfaces from nanocrystal suspensions. *Cellulose* 10:299-306.

141. Kontturi E, Thune PC, & Niemantsverdriet JW (2003) Cellulose model surfaces-simplified preparation by spin coating and characterization by X-ray photoelectron spectroscopy, infrared spectroscopy, and atomic force microscopy. *Langmuir* 19:5735-5741.

142. Bansal P, Hall M, Realff MJ, Lee JH, & Bommarius AS (2010) Multivariate statistical analysis of X-ray data from cellulose: A new method to determine degree of crystallinity and predict hydrolysis rates. *Bioresource Technol* 101:4461-4471.

143. Hollas JM (2002) *Basic atomic and molecular spectroscopy* (Wiley-Interscience, New York); Basic atomic and molecular spectroscopy pp vii, 184 p.

144. Derecskei B & Derecskei-Kovacs A (2006) Molecular dynamic studies of the compatibility of some cellulose derivatives with selected ionic liquids. *Mol Simulat* 32:109-115.

145. Barton AFM (1990) *CRC handbook of polymer-liquid interaction parameters and solubility parameters* (CRC Press, Boca Raton); CRC handbook of polymer-liquid interaction parameters and solubility parameters p 753 p.

146. Zhang J, *et al.* (2010) The dependence of pyrolysis behavior on the crystal state of cellulose. *Carbohyd Polym* 79:164-169.

147. Oh SY, *et al.* (2005) Crystalline structure analysis of cellulose treated with sodium hydroxide and carbon dioxide by means of X-ray diffraction and FTIR spectroscopy. *Carbohyd Res* 340:2376-2391.

148. Carrillo A, Colom X, Sunol JJ, & Saurina J (2004) Structural FTIR analysis and thermal characterisation of lyocell and viscose-type fibres. *Eur Polym J* 40:2229-2234.

149. Schmidt PW (1991) Small-Angle Scattering Studies of Disordered, Porous and Fractal Systems. *J Appl Crystallogr* 24:414-435.

150. Watanabe A, Morita S, & Ozaki Y (2006) Temperature-dependent structural changes in hydrogen bonds in microcrystalline cellulose studied by infrared and near-infrared spectroscopy with perturbation-correlation moving-window two-dimensional correlation analysis. *Appl Spectrosc* 60:611-618.

151. Appaw C, Gilbert RD, & Khan SA (2007) Viscoelastic behavior of cellulose acetate in a mixed solvent system. *Biomacromolecules* 8:1541-1547.

152. Arita T, Ueda Y, Minami K, Naka T, & Adschiri T (2010) Dispersion of Fatty Acid Surface Modified Ceria Nanocrystals in Various Organic Solvents. *Ind Eng Chem Res* 49:1947-1952.

153. Marcus Y (2002) *Solvent mixtures : properties and selective solvation* (Marcel Dekker Inc., New York); Solvent mixtures : properties and selective solvation pp xvi, 258 p.

154. Bayer EA, Lamed R, & Himmel ME (2007) The potential of cellulases and cellulosomes for cellulosic waste management. *Curr Opin Biotech* 18:237-245.

155. Thompson G, Swain J, Kay M, & Forster CF (2001) The treatment of pulp and paper mill effluent: a review. *Bioresource Technol* 77:275-286.

156. Naqvi M, Yan J, & Dahlquist E (2010) Black liquor gasification integrated in pulp and paper mills: A critical review. *Bioresource Technol* 101:8001-8015.

157. Kacurakova M, Capek P, Sasinkova V, Wellner N, & Ebringerova A (2000) FT-IR study of plant cell wall model compounds: pectic polysaccharides and hemicelluloses. *Carbohyd Polym* 43:195-203.

158. Kubo S & Kadla JF (2005) Hydrogen bonding in lignin: A Fourier transform infrared model compound study. *Biomacromolecules* 6:2815-2821.

159. Cheng G, *et al.* (2008) Association and structure of thermosensitive comblike block copolymers in aqueous solutions. *Macromolecules* 41:4824-4827.